Development of Polymeric Nanocarriers for Dual Magnetic Resonance Imaging and Drug Delivery

Nipon Pothayee

Dissertation Submitted to the Faculty of the Virginia Polytechnic Institute and State University in Partial Fulfillment of the Requirements for the Degree of

Doctor of Philosophy
In
Macromolecular Science and Engineering

Judy S. Riffle
Richey M. Davis
Kevin J. Edgar
Richard S. Turner
Nammalwar Sriranganathan

September 24, 2013
Blacksburg, VA

keywords; magnetite, manganese, block, graft ionomers, contrast agents, drug delivery

Development of Polymeric Nanocarriers for Dual Magnetic Resonance Imaging and Drug Delivery

Nipon Pothayee

ABSTRACT

Two types of (polymer-imaging agent-drug) complexes were prepared and characterized. These included block and graft copolymer complexes with magnetite nanoparticles and manganese ions.

Magnetite block ionomer complexes (*MBICs*) were formed through binding of a portion of the anionic segment of poly(ethylene oxide)-*b*-poly(acrylic acid) (PEO-*b*-PAA) block copolymers with the magnetite nanoparticle surfaces. The remainder of the carboxylic acids were utilized to bind with high concentrations of the cationic antibiotic gentamicin (31 wt%). A near zero-order release of gentamicin (pH 7.4 in PBS) that reached ~35 wt% of the initial gentamicin within 10 hours was observed, and this was followed by slower release of another 7 % by 18 hours. These nanoparticles were efficiently taken up by macrophages and appeared to enhance intracellular antimicrobial activities of gentamicin. To increase the complex sizes and NMR T_2 relaxivities, amine functional MBICs *(MBICs-NH_2)* were first assembled by adsorbing the polyacrylate block of an aminofunctional poly(ethylene oxide)-*b*-poly(acrylic acid)) (H_2N-PEO-*b*-PAA) copolymer onto magnetite nanoparticles. Amines at the tips of the H_2N-PEO corona were then linked through reaction with a PEO diacrylate oligomer to yield *MBIClusters* where the metal oxides in the precursor nanoparticles were distinctly separated by the hydrophilic polymer. These *MBIClusters* with hydrophilic intra-cluster space had transverse relaxivities (r_2*'s*) that increased from 190 to 604 s^{-1} mM Fe^{-1}

measured at 1.4 T and 37 °C as their average sizes increased. The clusters were loaded with up to ~38 wt% of the multi-cationic drug gentamicin. MRI scans focused on the livers of mice demonstrated that these *MBIClusters* are very sensitive contrast agents. These results indicate that these complexes could be potential theranostic agents for dual imaging and drug delivery.

Manganese graft ionomer complexes *(MaGICs)* comprised of Mn ions and a novel polyaminobisphosphonate-*g*-PEO copolymer were developed for use as T_1 weighted MRI positive contrast agents. The graft copolymers were prepared by free radical copolymerization of ammonium bisphosphonate methacrylate monomers with PEO-acrylate macromonomers. The complexes exhibited good colloidal stability without release of free manganese and did not show any in vitro toxicity against mouse hepatocytes. The T_1 relaxivities of the *MaGICs* were 2-10 times higher than that of a commercial manganese based contrast agent MnDPDP. These *MaGICs* with encapsulated anticancer drugs including doxorubicin, cisplatin and carboplatin have encapsulation efficiencies of 80-100 %. Drug release was sustained and depended on environmental pH, drug structure and drug concentration in the *MaGICs*. Moreover, these drug-loaded complexes exhibited high anticancer efficacy against MCF-7 breast cancer cells. The prominent MRI relaxivities and high anticancer efficacy suggest that these *MaGICs* have potential as effective dual imaging and chemotherapeutic agents.

Acknowledgement

First of all, I would like to thank my advisor Dr. Judy Riffle for her support, guidance, encouragement, and trust throughout my career at Virginia Tech. Her ability as an advisor to guide her students while nurturing and focusing their creativity towards a specific goal is one of her greatest talents. I am very fortunate to have her as my advisor ever since I came to Virginia Tech. It is also my honor to be advised by a group of prominent and brilliant committee members Dr. Richey Davis, Dr. Nammalwar Sriranganathan, Dr. Richard Turner and Dr. Kevin Edgar. All of these professors have my utmost respect. I would like to thank Angie Flynn, Mary Jane Smith and Cyndy Graham who has helped me organize all tools and materials required to conduct an experiment. Also, this dissertation would not be completed without great collaboration with Dr. Nikorn Pothayee, Dr. Neeta Jain, Dr. Yinian Lin, Nan Hu, and Sharavan Balasubramanium. I would like to extend my deepest thanks to all group members and friends that I have met and the others that walked through my life. I owe so much for the friendship and life lessons that we share. Finally, I am most grateful to my family for everything. To my mom, dad, brother, sister, grand moms, grand dads you always have been there for me through the bad and good times. I wouldn't be the person I am today without you all.

Table of Contents

Abbreviations

MBICs magnetic block ionomer complexes
MBIClusters magnetic block ionomer clusters
MaGICs manganese graft ionomer complexes
DOX doxorubicin
CPt cisplatin
CBPt carboplatin
GEN gentamicin
ATRP atom transfer radical polymerization
PEO poly(ethylene oxide)
PPO poly(propylene oxide)
PAA poly(acrylic acid)
SEC size exclusion chromatography
DLS dynamic light scattering
TGA thermal gravimetric analysis
TEM transition electron microscopy
ICP-AES inductively coupled plasma atomic emission spectroscopy
NMR nuclear magnetic resonance spectroscopy
SQuID superconducting quantum interference device
PMDETA N-N'-N'-N"-N"-pentamethyldiethylenetriamine
TMSBr trimethylsilyl bromide
$Fe(acac)_3$ iron (III) acetylacetonate
THF tetrahydrofuran
DMF dimethylformamide
DMSO dimethylsulfoxide
PB phosphate buffer
PBS phosphate buffered saline
ABS acetate buffer saline
CFU colony forming unit
M_n number average molecular weight
PDI polydispersity index
MTT methylthiazol tetrazolium assay

List of figures

List of tables

Chapter 1

Introduction

Advances in nanotechnology and molecular biology are rapidly enabling the development of nanoparticles with specific functional properties that address the shortcomings of traditional diagnostic and therapeutic agents.[1-3] In the past decade, the term "theranostics" was adopted to define ongoing efforts to combine diagnostic and therapeutic capabilities into a single agent. Clever combinations of nanoscale materials are under investigation to enable simultaneous in vivo drug delivery and diagnostic imaging for real-time tracking of drug-loaded nanocarriers.[4-5]

Magnetic resonance imaging (MRI) is a powerful tool for non-invasive clinical diagnostics. In MRI, relaxation phenomena including longitudinal relaxation (T1) and transverse relaxation (T2) of water protons are measured. The image contrast is generated from the differences in T1 and T2 relaxation times of the local protons, the proton density, and also the chemical and physical nature of the tissues within the specimen.[6-8] However, the low sensitivity of MRI often diminishes diagnostic quality. Thus, contrast agents are commonly employed to enhance sensitivity of MRI improving upon tissue contrast by altering relaxation rates of nearby water molecules. The key parameters in the properties of contrast agents are related to surface chemistry, size, and magnetic properties.[9] Thus, the development of next generation contrast agents that can specifically target, treat or illuminate damaged tissue together with drug delivery will require materials with tailored sizes, shapes, coatings, and surface modifications.

This dissertation focuses on designing nanocarriers that combine unique features of ion-containing block and graft copolymers with robust MRI contrast agents to create

novel platforms that encompass simultaneous real-time disease imaging and drug delivery. Chapter 3 introduces magnetic block ionomer complexes (*MBICs*) that combine the attributes of core-shell *BICs* containing electrostatically-bound drugs with magnetite nanoparticles designed for MR imaging. This strategy was to co-encapsulate cationic aminoglycoside antibiotics and magnetite with anionic PEO-*b*-PAA block copolymers to form nanoscale *MBICs* that were taken up by macrophage-like cells infected with pathogenic bacteria. Efficacy of the nanoparticles to enhance intracellular accumulation of MRI imaging agents and therapeutic drugs will be discussed.

Chapter 4 describes the formation of hydrophilic magnetic nanoclusters (*MBIClusters*) with controlled sizes and with significant hydrophilic space between the magnetite particles within the clusters. Their prominent longditudinal and transverse relaxivities together with high capacities for encapsulating cationic therapeutic agents makes these highly promising as future T2 weighted (negative) MRI probes.

Chapter 5 presents the formation of novel manganese graft ionomer complexes (*MaGICs*) for potential positive MRI contrast agents. Different types of graft copolymers including polycarboxylate-*g*-PEO and polyaminobisphosphonate-*g*-PEO were utilized to fabricate *MaGICs* through spontaneous self-organization with Mn^{2+} in aqueous solution. The relaxometric properties and applicability (lack of toxicity, colloidal stability, resistance against ion exchange with calcium) of each type of *MaGICs* was investigated. These agents were superior in contrast sensitivity relative to commercial contrast agents.

Chapter 6 describes the potential of using *MaGICs* as nanocarriers for various anticancer drugs. The drug loading efficiency and drug release characteristics were investigated. The effectiveness of these delivery vehicles to eradicate cancer cells in vitro

will be discussed.

References

1. O. Veiseh, J. W. Gunn, M. Zhang *Adv. Drug Deliv. Rev.* **2010**, *62*, 284.
2. N. Sanvicens, M.P. Marco *Trends Biotechnol.* **2008**, *26*, 425.
3. O.C. Farokhzad, R. Langer *Adv. Drug Deliv. Rev.* **2006**, *58*, 1456.
4. S. M. Janib, A. S. Moses, J. A. Mackey *Adv. Drug Deliv. Rev.* **2010**, *62*, 1052.
5. J. Xie, S. Lee, X. Chen *Adv. Drug Deliv. Rev.* **2010**, *62*, 1064.
6. J. Cheon *J. Am. Chem. Soc.* **2010**, *132*, 11015.
7. T. G. Park *Bioconjugate Chem.* **2010**, *21*, 505.
8. J. Gao *Adv. Mater.* **2012**, *24*, 6223.
9. J. Santamaría *Nanotoday*, **2007**, *2*, 22.

Chapter 2

Literature review

2.1 Overview

This literature review will discuss areas directly related to the research topic and is divided into four sections. The first section presents an overview of magnetite nanoparticles (MNPs) including synthesis and modification of these particles for use in biomedical applications. The applications of MNPs as MR imaging negative contrast agents and as carriers for drug delivery will be discussed in sections two and three. The last section will focus on the recent development in manganese-based nanoparticles for MR imaging positive contrast agents with a specific focus on the different manganese contrast agent families, their synthetic strategies and properties.

2.2 Fabrication of target-specific magnetite nanoparticles (MNPs)

2.2.1 Synthesis of magnetite nanoparticles (MNPs)

Different preparation methods have been developed to synthesize MNPs for biomedical applications. One main challenge is to define reproducible experimental conditions that produce narrow particle size distributions with suitable size. The most common procedure is the chemical co-precipitation of aqueous iron salts in the presence of strong bases such as ammonium hydroxide or sodium hydroxide. The properties of the particles are affected by different parameters including the temperature, pH and ratio of Fe^{2+}/Fe^{3+}.[1] The chemical reaction of magnetite formation can be written as shown in equation 1.

$$Fe^{2+} + 2Fe^{3+} + 8OH \rightarrow Fe_3O_4 + 4H_2O \quad (1)$$

According to the thermodynamics of this reaction, complete precipitation of

magnetite should be expected at pH between 8-14, with a stoichiometric ratio of 2:1 Fe^{3+}/Fe^{2+} in the absence of oxygen or other oxidizing agents.[2] Magnetite is prone to oxidation and transformed into maghemite (γ-Fe_2O_3) in the presence of oxygen.

The main advantage of the co-precipitation technique is that a large amount of nanoparticles can be prepared quickly. However, the size distribution of the magnetite nanoparticles obtained by this method is broad and uncontrollable.[3,4]

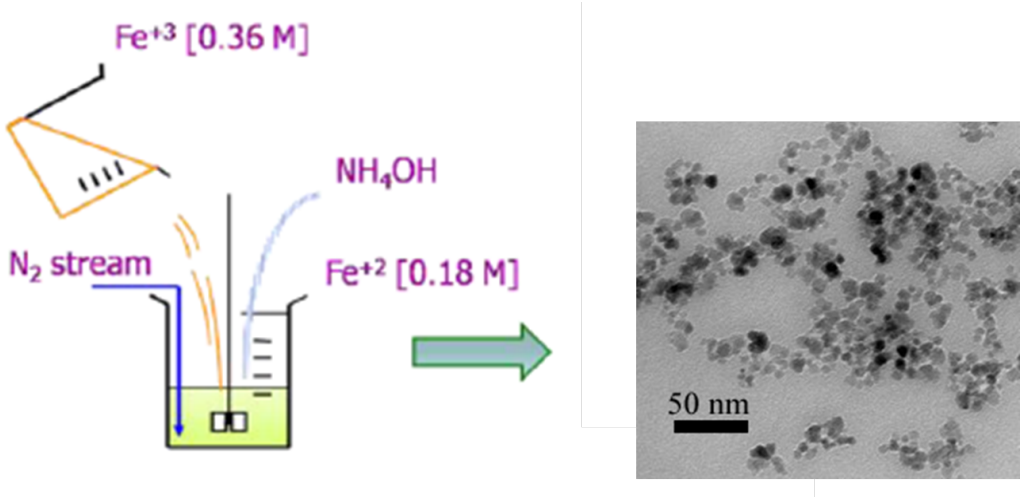

Figure 2.1 Illustration of the formation of small clusters of MNPs after synthesis by the co-precipitation method.

Since co-precipitation generates particles with a broad size distribution and aggregation, other approaches based on high temperature reduction of iron III organometallic precursors have been developed to produce particles with much more uniform dimensions.[5,6]

Sun et al. were the first group to pioneer a high-temperature reduction of iron(III) acetylacetonate with hexadecanediol in the presence of oleic acid and oleylamine in a high boiling point solvent such as benzyl ether to obtain monodisperse magnetite

nanoparticles.[6] In this method, oleic acid and oleylamine were used as surfactants while alkane-diol species was utilized as the reducing agent.

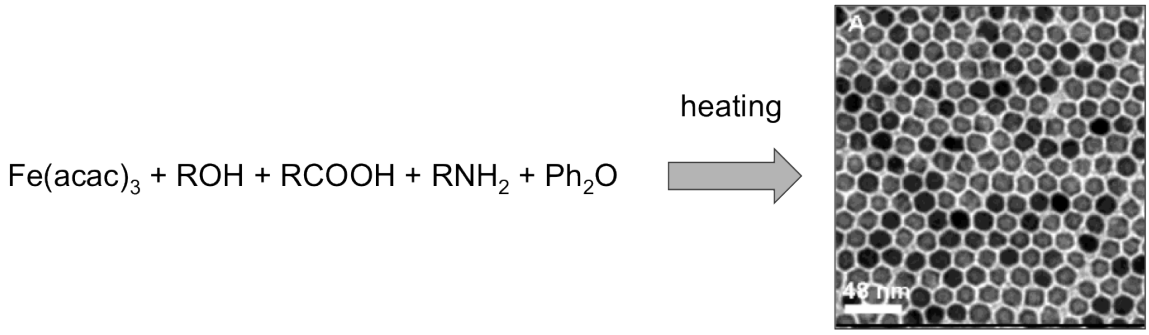

Figure 2.2 Illustration of the formation of monodisperse magnetite nanoparticles after synthesis by reduction of iron acetylacetonate.[6]

Other high boiling point solvents have been explored, especially when the solvent itself can act as the reducing agent to control growth of the particles. Pinna et al. reported the synthesis of MNPs with high crystallinity and magnetization by reducing iron (III) acetylacetonate in benzyl alcohol at the reflux temperature of 205 °C.[7] The particles were fairly narrowly dispersed and could be made soluble in organic solvents or water by coating with appropriate ligands.

2.2.2 Surface coating and functionalization to afford water-dispersible MNPs

One of the main challenges for utilizing MNPs in biomedical applications is to prepare water dispersible particles, which exhibit good colloidal stability in physiological media. Several approaches have been developed to coat and stabilize the surface of MNPs including in situ coating and post-synthesis coating.[8,9] These surface coatings function to provide binding sites for drug or targeting molecule loading, prevent particles aggregation and also limit non-specific cell interactions. The magnetic properties of MNPs are affected by coating materials and strategies. For example, Duan et al. showed

that decreasing hydrophobicity of the polymer coatings resulted in higher R_2 relaxivities[10], while LaConte et al. reported that R_2 relaxivities decrease with an increase of coating thickness.[11] This suggests that different parameters effect the final properties of the magnetite nanoparticles.

Various polymeric materials or surfactants have been used to produce water dispersible MNPs. In the literature reports so far, the most common materials are polysaccharides including dextran, alginate, chitosan or PEO-containing copolymers. The next sections will describe some of the most common polymer coatings, coating methods and examples of use.

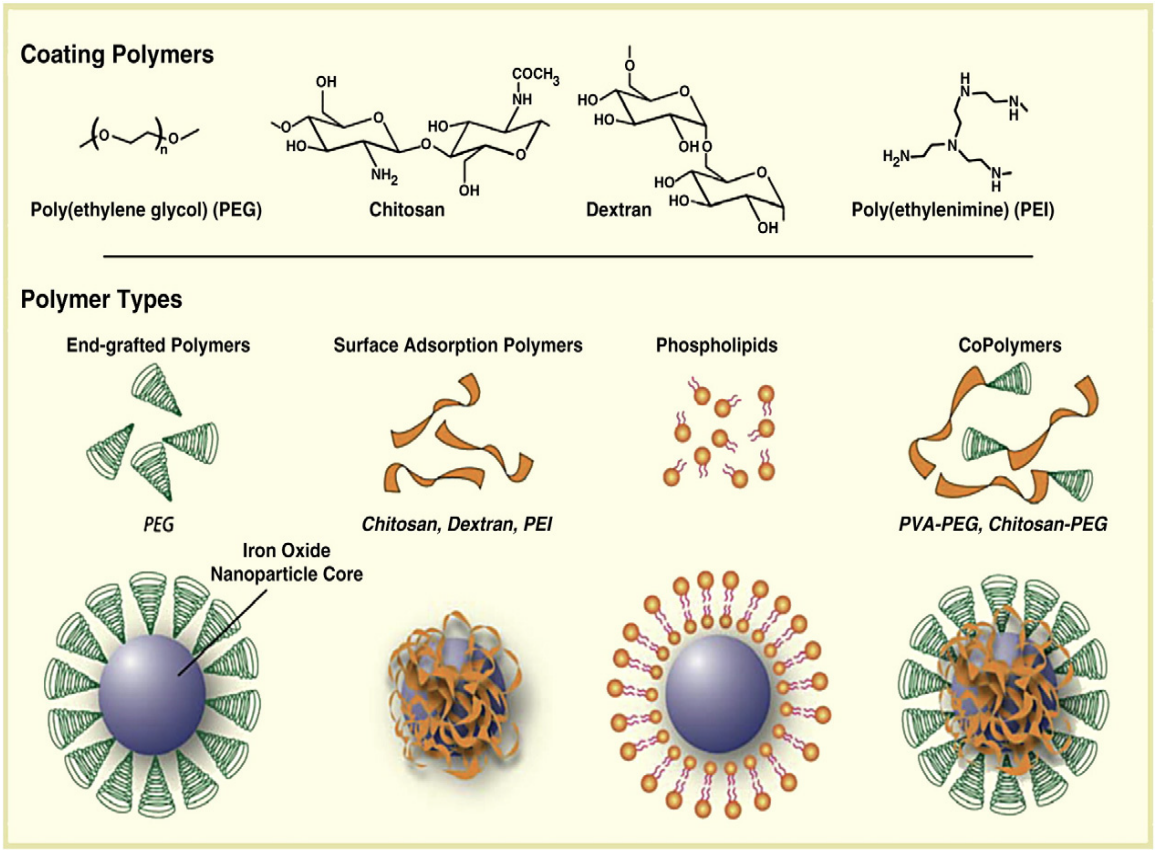

Figure 2.3 Surface modification of MNP with various types of polymer [9]

2.2.2.1 Polysaccharides

2.2.2.1.1 Dextran

Dextran is a branched polysaccharide polymer composed of glucose subunits. Due to its biocompatibility and its polar interactions (chelation and hydrogen bonding), dextran has been widely used in magnetite coatings.[12] Stabilization of MNPs with dextran was first reported by Molday and Mackenzie.[13] Ferumoxtran-10 and ferumoxides were produced by the Molday co-precipitation method with *in situ* coating by dextran. The same process was used for Ferucarbotran and Ferumoxytol with *in situ* coating by carboxymethyl dextran. Ferumoxtran-10 and Ferumoxytol, which have a small hydrodynamic diameters (15-30 nm), show prolonged blood residence times, which allows them to access macrophages located in deep and pathologic tissues. However, the dextran molecules can desorb from the MNP surfaces by heating or dilution.[14] Efforts to avoid desorption of dextran have been made including reacting it with a crosslinking agent such as epichlorohydrin.[15]

2.2.2.1.2 Alginate

Alginate (Alg) is the major structural polysaccharide of marine brown algae, and it has combined features of being abundant, low-cost, and is biocompatible. It is a linear copolymer of (1–4)-linked β-D-mannuronic acid and α-L-guluronic acid units with many carboxyl groups. Researchers have speculated that the carboxyl groups of the polyalginate can interact with iron ion and that electrostatic repulsion may create stable MNPs. Several investigations on preparation of MNPs coated with alginate have been carried out.[16,17] Typically, the chemical synthesis consists of three steps: (a) gelation of alginate with ferrous ions, (b) *in situ* precipitation of ferrous hydroxide through alkaline treatment of alginate, and (c) oxidation of ferrous hydroxide with an oxidizing agent such

as O_2 or H_2O_2. This method is, however, complex. Ma et al. developed a modified two-step co-precipitation method.[18] Their results revealed that typical MNPs had core diameters of 5-10 nm and that MNPs coated with alginate had hydrodynamic diameters of 193.8-483.2 nm, indicating agglomeration of particles.

2.2.2.1.3 Chitosan

Chitosan is one of the most abundant biopolymers and is used as a coating agent for MNPs. It is a cationic, hydrophilic polymer that is nontoxic, biocompatible, bioabsorbable and is easy to functionalize.[19] Therefore, preparations of MNPs coated chitosan are of great interest.[20] Kim et al. have synthesized MNPs by a sonochemical method and subsequently coated with chitosan for use as MRI contrast agents.[21] These particles with the size of 15 nm exhibited excellent superparamagnetic behavior. In another report, Lee et al. have prepared spherical MNPs with the size of 30 nm and embedded with chitosan. The MNPs-chitosan microspheres showed a strong enhancement of MR image contrast *in vitro*.[22]

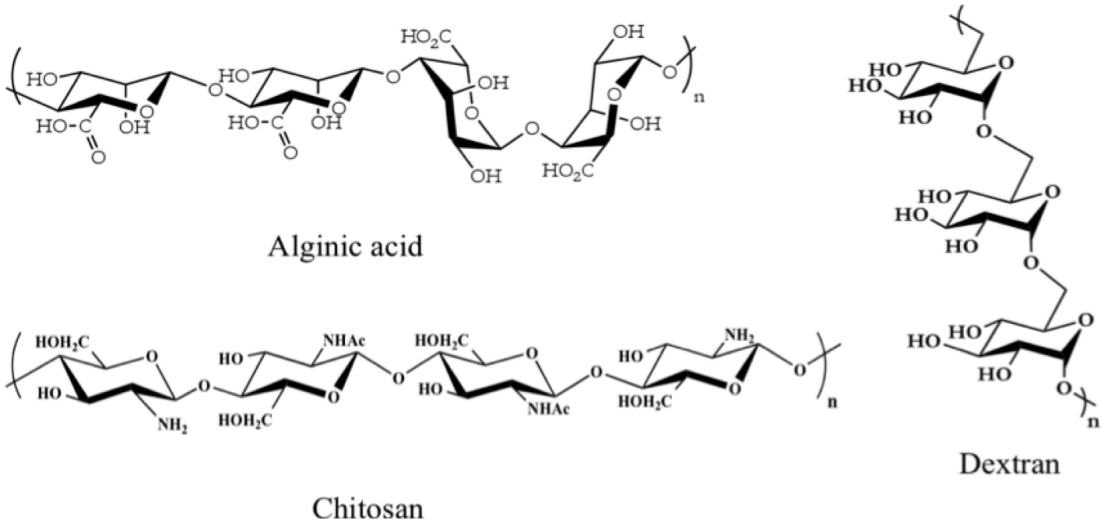

Figure 2.4 Chemical structures of polysaccharides that have been used to coat MNPs.

2.2.2.2 Liposomes

Liposomes are phospholipid bilayered vesicles with size ranging from 100 nm up to 5 um. They have been utilized for delivering small molecules, DNA, peptides, proteins, and contrast agents.[23] Liposomes can be utilized to stabilize MNPs in at least two ways including (1) post-synthesis incorporation, and (2) by synthesizing MNPs directly within their open core.[24-28] Liposomal coating provides MNPs with several advantages including simple surface modification, convenient encapsulation of drug molecules inside the amphiphilic substructures and delivery of drugs to the targeted site.[29] Recently, Martina et al. created magnetic fluid-loaded liposomes (MFLs) by encapsulating maghemite nanocrystals within unilamellar vesicles of egg phosphatidylcholine and 1,2-distearoyl-sn-glycero-3-phosphoethanolamine-N-[methoxy (poly(ethylene glycol))-2000] (DSPE-PEG2000).[30] MFLs with hydrodynamic sizes of 195 ± 33 nm were formed by film hydration coupled with sequential extrusion and were capable of encapsulating up to 1.67 moles of iron per mole of lipid. In vivo evaluation in mice using MR angiography demonstrated that these MFLs were still present in the blood 24 hours after intravenous injection confirming their long-circulating behavior.

2.2.2.3 PEO-containing copolymers

Copolymers exhibit unique properties due to the distinct functionalities derived from their constituents. The interesting properties that copolymers provide can be applied to MNP coatings. Many hydrophilic polymers, including polyacrylamide, poly(hydroxyethyl methacrylate), poly(*N*,*N*-dimethylacrylamide), poly(vinyl alcohol), poly(ethylene oxide) (PEO) have been copolymerized with several types of hydrophobic monomers. Among others, PEO has been most widely utilized due to its unique

properties. PEO has excellent solubility in water in a wide temperature range from room temperature to slightly below 100 °C.[31] It is also hydrophobic enough to dissolve in many organic solvents.[32] As an excellent solute, PEO has high surface mobility and the interfacial energy between PEO and water is very low. These attractive properties make PEO particularly effective at resisting protein adsorption.[33,34] In addition, PEO has low toxicity. It is FDA-approved for parenteral administration.[35] It was reported that 10% PEO solution (M_w=4000 g/mol) could be administered intravenously to rats, guinea pigs, rabbits, and monkeys up to 16 g/kg without any noticeable toxicity.[36]

2.2.2.3.1 PEO-polyester copolymers

Polyesters are widely used and studied as an important class of biodegradable polymers. These polymers include poly(ε-caprolactone) (PCL), poly(lactic acid) (PLA), poly(glycolic acid) (PGA) and their copolymers.[37,38] They can be non-specifically biodegraded into non-harmful small molecules in aqueous media. Metha et al. have developed water–dispersible magnetite nanoparticles stabilized with oleic acid primary surfactants and mPEG-PCL block copolymer secondary surfactant to form bilayer stabilizers having hydrophobic inner shells and hydrophilic cores.[39] The PCL segments were hypothesized to adsorb onto the particle surface coated with oleic acid and mPEG hydrophilic blocks extended to the carrier fluid to provide steric stabilization. The particles were about 9.0 nm in diameter and exhibited superparamagnetic behavior at room temperature with magnetization of 35 emu/g magnetite. Misara et al. reported the preparation of poly L-lactic acid (PLLA) based magnetite nanoparticles by using an emulsion evaporation technique.[40] The particle sizes were varied from 320 to 1500 nm. The particles showed superparamagnetic behavior with a saturation magnetization

increasing with the increased magnetite amount used in the formulation. In vitro MRI study showed that these particles had a good T2 relaxivity of 228 s^{-1} mM^{-1} rendering them practically useful as a negative contrast agent for MRI. Gao et al. have developed superparamagnetic polymeric micelles based on amphiphillic diblock copolymers of poly(caprolactone)-b-poly(ethylene glycol) (PCL-b-PEG) as a class of magnetic resonance imaging (MRI) probes with high spin-spin (T2) relaxivity and sensitivity.[41] It was hypothesized that the micelles consisted of a cluster of hydrophobic magnetite particles encapsulated inside the hydrophobic cores of polymeric micelles whose surface was stabilized by the PEG shell. The micelle sizes ranged from 75 to 110 nm. All micelle formulations had comparable r_2 values in the range of 169 to 471 Fe $mM^{-1}s^{-1}$, suggesting that these would be effective MRI contrast agents for T2-weighted imaging.

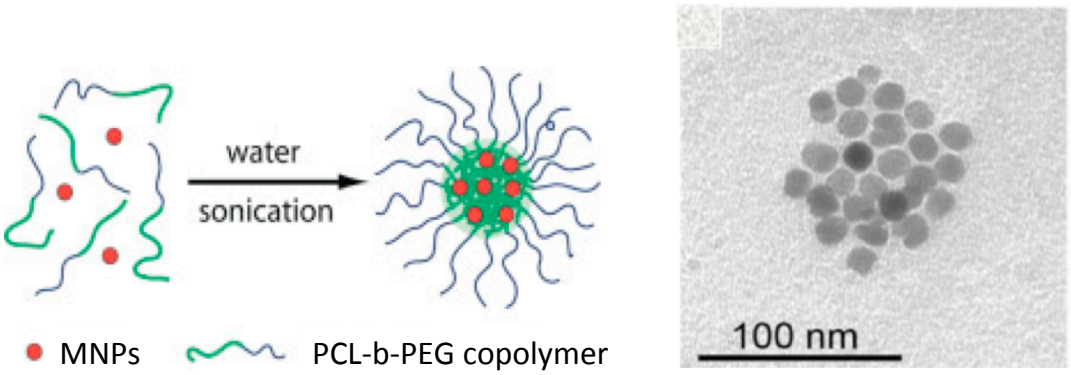

Figure 2.5 Formation of PCL-*b*-PEG coated MNPs.[41]

2.2.2.3.2 PEO-poly(amino acid) copolymers

Poly(aminoacid)s have excellent potential in drug delivery systems, especially copolymers based on PEO-*b*-poly(amino acid). An attractive feature of PEO-*b*-poly(amino acid)s is that functional groups, e.g., carboxyl groups, introduced by the poly(amino acid) blocks can be used to conjugate drugs chemically.

Pison et al. reported the formation of maghemite coated with poly(ethylene oxide)-*b*-poly(glutamic acid) (PEO-*b*-PGA) nanoparticles with the size of 60 nm.[42] The superparamagnetic maghemite core and the highly polyanionic coating enable *in vivo* detection by MRI. The nanoparticles were colloidally stable in water and physiological media for over six months and were well tolerated without acute or chronic toxicity in animal studies. Moreover, it was observed that the particles have long circulation time in the blood compartment after IV injection.

2.2.2.3.3 PEO-PPO-PEO triblock copolymers

Triblock copolymers based on poly(ethylene oxide-*b*-propylene oxide-*b*-ethylene oxide) (PEO-*b*-PPO-*b*-PEO) (e.g., Pluronics) are well established. These copolymers have been widely investigated as excipients in drug formulations. Wide ranges of molecular weights of Pluronics are commercially available. Above the critical micelle concentration (CMC), PEO-*b*-PPO-*b*-PEO can form spherical micelles in aqueous solution by self-assembly, with PEO blocks forming the shells and PPO blocks forming the core. Poorly water-soluble drugs might be encapsulated into the hydrophobic cores of PEO-*b*-PPO-*b*-PEO micelles and be stabilized by the PEO shells. This attractive feature makes PEO-*b*-PPO-*b*-PEO copolymers potential copolymers for drug delivery vehicles.

Recently, Pluronic F127 stabilized MNPs were created by Labhasetwa et al.[43] A water-insoluble anticancer therapeutic was loaded into the hydrophobic cores of these MNPs with high loading efficiency. The release rate of encapsulated drug was found to be significantly slower than that of free drug. The r_2 of MNPs coated F127 was higher than that of commercial contrast agent Feridex, suggesting better sensitivity in T_2 weighted MR imaging. Furthermore, they reported that the circulation time of the MNPs

coated F127 in carotid arteries in mice was longer than for Feridex IV. Therefore, they suggested that MNPs stabilized with F127 might be potentially used as effective contrast agent sand drug nanocarriers.

2.3 Application of MNPs for Magnetic Resonance Imaging (MRI)

MRI has been recognized as the most powerful tool for non-invasive clinical diagnosis. The technique is based on the property that protons align and precess around an applied magnetic field. Upon application of a transverse RF pulse, these protons are perturbed by the magnetic field. The subsequent process through which these protons return to their original state is referred to as the relaxation phenomenon, including longitudinal relaxation (T1) and transverse relaxation (T2).[44] The image contrast is generated from the differences in T1 and T2 relaxation times of the local protons, the proton density, and also the chemical and physical nature of the tissues within the specimen. However, the low sensitivity of MRI often diminishes diagnosis quality. Therefore, various types of contrast agents have been created and utilized to improve imaging quality.

Among the others, MNPs have been widely used as effective T2 contrast agents in MRI. MNPs provide MR contrast enhancement mostly by shortening the transverse relaxation times of surrounding protons upon accumulation in tissues. The T2 shortening process is caused by the large susceptibility difference between the MNPs and surrounding medium resulting in microscopic magnetic field gradients. Diffusion of protons through these field gradients results in dephasing of the proton magnetic moments and therefore shortening their transverse relaxation times.[45] Thus, MNPs are usually employed to provide negative contrast enhancement using T2-weighted pulse

sequences.

The relaxivities of MNPs are influenced by various factors such as particle size and coating material. The coordination chemistry of the ligand and the hydrophilicity of the coating layer are important influences on particle relaxivity. Daou et al. have reported that coating of MNPs with carboxylate ligands results in the spin canting and decreased net magnetization. In contrast, this effect was not observed with phosphonate ligand coated MNPs.[46] Additionally, polymer chain length, which corresponds to coating thickness, also has significant effects on relaxivity. LeConte et al. reported that increasing the outer hydrophilic PEG chain length led to a reduction in r_2 values.[47]

Over decades, many attempts have been made to prepare MNPs for use in MR imaging. Recently, Sun et al. have developed biocompatible MNPs comprised of PEG bounded with targeting peptide chlorotoxin (CTX) that was capable of targeting glioma tumors.[48] The nanoparticles with a core size of 10-15 nm were stable in physiological medium without aggregation for several months. It was suggested that PEG could improve the colloidal stability of the particles by reducing protein adsorption, non-specific macrophage uptake and prolonging serum half-life in vivo. In addition, PEG also provides amine terminal functional groups for the conjugation of CTX with MNPs through a three-step reaction, illustrated in Figure 2.6.

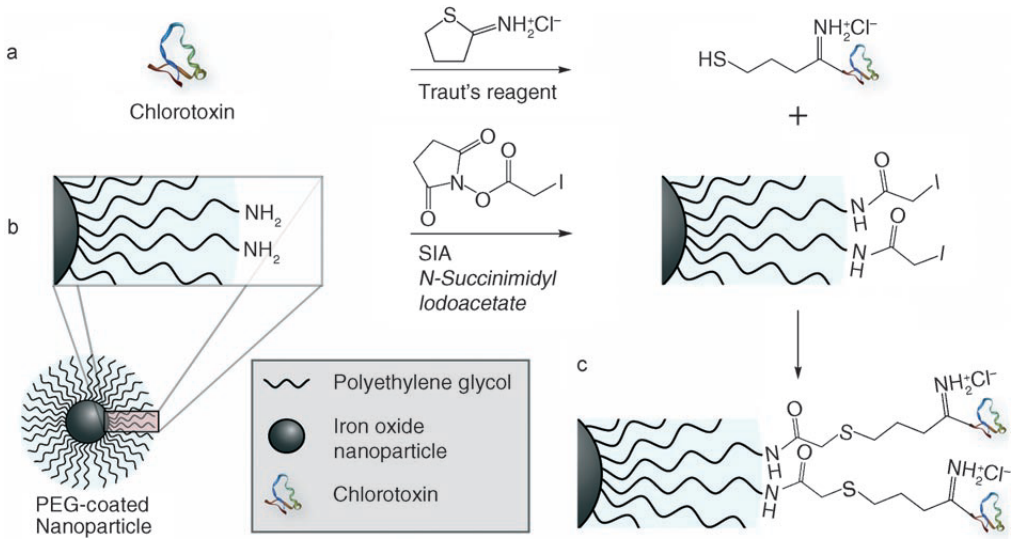

Figure 2.6 Conjugation of CTX with MNPs-PEG-NH_2 a) addition of a free sulfhydryl reactive group to CTX via Traut's Reagent, b) functionalization of MNPs-PEG-NH_2, with iodoacetate and c) formation of a thioether linkage between MNPs and CTX.[48]

The nanoparticles were preferably accumulated within glioma tumors of mouse model and subsequently generated MRI contrast enhancement. Histological analysis of selected tissues revealed that there were no acute toxic effects from these nanoparticles. They suggested that these nanoparticles could be used as a potential diagnostic agents and treatment of glioma tumors due to their high targeting specificity and benign biological response.

Another successful application of MNPs in MRI is specific cell tracking. MNPs coated with appropriate surface ligands can be effectively transported inside cells. Song et al. have developed a biocompatible magnetic nanocrystal probe for efficient intracellular labeling and in vivo MR tracking.[49] In their study, magnetite nanocrystals were prepared by thermal decomposition of $Fe(CO)_5$ and coated with hydrophobic

ligands (lauric acid). The nanoparticles were subsequently coated with either (3-carboxypropyl) trimethylammonium chloride (cationic ligand) or 2-carboxyethyl phosphonate (anionic ligand) (figure 2.7) creating a material having either cationic ammonium or anionic phosphonate groups to promote water solubility.

It was found that the cationic ligand-coated MNPs had much higher transfection efficiency into neural stem cells than both the anionic ligand coated MNPs and conventional poly-l-lysine-Feridex. They suggested that since cell membranes are weakly negatively charged, only cationic MNPs can easily anchor to cell membranes through electrostatic interactions and are internalized into cells by charge-mediated endocytosis pathway. This improved cellular transfection capability allows for the in vivo cellular MRI of stem cell trafficking, in which the longitudinal migration of stem cells is clearly observed in MR images as an elongated dark region along the spinal cord (Figure 2.8).

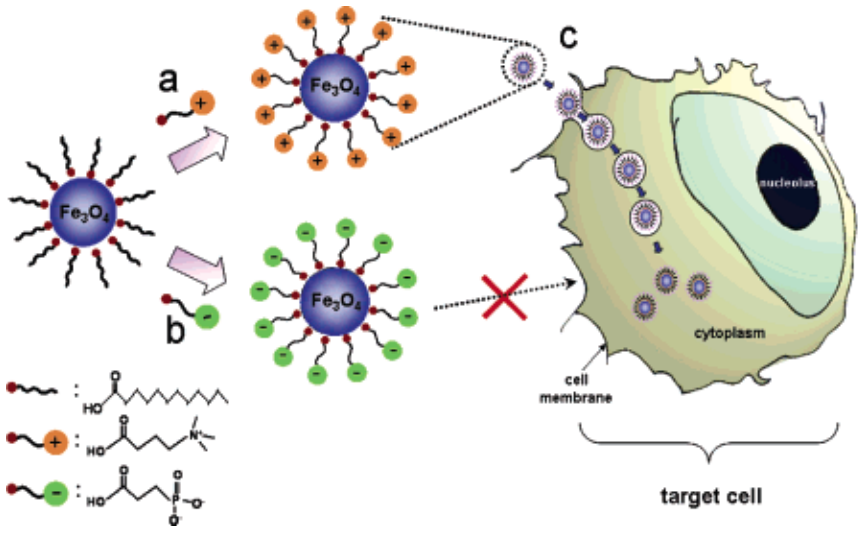

Figure 2.7 Illustration of surface exchange of magnetite nanocrystals with (a) cationic ligand (b) anionic ligand (c) their utilization for cell labeling application.[49]

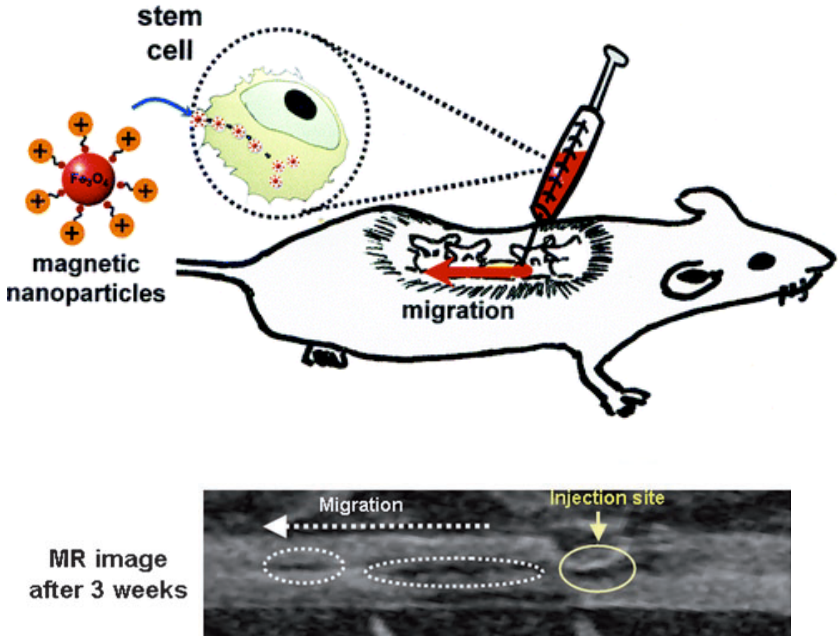

Figure 2.8 In vivo trafficking of cationic MNPs labeled neural stem cells (NSCs) introduced into the spinal cord of a mouse. [49]

2.4 Application of MNPs for Drug Delivery

Organic materials including polymeric nanoparticles, liposomes and micelles have been widely explored as drug nanocarriers (figure 2.9) using passive targeting, active targeting with a recognition moiety or active targeting by a physical stimulus. However, these purely organic systems present limited colloidal stability, swelling, susceptibility to microbiological attack, and burst drug release rate.[50-52]

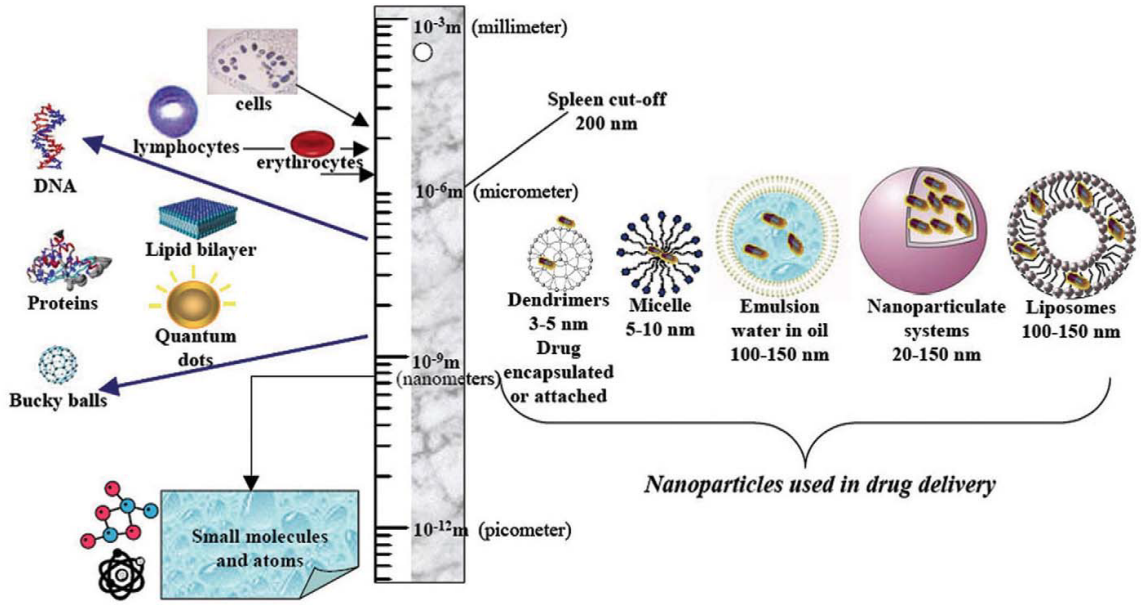

Figure 2.9 Various types of nanoparticle used in drug delivery [52]

Due to disadvantages of purely organic drug nanocarriers, inorganic nanocarriers MNPs comprise interesting options. The main advantages of MNPs are that they can be: (1) visualized; (2) guided or held in place by magnetic field; and (3) heat dissipators by exposing to the oscillating magnetic field for hyperthermia application. The behaviors of MNPs are correlated to coating material, size and magnetic properties. The coating material can prevent the MNPs from being cleared by the reticuloendothelial system (RES), thus increasing the circulation time in the blood compartment. Coating the MNPs with a neutral and hydrophilic compound such as polyethylene glycol was found to increase the blood circulation time of MNPs.[51, 52]

Several types of therapeutic drug have been incorporated into MNPs for potential treatment of various diseases. Drug loading capacities and their release behavior from MNPs can be tuned by controlling the interaction between drug molecules and MNPs.

Previously, Yang et al. prepared MNPs coated with poly(ethyl-2-cyanoacrylate)

(MNPs-PECA) by an interfacial polymerization method, producing the spherical nanoparticles with the size of 250 nm.[53] Anticancer drugs, cisplatin and gemcitabine, were separately loaded into the particles with drug loading capacities of 38 % and 9 % w/w respectively. The release rate of cisplatin was found to be slower than that of gemcitabine. (Figure 2.10) They explained the mechanism of drug release from MNPs-PECA is mainly a diffusion process from the oil core through the polymeric shell. Since the affinity of cisplatin for the oil phase was higher than that of gemcitabine, this results in more sustained release.

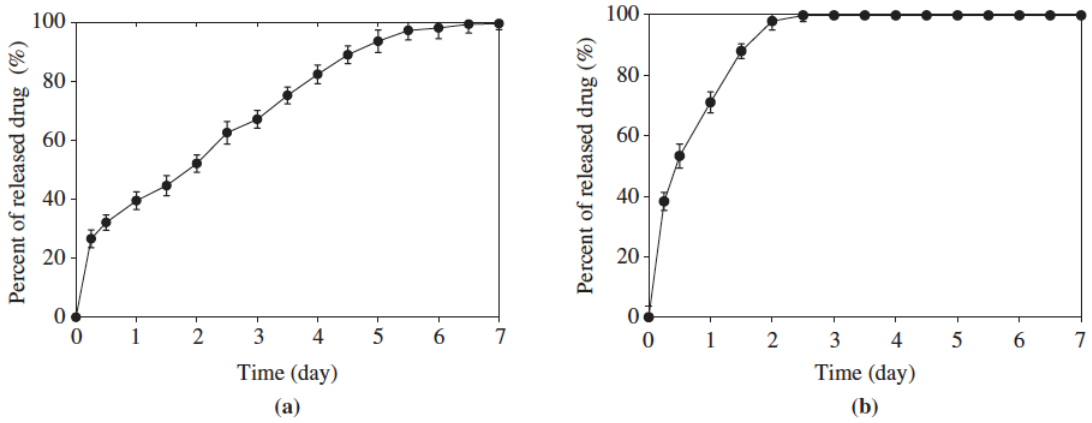

Figure 2.10 Release profiles of MNPs-PECA containing (a) Cisplatin and (b) Gemcitabine in phosphate buffer pH 7.4 at 37 °C. [53]

Kohler et al. have developed MNPs loaded with the antitumor drug methotrexate (MTX).[54] The MNPs were synthesized by using a co-precipitation technique, then were coated with(3-aminopropyl)-trimethoxysilane (APS). Consequently, MTX was linked to the MNP surface via amidation reaction. (Figure 2.11)

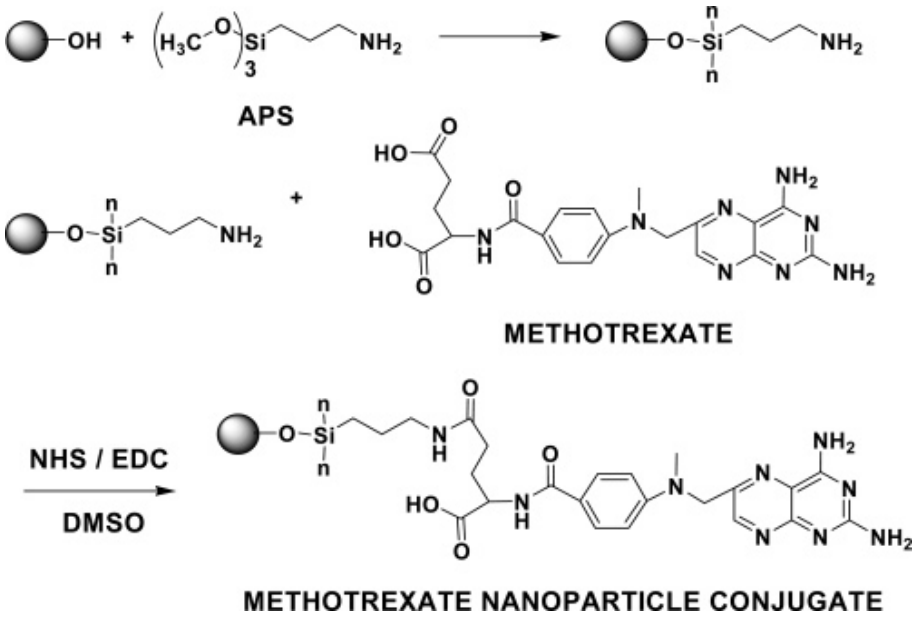

Figure 2.11 Surface modification of MNPs with MTX [54]

It was found that the cleavage and release of MTX only occurred in a low pH environment and through intracellular enzymatic degradation within human breast cancer cells or human cervical cancer cells. They concluded that covalently binding MTX onto nanoparticles could prevent the release of MTX until the nanoparticles reached the tumor cells and were cleaved by intracellular enzymes. Thus, this could minimize drug side effects to normal cells.

In addition, MNPs have also been utilized as nanocarriers for DNA or antisense RNA (siRNA) for therapeutic gene expression and silencing expression of defective gene.[55] MNPs coated with positively charged polymers such as PEI,[56] polyamidoamine,[57] or chitosan[58] were used to form complexes with negatively charged nucleic acids. Such complexes protect the nucleic acids from enzymatic degradation and assist endosomal release by inducing acidification of endosomal vesicles.[59,60]

Recently, Pan et al. developed a MNP coated polyamidoamine dendrimer

(PAMAM) to deliver antisense survivin oligodeoxynucleotide (asODN) to tumor cells.[61] They observed that the MNPs loaded with asODN were quickly taken up by tumor cells and exhibited cellular transfection and efficiently inhibited cell growth. These results indicated that MNP coated PAMAM might be a good candidate as a gene delivery nanocarrier and also for diagnostic molecular imaging.

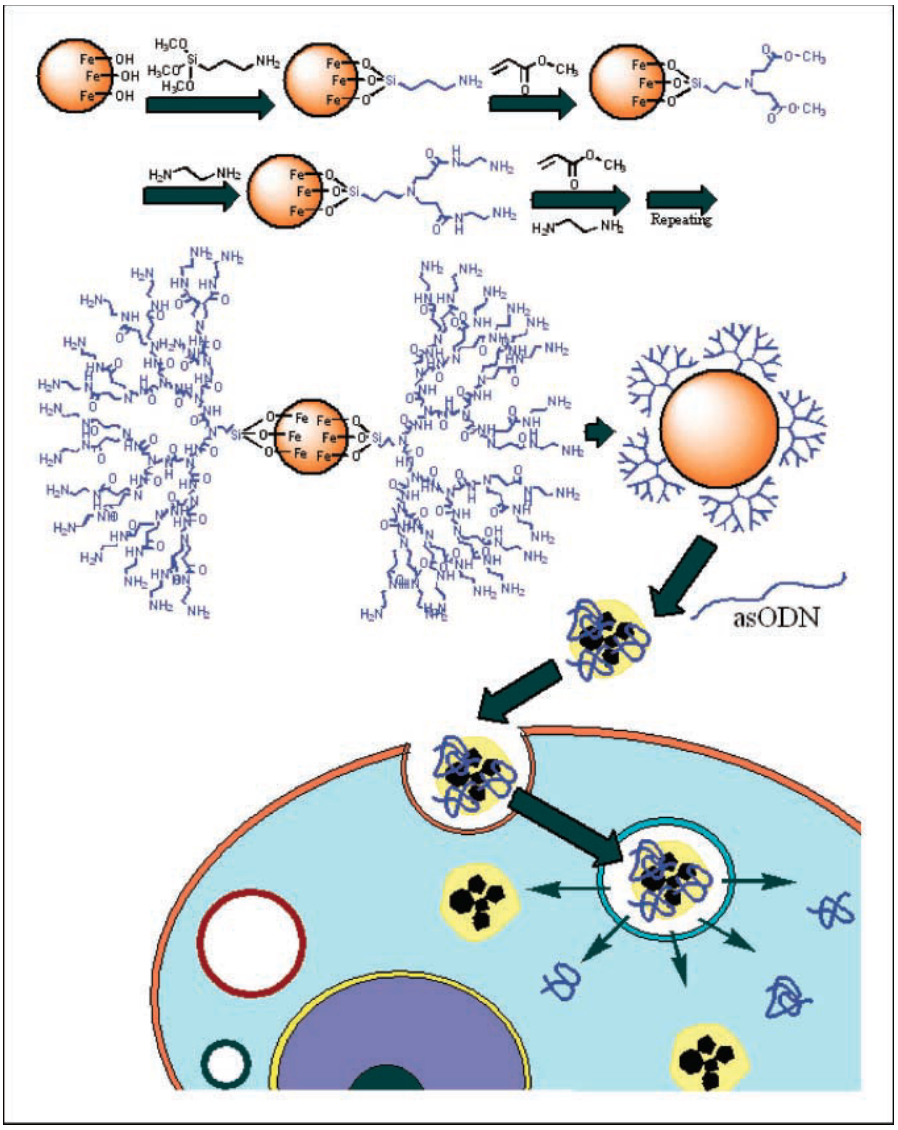

Figure 2.12 Modification of MNPs with PAMAM dendrimer and subsequent complexing with an asOD for nonviral gene transfection.[61]

2.5 Manganese based contrast agents (MnCAs)

The non-lanthanide metal manganese (Mn) is one of the paramagnetic materials that has been explored as contrast agent for T1-weighted MRI.[62,63] Manganese ions enhance MR imaging contrast by shortening the T1 of water protons, therefore increase the signal intensity and generate bright contrast signal in accumulated tissue in T1-weight MR images. Hence, these are normally called positive contrast agents. Manganese-based contrast agents can be divided into two broad classes including small molecule agents and macromolecular agents/nanoparticulates.[64-66]

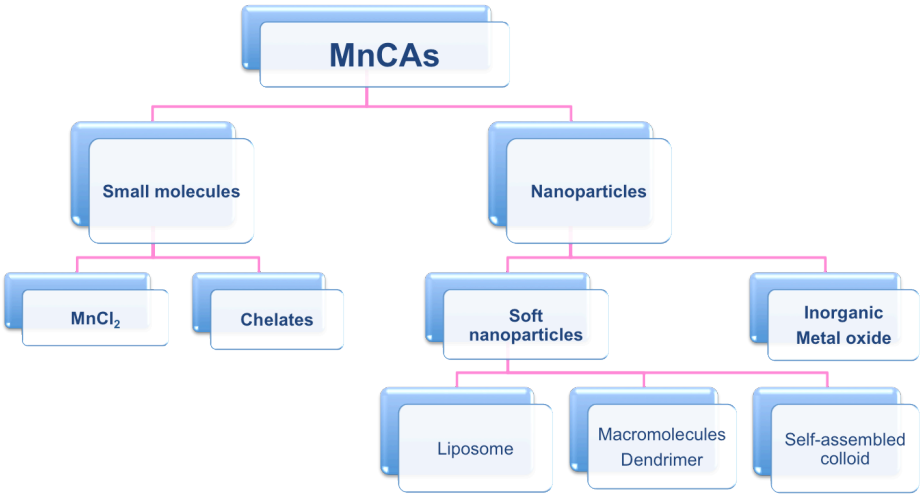

Figure 2.13 Manganese-based contrast agent families

2.5.1 Small molecule agents

2.5.1.1 Free ionic manganese ($MnCl_2$)

$MnCl_2$ was the first generation of a manganese based contrast agent. The r_1 value of $MnCl_2$ is 6.0 $mM^{-1}s^{-1}$ at 40 MHz, 40 °C.[67] Lumenhance® was the first $MnCl_2$-based contrast agent approved for medical use. However, a major disadvantage of using manganese in ionic form is its cellular toxicity. The aqueous manganese (II) was found to

cause neurotoxicity with an LD50 in mice of 0.3 mmol kg^{-1} injected via IV.[68-70] In addition, free manganese has a very short blood circulation time and therefore cannot be used as an effective MRI contrast agent.

2.5.1.2 Chelated manganese

Free manganese ions have been chelated with various types of small molecule ligands including polycarboxylic acid ligands (e.g., ethylenediaminetetraacetic acid) and porphyrins (e.g., sulfonatoporphyrins) (Figure 2.14) to decrease their cellular toxicity.[71-73] The only clinically approved chelated manganese is manganese (II) dipyridoxal diphosphate (Mn-DPDP) for liver imaging which has the r_1 value of 2.8 mM^{-1} s^{-1} and r_2 of 3.7 mM^{-1} s^{-1} at 1.0 T, 37 °C.[74]

Mn chelated phosphyrin complexes are also of great interest, not only because metallo-porphyrins are known to display selective retention in tumors, but also because they have high stability constants. Mn(III)TPPS4, where TPPS4 is the water-soluble tetraphenylsulfonylporphyrin, was one of the first Mn(III)porphyrin complexes tested for MRI. It has a greater effect on water relaxation time than $MnCl_2$ as a r_1 of 10.4 mm^{-1} s^{-1} was obtained at 20 MHz and 37 °C compared to 6.0 mm^{-1} s^{-1} for $MnCl_2$ under the same conditions. This high r_1 value led researchers to evaluate a wide range of Mn(III)–porphyrins as potential tumor specific MRI contrast agents.[72]

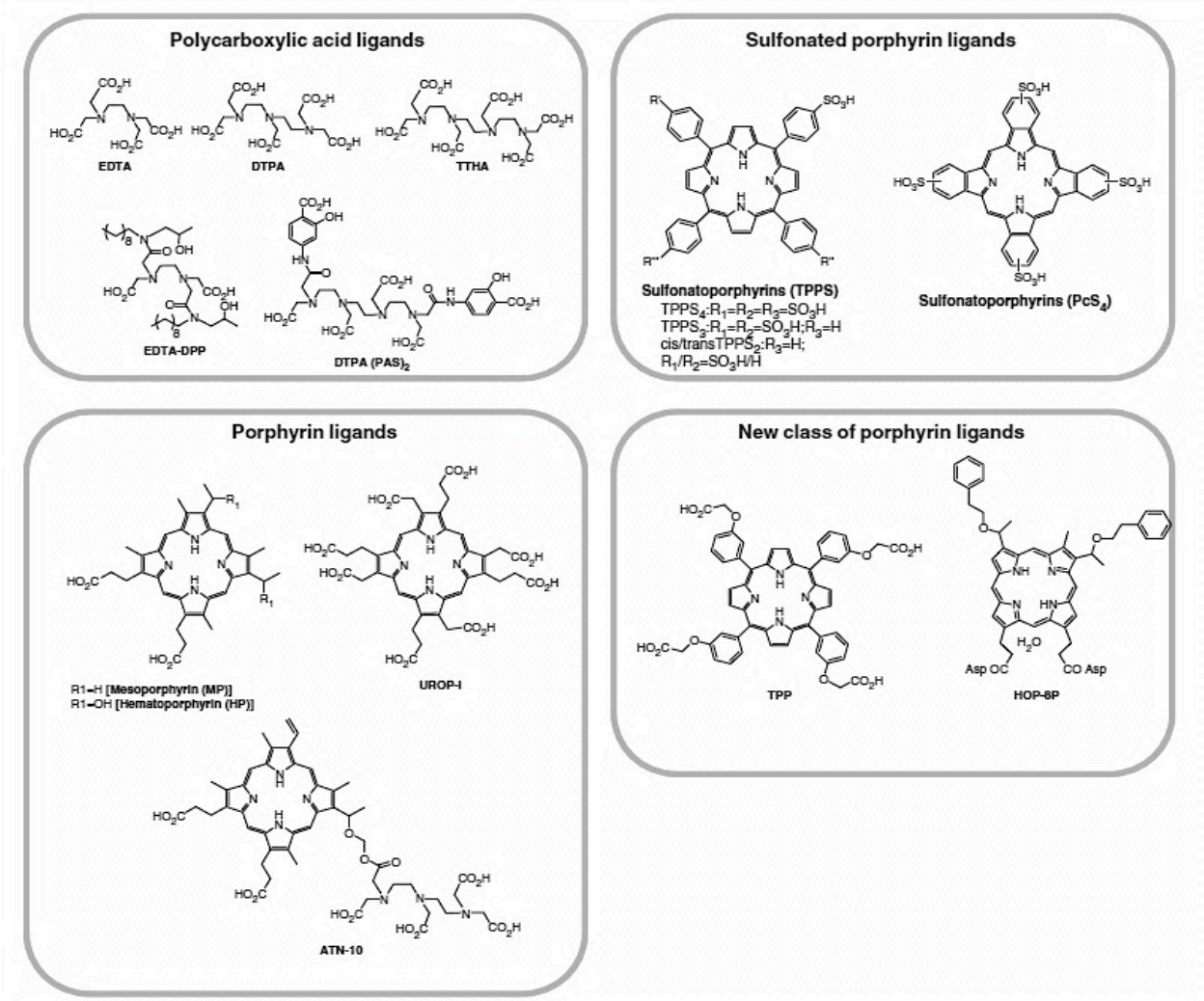

Figure 2.14 Examples of small molecule ligands used for chelation with Mn [73]

2.5.2 Macromolecular agents

2.5.2.1 Inorganic metal oxide

Among the most widely investigated, inorganic metal oxide nanoparticles such as MnO or Mn_3O_4 have been widely explored. (Figure 2.15) Many approaches have been established to synthesize manganese oxide nanoparticles. One common method is called thermal decomposition in which manganese oleate was heated in a high boiling solvent to promote nucleation and particle growth. This method allows the formation of nanoparticles with narrow size distribution.[75] However, one major drawback is the water

insolubility of these nanoparticles due to their high hydrophobicity. To overcome this issue, a surface modification with hydrophilic molecules is needed.

In order to alter the relaxation process of the water protons, *T1* contrast agents must directly interact with the water molecule. Therefore, for spherical Mn oxide nanoparticles, only Mn ions on the surface are efficient. The smaller size nanoparticles have larger surface areas and thus higher r_1 than the bigger nanoparticles.[75-77] Recently, various sizes of manganese oxide nanoparticles including 3, 5, 11 and 13 nm were prepared. It was reported that the smallest particles exhibited the highest r_1 (2.38 $mM^{-1}s^{-1}$).[75]

In addition to the size, the surface chemistry is also an important parameter. For example, Huang et al. reported the comparison of r_1 between dopamine-plus-human serum albumin (HSA) coated MnO nanoparticles and dopamine-plus-phospholipid coated MnO nanoparticles.[78] It was found that the dopamine/HSA coated particles exhibited five times higher r_1 than the dopamine/phospholipid-coated one. (Figure 2.16) It was suggested that HSA is more hydrophilic compared to the hydrophobic phospholipids therefore allows more efficient water interaction and results in the higher r_1.

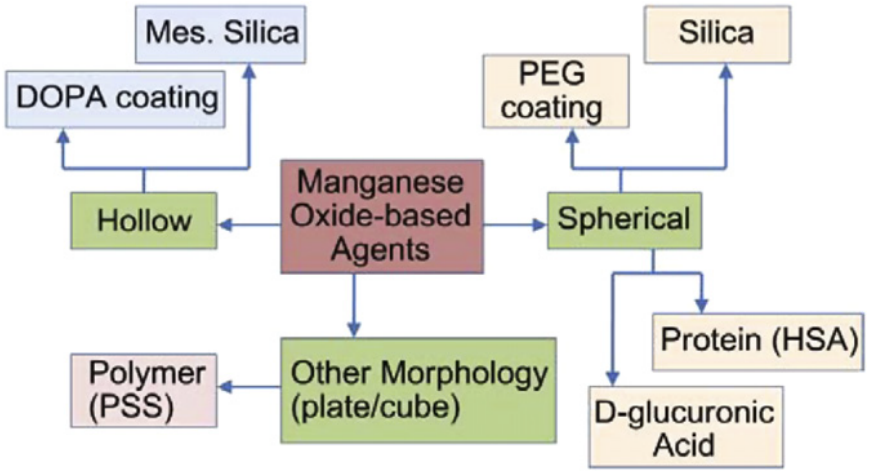

Figure 2.15 Example of manganese oxide based MRI contrast agents.[64]

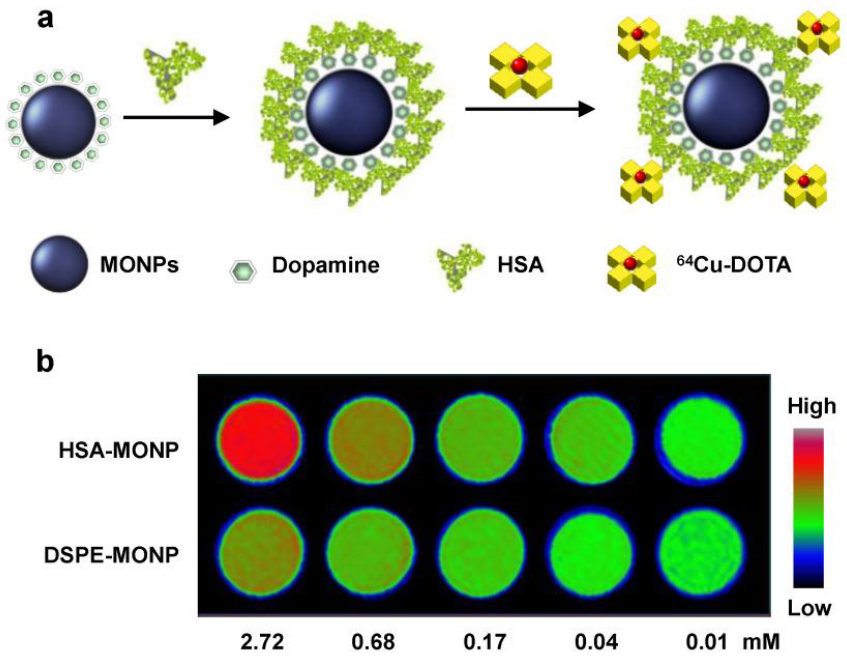

Figure 2.16 a) Surface modification of MnO nanoparticles with dopamine/HSA. b) Phantom image shows that HSA coated MnO nanoparticles (HSA-MONP) exhibited better contrast enhancement than the phospholipid coated one (DSPE-MONP).[78]

In addition, it has been reported by Lee et al. that the relaxivities of manganese oxide nanoparticles can be controlled by manipulation of their curvature. Three different types of manganese oxide nanoparticles (MONs) including spherical MONs coated oleic acid, spherical MONs coated PEG and hollow manganese oxide nanoparticles (HMONs) were prepared. It was found that HMONs showed the highest relaxivities and drug encapsulation efficiency. They suggested that HMONs have larger surface area compared to spherical MONs-oleic acid and MONs-PEG, thus leading to better water accessibility and larger binding sites for drug loading.[79]

2.5.2.2 Organic/Polymeric nanoparticles

In addition to inorganic metal and metal oxide, organic and polymeric Mn-based

nanoparticles also have been widely explored. These so-called 'soft particles' have shown excellent relaxivities and colloidal stability in physiological media. Rongved and Klaveness et al. were the first groups to report the formation of polymeric nanoparticles based manganese contrast agent.[80] In their first attempt, direct coupling of Mn^{2+} ions with polysaccharides without the use of any chelating agent led to unstable complexes. Thus, a chelating agent such as EDTA was used to link the polysaccharides to the manganese ion. Furthermore, Zhang et al. reported the formation of a dextran-Mn (III) porphyrin complex. The complex shown enhanced of r_1 relaxivity and lower toxicity compared to GdDTPA. In addition, the complex was able to selectively target tumors in vivo.[81]

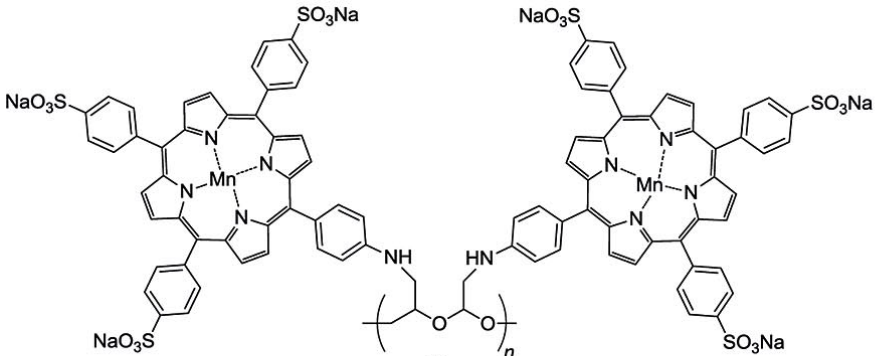

Figure 2.17 Modified dextran linked Mn(III) pophyrin complex[81]

Huang et al. covalently linked MnDTPA to chitosan oligosaccharides through an amide linkage[82] (figure 2.18) The complex showed higher relaxivity than that of GdDTPA and was stable in physiological media without the release of free Mn ions, thus preventing their toxicity side effect. These results suggested that the complex could be used as a promising MRI contrast agent.

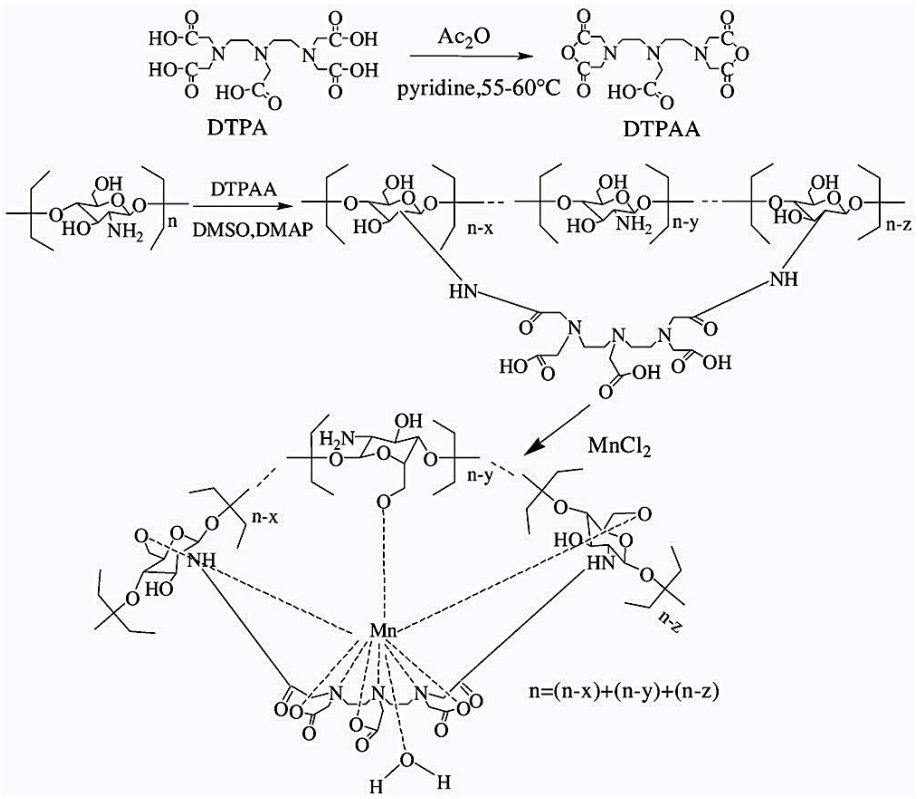

Figure 2.18 Synthesis of chitosan linked MnDTPA complex[82]

2.6 References

1) Lu, A.H.; Salabas, E.L.; Schuth, F. *Angew. Chem. Int. Ed.* **2007**, *46*, 1222.

2) Jolivert, J. P.; Chaneac, C.; Tronc, E. *Chem. Commun.* **2004**, *5*, 481.

3) Gupta, A.K.; Gupta, M. *Biomaterials* **2005,** *26*, 3995.

4) Calero-DdelC, V.; Rinaldi, C., *J. Magn. Mater.* **2007**, *314,* 60.

5) Sun, S.H.; Zeng, H. *J. Am. Chem. Soc.* **2002**, *124*, 8204.

6) Lee, J.H.; Huh, Y.M.; Jun, Y.; Seo, J.; Jang, J.; Song, H.T.; Kim, S.; Cho, E.J.; J. Cheon, J. *Nat. Med.* **2007,** *13*, 95.

7) Pinna, N.; Grancharov, S.; Beato, P.; Bonville, P.; Antonietti, M.; Niederberger, M. *Chem. Mater.* **2005**, *17*, 3044.

8) Laurent, S.; Forge, D.; Port, M.; Roch, A.; Muller, R.N. *Chem. Rev.* **2008**, *108*, 2064.

9) Omid Veiseh, Jonathan W. Gunn, Miqin Zhang *Adv. Drug Deliv. Rev.* **2010**, *62*, 284.

10) Duan, H.W.; Nie, S.M. *J. Phys. Chem.* **2008**, *112,* 8127.

11) LaConte, L.E.W.; Bao, G. *J. Magn. Res. Im.* **2007**, *26,* 1634.

12) P. Tartaj, M.P. Morales, S. Veintemillas-Verdaguer, T. Gonzalez-Carreno, C.J. Serna, *Elsevier*, **2006**, Amsterdam, Netherlands,.

13) Molday, R. S.; Mackenzie, D. J. *J. Immunol. Methods* **1982**, *52*, 353.

14) Cabuil, V. *Curr. Opin. Colloid Interface Sci.* **2000**, *5,* 44.

15) Fournier, C.; Leonard, M.; Le Coq-Lenard, I.; Delacherie, E. *Langmair* **1995,** *11*, 2344.

16) Kroll, E.; Winnik, F. M.; Ziolo, R. F., *Chem. Mater.* **1996**, *8*, 1594.

17) Nishio, Y.; Yamada, A.; Ezaki, K.; Miyashita, Y.; Furukawa, H.; Horie, K., *Polymer* **2004,** *45*, 7129.

18) Ma, H. L.; Qi, X. R.; Maitani, Y.; Nagai, T. *Int. J. Pharmaceut.* **2006.**

19) Kumar, M.; Domb, A.J. *Chem. Rev.* **2004**, *104*, 6017.

20) Jia, Z.; Yujun, W.; Yangcheng, L.; Jingyu, M.; Guangsheng, L. *Reac. Funct. Polym.* **2006,** *66*, 1552.

21) KIm, E. H.; Lee, H. S.; Kwak, B. K.; Kim, B. K., *J. Magn. Magn. Mater.* **2005,** *293*, 328.

22) Lee, H. S.; KIm, E. H.; Shao, H.; Kwak, B. K., *J. Magn. Magn. Mater.* **2005,** *293*, 102.

23) Torchilin, V. P. *Nat. Rev. Drug. Discov.* **2005,** *4*, 145.

24) Mornet, s.; Duguet, E. *J. Magn. Magn. Mater.* **2005,** *293,* 127.

25) Martina, M.S.; Lesieur, S.; *J. Am. Chem. Soc.* **2005**, *127*, 10676.

26) Bulte, J.W.M.; Frank, J.A. *J. Magn. Reson. Im.* **1999**, *9*, 329.

27) Decuyper, M.; Joniau, M. *Eur. Biophys. J. Biophy.* **1988,** *15***,** 311.

28) Yang, J.; Lee, C.H.; Haam, S. *Chem. Mater.* **2007,** *7,* 3870.

29) Mulder, W.J.M.; Nicolay, K. *NMR in Biomedicine* **2006**, *19*, 142.

30) Martina, M.S.; Lesieur, S. *J. Am. Chem. Soc.* **2005**, *127*, 10676.

31) Bailey, F. E.; Koleske, J. Y., *Eds.; Academic Press: New York,* **1976**.

32) Zhang, F.; Kang, E. T.; Neoh, K. G.; Huang, W. J. *Biomat. Sci-Polym.* **2001**, *12*, 515.

33) Wang, P.; Tan, K. L.; Kang, E. T. J. *Biomat. Sci-Polym.* **2000**, *11*, 169.

34) Lee, J. H.; Lee, H. B.; Andrade, J. D. *Prog. Polym. Sci.* **1995**, *20*, 1043.

35) Adams, M. L.; Lavasanifar, A.; Kwon, G. S. *J. Pharm. Sci.* **2003**, *92*, 1343.

36) Newman, P.K. *American Chemical Society* **1997.**

37) Peppas, L. B. *Int. J. Pham.* **1995**, *116*, 1.

38) Gan, Z.; Wu, C. *Macromolecule* **1999**, *32*, 590.

39) Meerod, S.; Rutnakornpituk, M. *Polymer* **2008**, *49*, 3950.

40) Hamoudeh, M.; Fessi, H. *Int. J. Pharm.* **2007**, *338*, 248.

41) Hua A.; Gao, J.; *Adv. Mater.* **2005**, *17*, 1949.

42) Kaufner, L.; Pison U. *Nanotechnology* **2007**.

43) Tapan K. J.; Vinod L. *Biomaterials* **2008,** *29*, 4012.

44) Mitchell, D. *MRI Principles*, Saunders, Philadelphia, PA**, 2004.**

45) Weissleder, R.; Papisov, M. *Adv. Drug. Deliv. Rev.* **1995**, *16*, 321.

46) Daou, T. J. *Chem. Mater.* **2008**, *18,* 5869.

47) LaConte, L. E. W. *J Magn Reson Imag* **2007**, *6*,1634.

48) Conroy S.; Omid V.; Jonathan G.; Miqin Z. *Small* **2008**, *3*, 372.

49) Song, H.T.; Cheon, J. *J. Am. Chem. Soc*. **2005**, *127*, 9992.

50) Arruebo, M. *Chem. Mater.* **2006**, *18,* 1911.

51) Fr.chet, J. M. J. *Prog. Polym. Sci.* **2005,** *30,* 844.

52) J. Santamaría *Nanotoday*, **2007**, *2*, 22.

53) Yang, J.; Haam, S. *J. Microencapsul.* **2006,** *23*, 203.

54) Kohler, N.; Sun, C.; Zhang, M.Q. *Langmuir* **2005**, *21,* 8858.

55) McBain, S.C.; Alton, E.; Dobson, J. *Nanotechnology* **2008**, *19*.

56) Park, I.K.; Zhang S.; Pun, S.H. *Biomaterials* **2008**, *29*, 724.

57) Pan, B.F.; Cui, D.X.; Huang, T. *Cancer Res.* **2007,** *67* 8156.

58) Bhattarai, S.R.; Kim, H.Y.; Hwang, P.H. *J. Virol. Methods.* **2008,** *147*, 213.

59) Huth, S.; Rosenecker, J. *J. Gene. Med.* **2004**, *6*, 923.

60) Petri-Fink, A.; Steitz, B.; Hofmann, H. *Eur. J. Pharm. Biopharm.* **2008**, *68*, 129.

61) Pan, B.F.; Cui, D.X.; Huang, T. *Cancer Res.* **2007,** *67*, 8156.

62) Lauterbur PC. *Sem. Nucl. Med.* **1983**, *13*, 364.

63) Wendland MF, *NMR Biomed* **2004**, *17*, 581.

64) G. M. Lanza et al., *Tetrahedron*, **2011**, *67*, 8431.

65) Pearson, T. C. J. et al., *Magn. Reson. Imaging* **2010**, *31*, 440.

66) Zipeng zhen and Jin xie, *Theranostics* **2012**, *2*, 45.

67) Bernardino, M. E. et al., *J. Magn. Reson. Imaging* **1994**, 4, 872.

68) Cuthbertson, E. M. et al., *J. Biol. Chem.* **1943**, *147*, 749.

69) Shin-o, T. et al., *Chem. Pharm. Bull.* **1983**, *31*, 2459.

70) Lo nnerdal, B. et al., *Acta. Pharmacol. Toxicol.* **1986**, *59*, 60.

71) Caravan, P. et al. *Inorg. Chem.* **2004**, *43*, 6313.

72) Buchler, J. W. et al.; *Academic: New York*, **1979**, *IA*, 389.

73) G. M. Lanza et al., *Advanced review* **2011**, *3*, 162.

74) Ferrucci, J. T. *Radiology* **1991**, *178*, 73.

75) Hyeon *Eur. J. Inorg. Chem.* **2012**, 2148.

76) Huang CC, Khu NH, Yeh CS. *Biomaterials* **2010**, *31*, 4073.

77) Baek MJ, Park JY, Xu W, Kattel K, Kim HG, Lee EJ *ACS Appl. Mater. Interfaces.* **2010**, *2*, 2949.

78) Huang J, Xie J, Chen K, Bu L, Lee S, Cheng Z *Chem. Commun. (Camb)* **2010**, *46*, 6684.

79) Shin, J.; Anisur, R. M.; Ko, M. K.; Im, G. H.; Lee, J. H.; Lee, I. S. *Angew. Chem., Int. Ed.* **2009**, *48*, 321.

80) P. Rongved, J. Klaveness *Carbohydr. Res.* **1991**, *214*, 315.

81) Z. Zhang, R. He, K. Yan, Q.-n. Guo, Y.-g. Lu, X.-x. Wang, H. lei, Z.-y. Li *Bioorg. Med. Chem. Lett.* **2009**, *19*, 6675.

82) Y. Huang, X. Zhang, Q. Zhang, X. Dai, J. Wu *Magn. Reson. Imaging*, **2011**, *29*, 554.

Chapter 3

Design and Synthesis of Magnetic Block Ionomer Complexes (*MBICs*) for Potential Dual Imaging and Therapeutic Agents

Adapted with permission from N. Pothayee, N. Pothayee, N. Jain, N. Hu, S. Balasubramaniam, L. M. Johnson, R. M. Davis, N. Sriranganathan and J. S. Riffle, *Chemistry of Materials*, 2012, 24, 2056-2063. DOI: 10.1021/cm3004062.

3.1 Introduction

Intracellular bacterial pathogens such as *Brucella, Salmonella* and *Listeria* have developed mechanisms to evade host defenses in phagocytic cells and they can establish persistent infections.[1] Brucellosis, caused by *Brucella spp.,* is the most common zoonotic disease worldwide. The pathogen can be transferred from infected animals to humans and also has the potential to be weaponized. It is, thus, categorized as a BioSafety Level-3 pathogen.[2] Prolonged treatment is required that often causes toxicity, yet relapse rates remain high.[1] These bacteria enter mononuclear phagocytes such as blood-borne monocytes, tissue macrophages, dendritic cells, and microglia and replicate in them.[3] Eradication is difficult since the bacteria reside within the phagocytic cells.[4-6] Recommended antibiotics for treating the disease include aminoglycosides that have multiple ammonium ions at physiological pH, but their polar, charged structures prevent them from transporting into the cells in sufficient concentrations to adequately treat the intracellular bacteria. Therefore, polymeric nanocarriers to enhance entry of aminoglycosides into the cells where they can reach the bacteria are desirable.

Multifunctional magnetite nanocarriers that also contain therapeutic agents are of great interest for delivering drugs and tracking their biodistribution via MRI.[7-13] The concept is challenging since the complexes containing the contrast agent can disperse broadly in vivo and sufficient concentrations of the agents must accumulate in close

proximity to provide good contrast. In this chapter, we introduce magnetic block ionomer complexes (MBICs) that combine the attributes of core-shell BICs containing electrostatically-bound drugs with magnetite nanoparticles designed for MR imaging. Our strategy is to co-encapsulate cationic aminoglycoside antibiotics and magnetite with anionic PEO-*b*-PAA block copolymers to form nanoscale MBICs (figure 3.1) that will be taken up by macrophage-like cells infected with pathogenic bacteria. Our hypothesis is that the phagocytic nature of the cells that contain these pathogens *in vivo* will recruit sufficient concentrations of the multifunctional drug carriers to provide MR contrast, so that the approach will afford a means to image biodistribution of the drugs. The capability for imaging the drug complexes will also minimize the need for repeated collection of blood, urine or feces to analyze for drug concentrations. This chapter describes the materials chemistry for assembling high concentrations of the cationic drug, gentamicin, and magnetite nanoparticles in MBICs and for controlling their dispersion in aqueous fluids through steric repulsion of nonionic PEO brushes. Uptake of the MBICs by macrophages was demonstrated by iron accumulation assays and flow cytometry analyses.

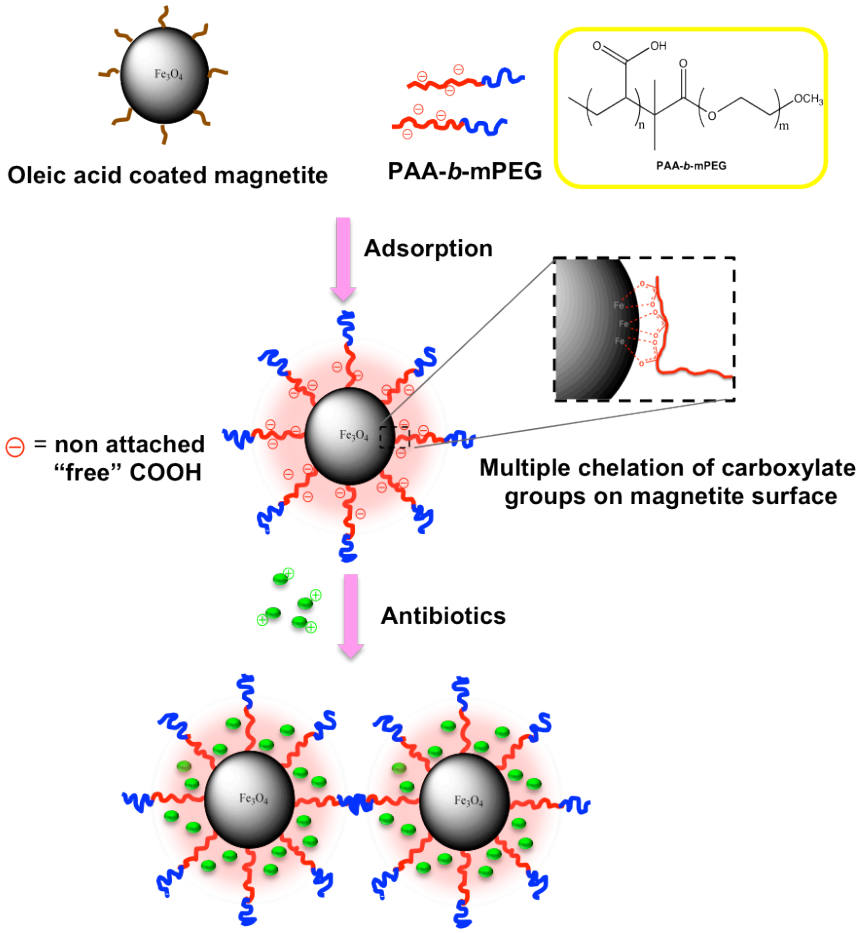

Figure 3.1 Synthesis of MBICs and subsequent drug loading via electrostatic interactions of complementary charged molecules

3.2 Experimental

3.2.1 Materials

Benzyl alcohol (>98%), diethyl ether, iron (III) acetylacetonate ($Fe(acac)_3$), oleic acid (90%, technical grade), triethylamine (>99.5%), pentamethyldiethylenetriamine (PMDETA), bromoisobutyryl bromide, and poly(ethylene oxide) monomethylether (mPEO) were purchased from Aldrich and used as received. 3-Hydroxypropyldimethylvinylsilane (3-HPMVS) and N-(*tert*-butoxycarbonyl)-2-amino-ethanethiol were synthesized by following a previously published procedure.[14] *tert*-Butyl

acrylate (tBA) was distilled from calcium hydride before polymerization. Tetrahydrofuran was dried over sodium using benzophenone as an indicator and was freshly distilled prior to use. Toluene (anhydrous), dichloromethane (HPLC grade), hexane (HPLC grade) and acetone were purchased from Fisher Scientific and used as received. Dialysis tubing was obtained from Spectra/Por. Phosphate buffered saline (PBS) was obtained from Mediatech Inc. (VA, USA). Fetal bovine serum (FBS) and DMEM were purchased from Sigma Aldrich.

3.2.2 Characterization

^{1}H NMR spectral analyses of compounds were performed using a Varian Unity 400 NMR or a Varian Inova 400 NMR operating at 399.97 MHz. An Alliance Waters 2690 Separations Module with a Viscotek T60A dual viscosity detector and laser refractometer equipped with a Waters HR 0.5 + HR 2 + HR 3 + HR 4 styragel column set was used for size exclusion chromatography (SEC) analyses. SEC data were collected in chloroform at 30 °C. Data were analyzed utilizing a Universal calibration made with polystyrene standards to obtain absolute molecular weights.

Thermogravimetric analyses (TGA) were carried out on the mPEO-*b*-PAA-magnetite nanoparticles using a TA Instruments TGA Q500 to determine the fraction of each complex that was comprised of magnetite. Each sample was first held at 110 ºC for 10 min to drive off any excess moisture. The sample (10-15 mg) was then equilibrated at 100 ºC and the temperature was ramped at 10 °C min^{-1} to 700 ºC in a nitrogen atmosphere. The mass remaining was recorded throughout the experiment. The mass remaining at 700 °C was taken as the fraction of magnetite in the complexes. The experiments were conducted in triplicate.

DLS measurements were conducted with a Malvern Zetasizer NanoZS particle analyzer (Malvern Instruments Ltd) at a wavelength of 633 nm from a 4.0 mW, solid-state He-Ne laser at a scattering angle of 173° and at 25 ± 0.1 ˚C. Intensity, volume and number average diameters were calculated with the Zetasizer Nano 4.2 software utilizing an algorithm based upon Mie theory that transforms time-varying intensities to particle diameters. For DLS analysis, the dialyzed complexes were dispersed in DI water at a concentration of 1.0 mg mL^{-1}, and the dispersion was sonicated for 1 min in a 75T VWR Ultrasonicator (120 W, 45 kHz), then filtered through a 1.0 μm, Teflon^{TM} filter directly into a polystyrene cuvette for analysis.

A 7T MPMS SQuID magnetometer (Quantum Design) was used to determine magnetic properties. Hysteresis loops were generated for the mPEO-*b*-PAA-magnetite nanoparticles at 300K. Inductively coupled plasma-atomic emission spectroscopy (ICP-AES) was performed with a SPECTRO ARCOS 165 ICP spectrometer (SPECTRO Analytical Instruments, Germany). The particles were digested to release free iron by reacting them with concentrated nitric acid at a concentration of 0.2 mg mL^{-1} for 5 days at 25 °C. They were diluted to 0.01 mg mL^{-1} with DI water prior to measurement.

Transmission electron microscopy was performed on a Philips EM-420 field emission gun TEM operating at an acceleration voltage of 100 kV. Samples were prepared by casting a drop of a dilute aqueous solution of the MBICs onto amorphous carbon-coated copper grids. Images were acquired at a magnification of 96,000X, corresponding to a resolution of 3.88 pixels nm^{-2}. The sizes of over 2000 particles from different regions of the grid were measured using Reindeer Graphics' Fovea Pro 4 plug-in

for Adobe Photoshop 7.0® and fitted using a log-normal distribution function to obtain the average radii of the nanoparticle cores.

3.2.3 Synthesis of a PEO-b-PAA block ionomer

mPEO (6.0 g, 3.0 x 10^{-3} mol) was dissolved in 50 mL of THF in a 100-mL round-bottom flask. Triethylamine (0.840 mL, 6.0 x 10^{-3} mol) was added to the mixture, and then 2-bromoisobutyryl bromide (0.740 mL, 6.0 x 10^{-3} mol) was added dropwise at room temperature. After 48 h, the reaction mixture was filtered and concentrated by rotary evaporation. mPEO-Br was dissolved in 100 mL of dichloromethane and washed twice with DI water. The polymer was isolated by precipitation into a large amount of hexane (~500 mL) twice and dried under vacuum at 40 °C.

mPEO-Br was used as a macroinitiator for polymerization of *t*-butyl acrylate by atom transfer free radical polymerization (ATRP). mPEO-Br (M_n 2,150 g mol^{-1}, 1.075 g, 5.0 x 10^{-4} mol), *t*-butyl acrylate (8.75 mL, 5.0 x 10^{-2} mol), and 9 mL of dry toluene were added into a 50-mL Schlenk flask. After degassing, 72 mg of cuprous bromide (CuBr, 5.0 x 10^{-4} mol) and 0.100 mL of PMDETA (5.0 x 10^{-4} mol) were added quickly under nitrogen. The reaction mixture was deoxygenated with 3 freeze-thaw cycles, and then heated at 80 ^{o}C for 12 h. After the polymerization, the catalyst was removed by filtering the reaction mixture through neutral alumina using dichloromethane as the eluent. The solvent was evaporated and the block copolymer was dried under vacuum at 50 ^{o}C overnight. The *t*-butyl ester groups were removed by dissolving mPEO-*b*-P*t*BA (2.0 g, 1.09 x 10^{-2} eq of *t*-butyl ester groups) in 50 mL of dichloromethane. Trifluoroacetic acid (5 mL, 6.50 x 10^{-2} mol) was added and the reaction mixture was stirred at room temperature for 24 h. The polymer was precipitated into hexane and dried under vacuum

at room temperature. The polymer was dissolved in THF and dialyzed against 4 L of DI water through a cellulose acetate membrane (MWCO 3,500 g mol^{-1}) for 24 h. The Mn was calculated to be 2K PEO-13K P*t*BA by ^{1}H NMR. The mPEO-*b*-PAA with PEO M_n of 2,000 g mol^{-1} and PAA M_n of 7,300 g mol^{-1} was recovered by freeze-drying.

3.2.4 Synthesis of tert-butoxycarbonylamine-functional PEO (tBoc-HN-PEO).

Ethylene oxide was initiated with 3-hydroxypropyldimethylvinylsilane (3-HPMVS). Ethylene oxide (14.6 g, 0.332 mol) was distilled from a lecture bottle into a 300-mL Parr reactor cooled with a 2-propanol-dry ice bath. An initiator and catalyst solution consisting of 3-HPMVS (1.08 g, 7.5 mmol), THF (10 mL), and a double metal zinc hexacyanocobaltate catalyst (13 mg) was prepared in a flame-dried, 50-mL round-bottom flask and stirred at 25 °C for 24 h. The initiator-catalyst solution was added to the Parr reactor via syringe. The cooling bath was removed, and the reaction mixture was heated to 90 °C. The reaction began after ~15 min as evidenced by an exotherm from 90 to 180 °C and a pressure increase from 110 to 280 psi. After the exotherm subsided, the temperature and the pressure dropped to 95 °C and 60 psi, then the reaction was stirred for an additional 12 h. The reactor was purged with N_2 for 1 h and then opened, and its contents were diluted with 100 mL of dichloromethane. The mixture was filtered through celite using dichloromethane as the eluent (2x) to remove the catalyst. The dichloromethane was evaporated and the dimethylvinylsilyl-functional PEO was dried at 50 °C under vacuum overnight. The M_n was calculated to be 2800 g mol^{-1} by ^{1}H NMR. *tBoc*-HN-PEO-OH was obtained via an ene-thiol addition of N-(*tert*-butoxycarbonyl)-2-amino-ethanethiol across the vinylsilane double bond. Dimethylvinylsilyl-functional PEO (2 g, 0.7 mmol), N-(*tert*-butoxycarbonyl)-2-amino-ethanethiol (0.43 g, 2.4 mmol) and

AIBN (98.5 mg, 0.6 mmol) were dissolved in deoxygenated DMF (7 mL) in a 100-mL round-bottom flask. The reaction was conducted at 80 °C for 24 h with stirring, then cooled to room temperature. Dichloromethane (70 mL) was added, and the mixture was washed with DI water (4x). The dichloromethane was evaporated and the *tBoc*-HN-PEO was dried at 50 °C under vacuum.

3.2.5 Synthesis of an amine-functional poly(ethylene oxide-b-acrylic acid) copolymer (H_2N-PEO-b-PAA) by ATRP

tBoc-NH-PEO was functionalized with bromoisobutyryl bromide, then the protected amine-functional polymer was used as a macroinitiator for preparing *tboc*-NH-PEO-*b*-P*t*BA using a similar procedure to that described for the mPEO-*b*-P*t*BA. Removal of the t-butyl ester groups and the *tboc* group was achieved by dissolving the *tboc*-NH-PEO-*b*-PtBA (2.0 g, 1.09 x 10^{-2} eq of *t*-butyl ester groups) in 50 mL of dichloromethane. Trifluoroacetic acid (5 mL, 6.50 x 10^{-2} mol) was added and the reaction was stirred at 25 °C for 24 h. The polymer was precipitated in hexane and dried under vacuum, then dissolved in THF and dialyzed against 4 L of DI water through a cellulose acetate membrane (MWCO 3,500 g mol^{-1}) for 24 h. The H_2N-PEO-*b*-PAA had a PEO M_n of ~3,500 g mol^{-1} and PAA M_n of ~6,800 g mol^{-1} as measured by ^1H NMR.

3.2.6 Reaction of H_2N-PEO-b-PAA with fluorescein isothiocyanate (FITC).

H_2N-PEO-*b*-PAA (0.4 g, 0.050 mmol), FITC (9.7 mg, 0.025 mmol) and DMF (2 mL) were added to an aluminum foil covered 20-mL vial equipped with a stir bar. The reaction was conducted at room temperature overnight under dark conditions.

3.2.7 Synthesis of magnetic iron oxide nanoparticles.

The nanoparticles were prepared using a procedure adapted from Pinna et al.[15] $Fe(acac)_3$ (2.14 g, 8.4 mmol) and benzyl alcohol (45 mL, 0.43 mol) were charged to a 250-mL, three-neck, round-bottom flask equipped with a water condenser and placed in a Belmont metal bath with an overhead stirrer with thermostatic (±1 °C) control. The solution was dehydrated at 110 °C for 1 h under a N_2 stream. The temperature was increased in 25 °C increments and held at each step temperature for 1 h, until it reached the reflux temperature of benzyl alcohol at 205 °C, then the temperature was maintained for 40 h. The reaction was cooled to room temperature and the particles were collected by centrifugation (4000 rpm, 30 min). The magnetite nanoparticles were washed 3 times with acetone (100 mL each), then were dispersed in chloroform (20 mL) containing oleic acid (0.3 g). The solvent was removed under vacuum at room temperature, and the oleic acid-stabilized magnetite nanoparticles were washed 3 times with acetone (50 mL each) to remove excess oleic acid. The particles were dried under vacuum overnight at room temperature and stored as a dispersion in chloroform at a concentration of 20 mg mL^{-1} prior to use.

3.2.8 Synthesis of magnetic block ionomer complexes (*MBICs*)

Ligand adsorption from a homogeneous organic solvent mixture was employed to assemble the block ionomers onto the nanomagnetite. A representative method for preparing a targeted composition of 66:34 % by weight polymer to magnetite is provided. Oleic acid-stabilized magnetite nanoparticles (50.0 mg) were dispersed in chloroform (10 mL) and charged to a 50-mL round-bottom flask. mPEO-*b*-PAA (100.0 mg) was dissolved in DMF (10 mL) and added dropwise to the dispersion. The mixture was

sonicated in a VWR 75T sonicator (120 W, 45 kHz) for 4 h under N_2, and then stirred at RT for 24 h. The nanoparticles were precipitated in hexanes (200 mL). A permanent magnet was utilized to collect the magnetite nanoparticles and free oleic acid was decanted with the supernatant. The particles were dried under vacuum overnight at room temperature, then dispersed in DI water (20 mL) with adjustment of the pH to ~ 7 with 1 N NaOH and sonicated for 30 min. The particles were dialyzed against DI water (1 L) for 24 h in a 25,000 g mol^{-1} MWCO dialysis bag to remove free polymer. The dispersion was filtered through a 0.2 μm Teflon™ filter to sterilize and to remove any aggregates. A black-brown solid product was obtained after freeze-drying.

3.2.9 Synthesis of magnetic block ionomer complexes (*MBICs*) labeled with fluorescein (*MBICs-FITC*)

Oleic acid-stabilized magnetite nanoparticles (50.0 mg) were dispersed in chloroform (5 mL) and charged to a 50-mL round-bottom flask. mPEO-*b*-PAA (50.0 mg) and FITC-labeled H_2N-PEO-*b*-PAA (50.0 mg) were dissolved in DMF (2.5 mL each) separately and were added to the dispersion. The mixture was sonicated in a VWR 75T sonicator (120 W, 45 kHz) for 4 h under N_2, and then stirred at room temperature for 24 h under dark conditions. The nanoparticles were precipitated in hexanes (100 mL). A permanent magnet was utilized to collect the magnetite nanoparticles and free oleic acid was decanted with the supernatant. The particles were dried under vacuum overnight at room temperature, then dispersed in DI water (10 mL) with adjustment of the pH to ~ 7 with 1 N NaOH and sonicated for 30 min. The particles were dialyzed against DI water (1 L) for 24 h in a 25,000 g mol^{-1} MWCO dialysis bag to remove free polymer and any free

FITC. The dispersion was filtered through a 0.2 μm Teflon™ filter to sterilize and to remove any aggregates. A black-brown solid product was obtained after freeze-drying.

3.2.10 Preparation of gentamicin loaded *MBICs*

mPEO-*b*-PAA coated magnetite (40 mg, 2.18 x 10^{-4} eq COOH) was weighed into a 20-mL glass vial. Gentamicin sulfate solution in 10 mM phosphate buffer pH 7.2 (45 mg gentamicin sulfate, 27 mg gentamicin, 5 mL) was added. The solution was sonicated for 5 min and transferred to a centrifugal filter unit equipped with a cellulose acetate membrane (MWCO of 10,000 $gmol^{-1}$). The free drug and salt solution were removed by centrifuging the dispersion at 3750 rpm for 1 h. This allowed the liquid to pass through the membrane into the bottom of the centrifugation unit, and the particles were collected on the membrane. They were removed from the membrane by re-dispersing them in a small amount of DI water (10 mL), and then the dispersion was freeze-dried to obtain gentamicin-loaded MBICs.

3.2.11 Quantification of gentamicin in the *MBICs*

The amount of encapsulated gentamicin in the *MBICs* was measured by releasing the drug from the complex in borate buffer (pH 9.7), then by derivatizing the released gentamicin with a phthalaldehyde-mercaptoethanol assay solution and reading the fluorescence intensity of the derivative at 450 nm as compared to a calibration curve. An MBIC complex (5 mg) was dissolved in borate buffer (10 mL), and the dispersion was diluted with borate buffer by a factor of 10. The diluted solution (0.5 mL) was added to a scintillation vial. Phthalaldehyde-mercaptoethanol assay solution (0.5 mL) was added, followed by 0.2 mL of isopropanol and 1.8 mL of borate buffer, and the mixture was reacted at 25 °C for 1 h. The fluorescence emission intensity was measured in a

fluorimeter (Biotek, USA) using an excitation wavelength of 340 nm and an emission wavelength of 450 nm.[16-17] All samples including a series of standard solutions of gentamicin were transferred into 48-well plates and the fluorescence emission was measured. The concentration of gentamicin was calculated from a standardized calibration curve.

3.2.12 Drug release from gentamicin-loaded *MBICs*

To determine the release of gentamicin from the MBICs in PBS, 10 mg of gentamicin-loaded MBICs (equivalent to 3.1 mg gentamicin) were dispersed in 2 mL of PBS and placed in a 3,500 MWCO dialysis cassette (Fisher Scientific). The cassette was placed in a 250-mL beaker and 150 mL of either phosphate buffer saline (pH 7.4) or acetate buffer saline (pH 4.5) as the receptor medium was added to the beaker. The beaker was covered with Parafilm and maintained at 37 °C in a temperature-controlled Environ shaker agitated at 50 RPM. Aliquots of 3 mL were taken from the receptor medium and placed in separate scintillation vials at each time point. Each time, 3 mL of fresh PBS was added to the beaker to retain constant volume. The gentamicin in each aliquot was derivatized with a phthalaldehyde-mercaptoethanol assay solution as described above and the fluorescence intensity was measured at 450 nm. The amount of free drug (the control) that passed through the dialysis membrane was compared to the drug released at each time point using a standardized curve.

3.2.13 Transverse Relaxivities

The proton transverse relaxation times (T_2) were measured on a Model mq-60 NMR Analyzer (Bruker Minispec) at a magnetic field strength of 1.4 T corresponding to a proton Larmor frequency of 60 MHz. T_2 was obtained from fitting a monoexponential

decay curve to signal data generated by a Carr-Purcell-Meiboom-Gill (CPMG) spin-echo pulse sequence with an echo spacing of 0.5 ms and a repetition time of 5 s. Samples were filtered through a 1 μm Teflon™ filter and 500 μL were transferred into a 7.5 mm NMR tube and measurements were made at 37.5 °C after equilibration for 15 min. The transverse relaxivity (r_2) was calculated from the least-square fit of the relaxation rate ($1/T_2$) as a function of iron concentration. Fe concentrations were determined by ICP-AES on the dispersions that were measured by ICP-AES so that the relaxivity data could be normalized by the iron concentration.

3.2.14 Intracellular uptake of *MBICs* and gentamicin-loaded MBICs by ICP-AES

Murine 744A.1 macrophages were seeded in a 96-well plate at a density of 1 x 10^5 cells/well. Dispersions (250 μL) of a series of concentrations ranging from 12.5-200 μg mL^{-1} of gentamicin-loaded MBICs or MBICs without drug in DMEM media were added and incubated with the cells for 24 h at 37 °C with 5 % CO_2 to allow the cells to take up the complexes. After incubation, the supernatant was discarded and the remaining cells were washed twice with PBS (without Ca^{2+} and Mg^{2+}) to remove any particles that had not been taken into the cells. Concentrated nitric acid (70% w/w, 0.3 mL) was added to each well and reacted at room temperature for 5 days to digest the cells and particles, then the contents of 3 wells (for each concentration of iron that had been incubated) were combined in a vial and DI water (9.1 mL) was added to each solution. The mean weight of the cells in each vial was 0.74 ± 0.07 mg. The amount of iron that accumulated inside the cells was quantified by ICP-AES by analyzing each solution in triplicate and compared to non-treated control cells. The amount of iron found in the control cells was below the detectable limit as measured by ICP-AES.

3.2.15 Intracellular uptake of gentamicin-loaded *MBICs-FITC* by flow cytometry

J774A.1 murine macrophage like cells were cultured in DMEM media containing 10% heat inactivated FBS at 37°C with 5% CO_2. The cultured macrophage cells were gently scraped, then seeded at 1×10^6 cells/well in 12-well tissue culture plates and incubated for 24 h to reach 90% cell confluency in the wells. The next day, the cells were washed twice with PBS, then 1 mL of fresh cell culture medium was added to each well. The gentamicin-loaded MBIC-FITC complexes were dispersed in cell culture medium over a range of concentrations from 0.5-2.0 mg mL^{-1}. One mL of a dispersion was added to the cells in each well to achieve a final concentration ranging from 0.25-1.0 mg mL^{-1}, and the cells and complexes were incubated for 2 h at 37 °C. The control for this experiment was a cell culture incubated with MBICs without any fluorescent tag. The supernatant was discarded and the remaining cells were washed twice with PBS (without Ca^{2+} and Mg^{2+}) to remove any particles that had not been taken up by the cells. After washing the cells, 1 mL of non-enzymatic cell dissociation solution (Cell stripper solution, CellGro,) was added to the cells, and the cells were collected from the wells using sterile transfer pipettes for flow cytometry analysis. The fluorescence intensities were analyzed by fluorescence-activated cell sorter flow cytometry (BD FACS Aria) with an excitation wavelength of 488 nm and a 530/30-nm emission filter. Five thousand single-cell events were counted to compute the mean fluorescence intensities of the cells from duplicate samples.

3.2.16 Intracellular uptake of gentamicin-loaded *MBICs-FITC* by Confocal microscopy

For confocal microscopic examination, 1 x 10^5 J774A.1 cells/well were seeded in 10 mm diameter microwells of 35 mm petri dishes (Mat-tek Corporation). The cells were incubated with 2 mL DMEM + 10% FBS for 24 hours. After 24 hours, the medium was removed, MBICs-FITC (25 μg/well) suspended in culture medium were then added to the cells and incubated for an hour at 37 °C and 5% CO_2. Cells incubated with medium alone were the negative controls. To study localization, an image-iT live lysosomal and nuclear labeling kit (Invitrogen) was used to stain the lysosome/endosome and nuclear compartments. The wells were examined under a 40x water-immersion objective on a Ziess LSM 520 META confocal microscope.

3.2.17 Bioactivity of gentamicin in *MBICs*

The Minimum Inhibitory Concentrations (MICs) and Minimum Bactericidal Concentrations (MBCs) of gentamicin-loaded MBICs, MBICs without drug, and free gentamicin were determined for *B. melitensis* 16M (stock culture) and *E. coli* (ATCC 25922) using a broth microdilution method. *B. melitensis* and *E. coli* were freshly grown in tryptic soy broth for 24-48 h at 37 °C, then the bacterial concentration was adjusted to 5 x 10^6 CFUs mL^{-1}. Stock solutions of the gentamicin-loaded MBICs and of free gentamicin were prepared by adding each to DI water at a concentration of 128 μg mL^{-1} of the drug. Likewise, a stock solution of empty MBICs (without drug) was prepared by adding the MBICs into DI water at the same weight composition used for the gentamicin-loaded MBICs. Each stock solution (100 μL each) was added to 100 μL of tryptic soy broth in the first line of wells of a 96-well plate. A series of double dilutions were made in the 96-well plate. Bacterial suspension (100 μL) was added to each well to obtain a bacterial concentration between 2.5-3 x 10^5 CFUs/well. The final gentamicin

concentration ranged from 32–0.015 μg mL^{-1}. Wells without drug were considered as positive controls while wells without bacterial suspension were designated as negative controls. All the treatment groups were tested in duplicate. The 96-well plate was incubated for 24-48 h at 37 °C in the presence of 5% CO_2. MIC was defined as the minimal concentration of treatment that showed no growth in the well. Furthermore, 50 μL of each suspension was removed from each well, plated on tryptic soy agar and incubated for 36-48 h at 37 °C with 5% CO_2. The concentration of drug that showed 99.9% killing of *Brucella* was considered as the MBC.

3.2.18 In vitro efficacy of nanostructures against an intracellular brucellosis model

Brucella melitensis 16M was routinely grown at 37 ^{0}C in tryptic soy broth (TSB) or on tryptic soy agar (TSA, Difco). Efficacies of the MBIC complexes compared to free drug against intracellular Brucella were tested in murine J774A.1 macrophages. The cells were seeded at a density of $5x10^6$ cells/well in a 24-well cell culture plate (Corning) 24-36 h prior to infection. At 90% confluency, the cells were infected with B. melitensis for 1 h at a multiplicity of infection of 100:1. After phagocytosis, the media was removed and fresh media containing 50 **μ**g mL-1 gentamicin was added and the cells were incubated for 45 min to kill the extracellular bacteria. Again, the media was removed and finally the infected cells were incubated with DMEM containing 10% FBS for 24 h to set up the infection model. At 24 h post-infection, the cells were washed twice with DMEM and 50 μL of either free drug or the MBIC complexes containing 50 **μ**g gentamicin, resuspended in DNAase and RNAase enzyme-free water, was added to the infected cells along with 2 mL DMEM+10% FBS and incubated further for 24 h. The media was

removed and the cells were washed twice with PBS. To determine the intracellular bacterial load, the cells were lysed using 250 μL of 0.1% Triton X-100™ and 10-fold serial dilutions of lysates were prepared and spread on TSA plates. Colony forming units (CFUs) were determined after incubating the plates for 48 h at 37 °C under 5% CO_2.

3.3 Results and Discussion

3.3.1 Synthesis of PEO-*b*-PAA

The block copolymers of PEO and PAA were synthesized via controlled radical polymerization (Atom Transfer Radical Polymerization, ATRP) through a method adapted from the literature.[18] Hydroxyl functional CH_3O-PEO-OH was capped with bromoisobutyryl bromide to yield *tert*-bromoalkane endgroups, then utilized to initiate the *tert*-butylacrylate for preparing the diblock copolymers. Proton NMR spectra provided the compositions of the copolymers (figure 3.2). If one utilizes the block lengths of the macroinitiators and the relative compositions of the final polymers, and assumes that no premature termination occurs, one would predict that the diblock would be a PEO (2000 M_n)-*b*-P*t*BA (13,100 M_n). The actual molecular weights derived from SEC, however, were slightly higher than these predicted sizes, and this might due to some coupling during the controlled free radical polymerizations (figure 3.3). The *tert*-butyl groups were then quantitatively removed yielding the mPEO-*b*-PAA copolymer with a PEO M_n of 2,000 g mol^{-1} and PAA M_n of 7,200 g mol^{-1} as measured by ^1H NMR.

Figure 3.2 ^{1}H NMR spectrum of mPEO-*b*-P*t*BA in $CDCl_3$ (top) and mPEO-*b*-PAA sodium salt in D_2O (bottom) showing the complete disappearance of the *tert*-butyl resonance at ~1.3 ppm after deprotection

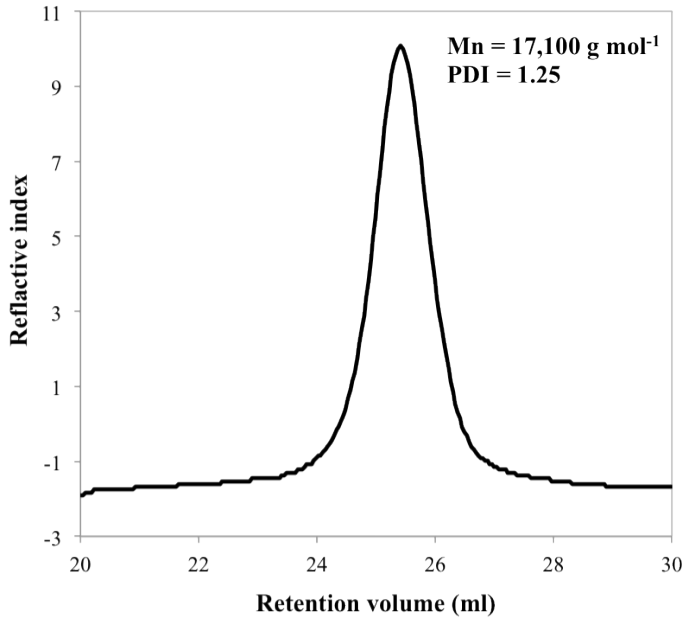

Figure 3.3 SEC analysis curve of mPEO-*b*-P*t*BA

3.3.2 Synthesis of H_2N-PEO-*b*-PAA

The H_2N-PEO-*b*-PAA block copolymers were synthesized through controlled radical polymerization of *t*-butyl acrylate initiated by a protected aminofunctional PEO macroinitiator (*tboc*-NH_2-PEO-Br). The *t*-butyl esters and the *tboc* protecting group on the amine terminus were subsequently removed to yield diblock H_2N-PEO-*b*-PAA copolymers with a PEO M_n of ~3,500 g mol^{-1} and PAA M_n of ~6,800 g mol^{-1} as measured by ^1H NMR (figure 3.4).

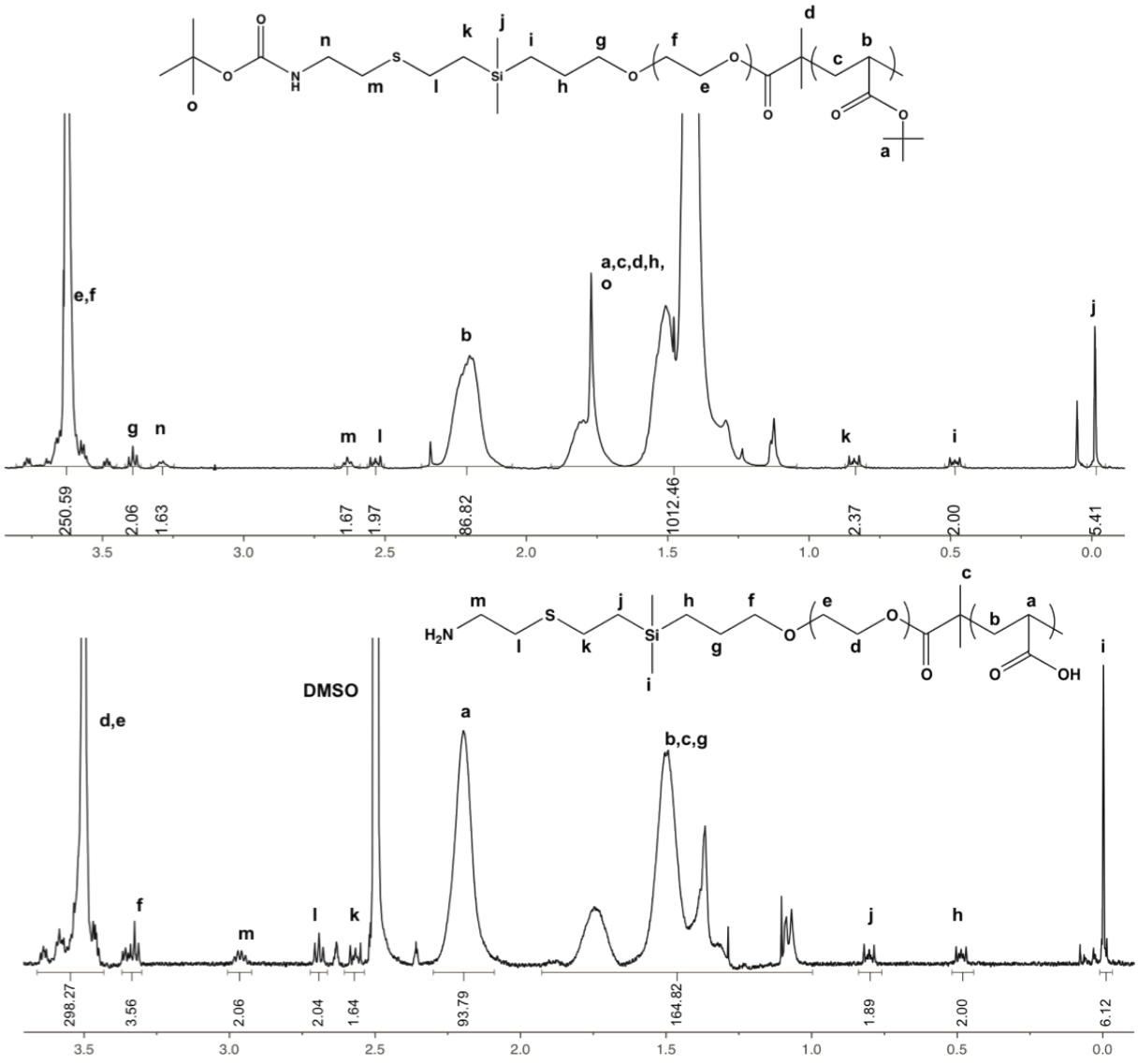

Figure 3.4 ^{1}H NMR spectrum of *tboc*-NH-PEO-*b*-P*t*BA in $CDCl_3$ (top) and NH_2-PEO-*b*-PAA in ^{6}D-DMSO (bottom)

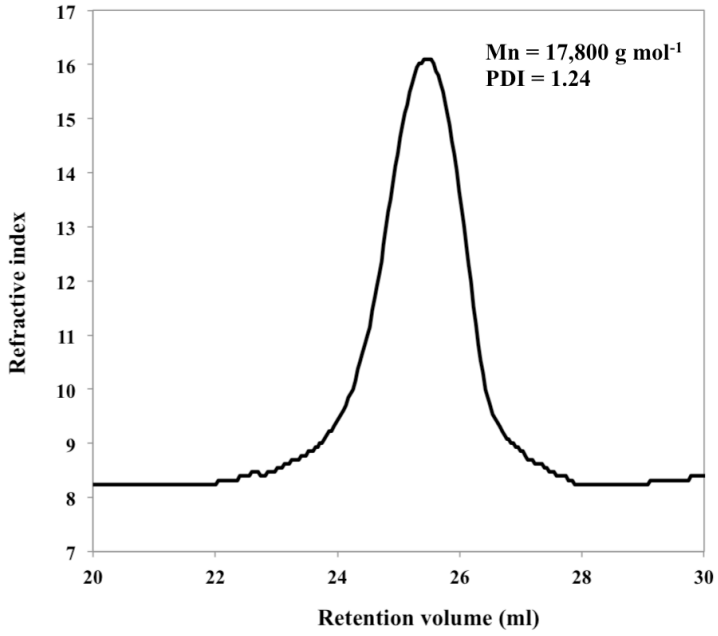

Figure 3.5 SEC analysis curve of *tboc*-NH-PEO-*b*-P*t*BA

3.3.3 Synthesis and characterization of *MBICs*

The MBICs were prepared using magnetite nanoparticles as substrates for mPEO-*b*-PAA and H_2N-PEO-*b*-PAA assembly through ligand adsorption of a portion of the carboxylates on the PAA block onto the nanoparticle surfaces. The copolymers were dissolved in DMF to provide a clear solution, and this was added dropwise into a magnetic particle dispersion in chloroform, then the mixture was sonicated and stirred at room temperature. This produced a stable colloidal dispersion of nanoparticles in the homogeneous DMF/chloroform solvent mixture. After purification, the polymer-magnetite complexes were recovered in high yields, usually exceeding 95 %.

The magnetic properties of the MBICs were characterized via SQuID analysis. Compositions of the MBICs were assessed by TGA and the example characterized with the SQuID data shown in figure 3.6 had 63 wt% polymer and 37 wt% magnetite. Hysteresis loops revealed that the complex was superparamagnetic at 300 K with a

saturation magnetization of ~54 $Am^2 kg^{-1}$.of magnetite (figure 3.6) which corresponds to ~75 $Am^2 kg^{-1}$ of Fe. It has been previously reported that the magnetization of iron oxide nanoparticles in this size range depends on particle size and the values reported herein are consistent with the mass magnetization values reported by others for similar sized Fe_3O_4 nanoparticles.[19] The magnetizations of maghemite nanoparticles also vary with size and are slightly lower than for magnetite.[20]

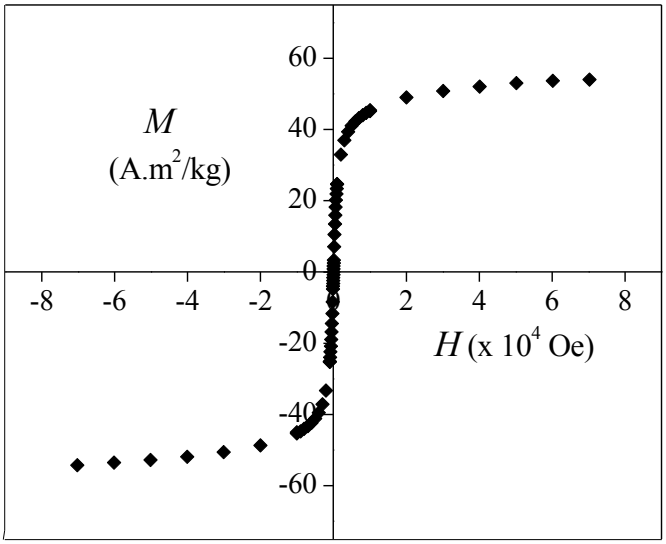

Figure 3.6 Hysteresis loop of MBICs at 300K

The nanoparticles were dispersible in water and aqueous buffers. TEM showed that the particles had relatively uniform sizes (figure 3.7) and suggested that they dispersed well. The average radius of the nanoparticles obtained by a log-normal fit to the measured particle sizes was 4.14 ± 1.5 nm. We have previously shown that weak ligands such as carboxylates can desorb from the surfaces of metals and metal oxides in aqueous

environments with high ionic strength through competitive binding from ligand-rich molecules such as phosphate ions,[14] but the polymeric nature of the PAA provided cooperative adsorption that led to excellent stability of the polymer on the magnetite.

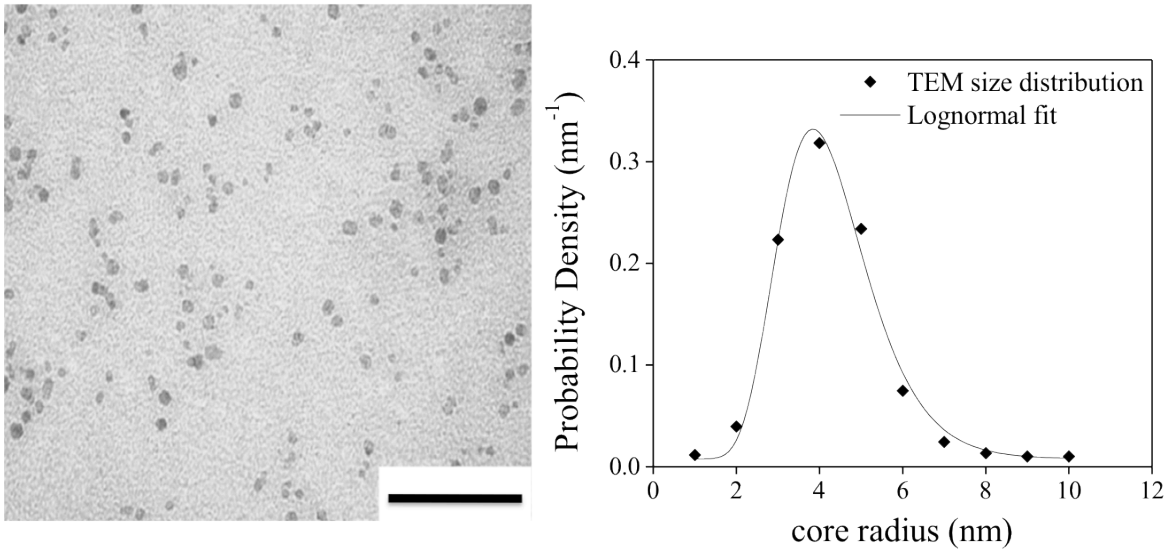

Figure 3.7 TEM image of MBICs cast from deionized water. Scale bar = 100 nm. The observed TEM particles sizes were described by a lognormal distribution function (continuous line) to yield an average radius of 4.14±1.52 nm.

To demonstrate that these nanostructures are potentialy suitable candidates for drug delivery vehicles, the stabilities of their sizes under simulated physiological condition was evaluated. Sizes of the MBICs remained constant in PBS containing 0.14 M NaCl for up to 10 days. This result clearly suggests that MBICs should be sufficiently stable under physiological conditions, and therefore suitable for use as a drug carrier.

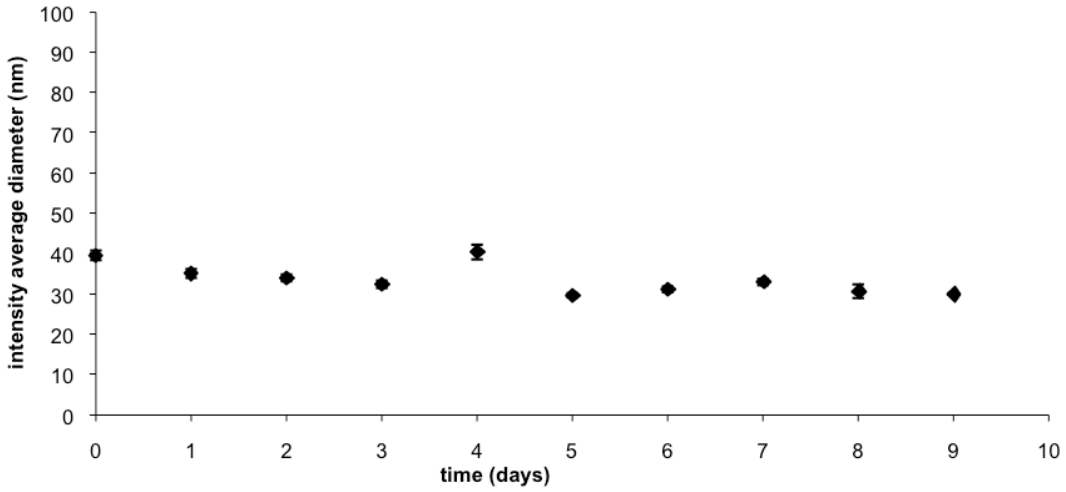

Figure 3.8 Stability of MBICs in PBS (0.14 M NaCl, pH 7.2)

3.3.4 Preparation and characterization of gentamicin-loaded nanostructures

Micellization of amphiphilic block copolymers with magnetite and drug molecules co-encapsulated in their cores has been previously explored.[22-23] The approaches, however, have been largely limited to relatively hydrophobic drugs in hydrophobic micelle cores. For example, Gao and co-workers described micelles comprised of PEO-*b*-poly(D,L-lactide) encapsulating doxorubicin and a cluster of magnetic nanoparticles by hydrophobic interactions, with a doxorubicin loading of 2.7%.[21] Yang et al. also reported doxorubicin- and magnetic nanoparticle-loaded micelles comprised of PEO-*b*-poly(lactide-*co*-glycolide) with a drug loading of 3.5%.[23]

Herein, we utilized a loading protocol where the model cationic drug gentamicin became entrapped through electrostatic interactions with carboxylate ions on the polymer by mixing the drug solution with the MBIC particles in phosphate buffer. Any drug that remained free was removed by centrifuging the dispersion through a membrane. The amount of gentamicin in the complexes was analyzed by releasing it from the complex,

derivatizing the aminoglycoside primary amines with phthalaldehyde and mercaptoethanol, then assaying the fluorescence intensity of the derivative.[17] Normally, this assay is conducted by measuring the absorbance of a solution of the derivative at 340 nm.[24] In this system, however, the magnetite absorbs radiation significantly at this wavelength. Thus, a fluorimetric assay was used to avoid interference from the magnetite. The derivatives were excited at 340 nm and the fluorescence intensities were measured at 450 nm and compared to a calibration curve.

The amount of charged gentamicin was based on a 1:1 equivalence ratio of cations to anions assuming all of the anions were free to complex with the drug (i.e., by assuming none of the anions were used up by assembly on the magnetite). After purification of the complexes, the assay showed that 78% of the charged concentration of gentamicin was encapsulated in the MBICs. This corresponded to a marked high gentamicin content of ~ 31 weight percent. Such high drug capacities are potentially advantageous clinically since a high payload can reduce the total required dosage of pharmaceutical formulations required for treatment.

The primary average particle radius of the magnetite, derived from the TEM images, was 4.14 ± 1.5 nm and upon adsorption of 67 weight percent polymer, DLS showed that the intensity weighted hydrodynamic diameter of the MBICs was 34 nm. The physicochemical properties of the MBICs were significantly altered upon gentamicin encapsulation (table 3.1). The hydrodynamic diameters of the particles increased from 34 to 62 nm. This could be partially attributed to formation of small clusters due to gentamicin acting as a bridging agent between particles. Moreover, the zeta potentials of the gentamicin-loaded MBICs dramatically decreased from ~ -40 to ~ -10 mV, indicating

that the cationic gentamicin had effectively neutralized negative charges on the polyacrylate component of the MBICs within the cores of the complexes. It is believed that the reduction in available negative charge on the polyacrylate chains due to complexation with the cationic drug led to reduction in electrostatic repulsion and that this may also have contributed to the formation of small aggregates. These results are clearly consistent with gentamicin being successfully loaded into the MBICs.

Particles	Intensity average diameter (nm)	PDI	Zeta potential (mV)
MBICs	34 ± 1	0.20	-39 ± 10
Gentamicin-loaded MBICs	62 ± 4	0.18	-13 ± 7
MBICs-FITC	35 ± 1	0.20	-40 ± 6
Gentamicin-loaded MBICs-FITC	153 ± 3	0.16	-15 ± 4

Table 3.1 Physicochemical properties of MBICs and gentamicin-loaded MBICs

3.3.5 NMR Relaxivities of *MBICs* and gentamicin loaded *MBICs*

The iron oxide nanoparticles led to a microscopic susceptibility effect, whereby the magnetization induced in the particles accelerates dephasing of the diffusing water protons, causing a reduction in the transverse relaxation times (increase in the relaxation rates). The degree of contrast brought about by the particles in T_2-weighted MRI is characterized by the transverse relaxivity – the relaxation rate enhancement per millimolar Fe. The unloaded complexes (no drug) had a transverse relaxivity of 81.9 s^{-}

^{1}(mM Fe)$^{-1}$, which is higher than that reported for commercial T_2 contrast agents such as Ferridex® (r_2 = 41 s^{-1}(mM Fe)$^{-1}$ at 37 °C and 1.5 T) (figure 3.9).[25] The increase in size of the complexes upon gentamicin encapsulation was accompanied by an increase in r_2 to 160.5 s^{-1}(mM Fe)$^{-1}$. The increase in r_2 with formation of small aggregates is consistent with recent findings in our group that controlled aggregation leads to considerably shorter T_2 relaxation times or higher r_2 relaxivities.[26]

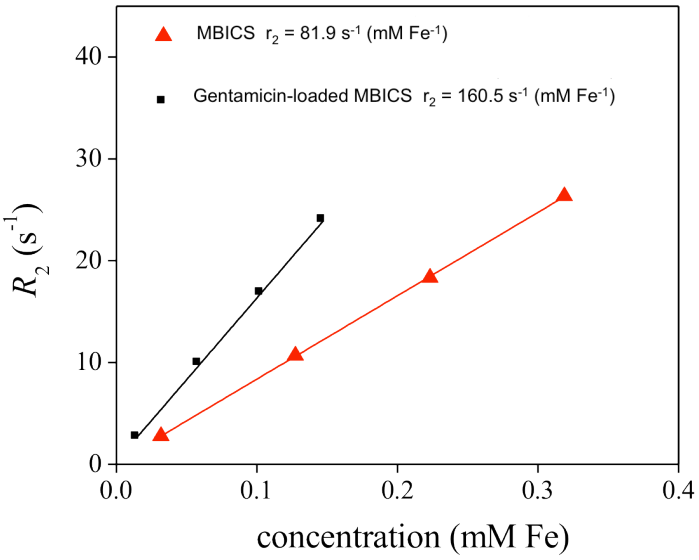

Figure 3.9 Transverse relaxation rates of the MBICs with and without gentamicin as a function of iron concentration

3.3.6 Gentamicin release behavior from gentamicin-loaded *MBICs*

Release studies of gentamicin from the magnetic nanoparticles were performed at pH 7.4 and 4.5 to simulate blood pH and intracellular pH conditions respectively. Either free gentamicin or gentamicin-loaded MBICs were dispersed in PBS and placed in a dialysis cassette. The cassettes were fully submerged in a beaker containing a 75-fold

volume of receptor medium to establish sink conditions. The release of gentamicin into the receptor medium was measured at respective time points. The free drug control fully diffused through the membrane into the receptor medium within five hours. Release of the gentamicin from the MBICs was sustained significantly longer. Approximately 35 wt% of the encapsulated gentamicin was released within 10 hours, then an additional 7% was released by 18 hours (figure 3.10). This second phase of the release behavior was slower. This was rationalized in that as cationic drug molecules were released, the ratio between negative and positive charge continued to increase. This may contribute to the slower release rate that was observed at later time points.

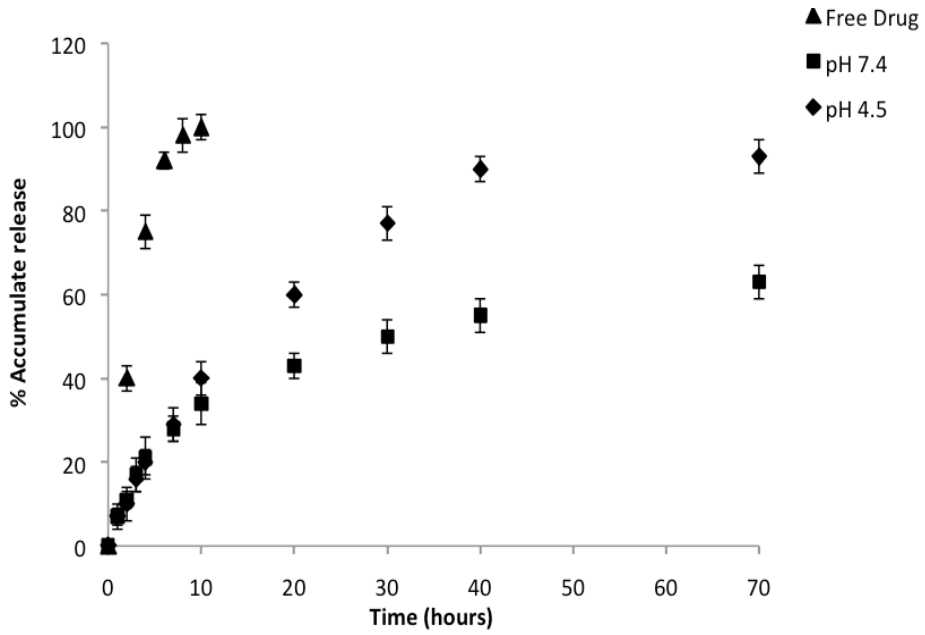

Figure 3.10 Release profiles of gentamicin from MBICs at pH 7.4 in PBS (squares) and at pH 4.5 in acetate buffered saline (diamonds) at 37 $^{\circ}$C

It is important to note that corresponding complexes between mPEO-*b*-PAA and gentamicin (without magnetite nanoparticles) instantaneously dissociate in saline buffer.[27] When the copolymer was adsorbed onto the magnetite nanoparticles, subsequent

complexation with gentamicin resulted in stable complexes that could withstand media with physiological ionic strength. The solid inorganic core of iron oxide particles serves as a multifunctional substrate for block ionomers to stably adsorb, and it acts as a pseudo-crosslinking site in the complexes, thus enhancing stability. The significantly improved stability of the complexes combined with sustained drug release may play a vital role in the efficacies of the complexes in animal models where delivery vehicles must avoid disintegration before reaching target sites and cells.

Release behavior of gentamicin from the MBICs was pH-dependent (figure 3.10). At pH 4.5, some of the carboxylate groups were protonated and this led to less electrostatic interaction with drug molecules. Thus faster release of gentamicin at pH 4.5 relative to pH 7.4 occurs.

3.3.7 Intracellular uptake of gentamicin-loaded MBICs

To investigate the amount of iron that accumulates inside the cells, the MBICs, with and without the drug, were incubated with macrophage cells for 24 hours, and iron uptake was measured by elemental analysis (ICP-AES). After incubation, the magnetic nanoparticles that were not taken up remained colloidally stable in the medium and were removed by washing with PBS. Figure 3.11 depicts the amount of iron taken up by the cells relative to the amount of charged iron. The concentrations of the complexes that were incubated with the cells in this experiment (with 31 weight percent of the drug versus without the drug) were based on iron content, so the concentrations of complexes that contained the drug were higher overall for each iron concentration than those without drug. Significant uptake of both types of complexes over all of the concentrations investigated was observed, thus revealing active endocytosis of the nanoparticles by the

cells. Under the conditions of the experiment, there were no discernible differences between the amount of iron taken up from the MBICs relative to the MBICs that were loaded with gentamicin. Details regarding the mechanism of uptake are not clear at this stage of the work.

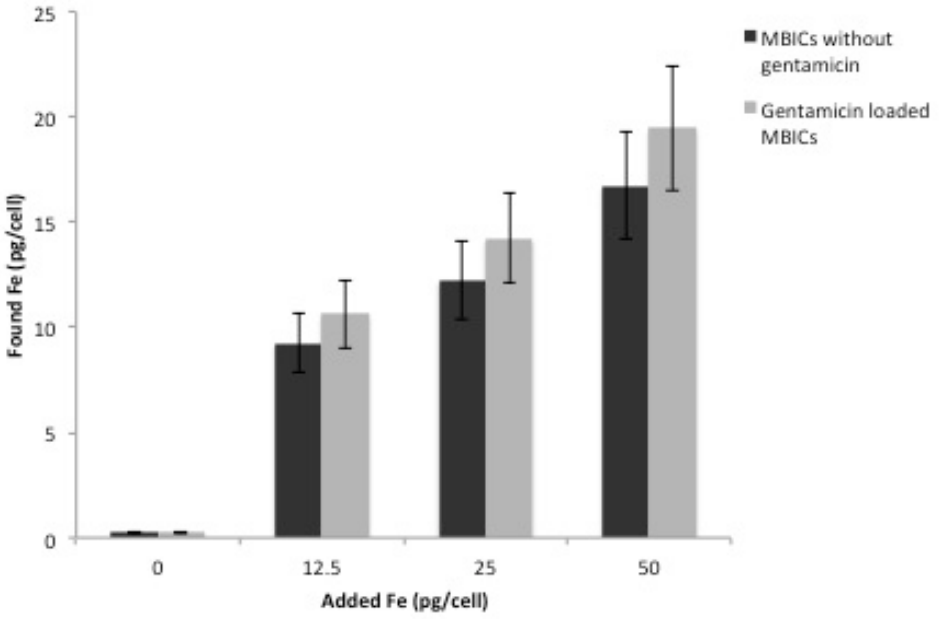

Figure 3.11 Intracellular uptake of MBICs and gentamicin-loaded MBICs by macrophage cells after incubation for 24 h.

In a second set of experiments, the poly(ethylene oxide) block of the copolymer was functionalized with an amine outer terminus, then some of those aminofunctional chains were derivatized with FITC so that the complexes could be detected by fluorescence measurements in the flow cytometry experiment. The PAA component of the copolymer was adsorbed onto the magnetite to produce a fluorescent MBICs-FITC

complex (that still retained some amino groups on the outer periphery). The remaining free carboxylate groups in the complexes were then bound with gentamicin, again with 31 weight percent uptake of the drug. Interestingly, the sizes of these aminofunctional MBICs-FITC complexes loaded with the drug were significantly larger in aqueous media relative to either the non-fluorescent analogues or to the MBICs-FITC complexes without the drug (table 3.1). Uptake of these drug-loaded aminofunctional MBICs-FITC complexes was assessed by their fluorescence intensities using flow cytometry (figure 3.12). While these complexes differed from those investigated by ICP in that these contained the FITC and amine moieties on their surfaces and they were larger, the uptake results complemented the other set of experiments. Significant uptake of the nanoparticles into the cells was observed.

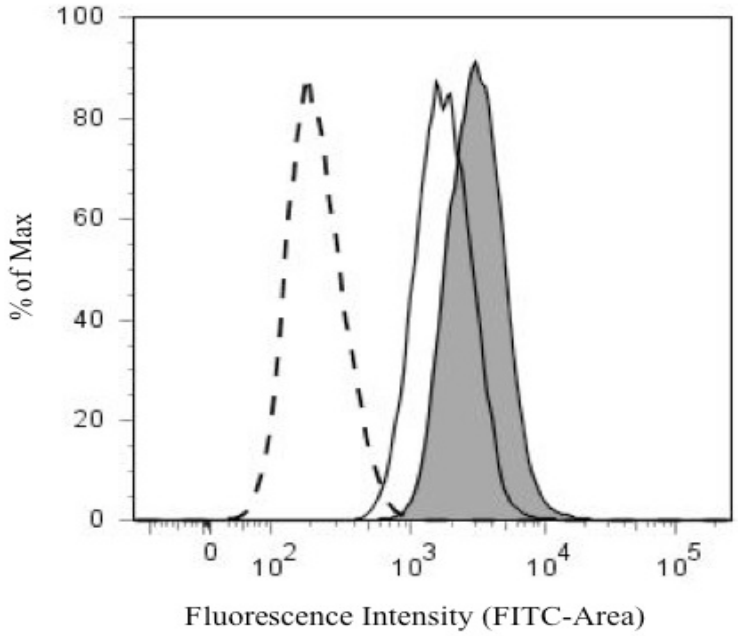

Figure 3.12 Fluorescence histograms from flow cytometry depicting the uptake of nanoparticles labeled with FITC into J774A.1 cells. Cells containing MBICs without FITC (control, dashed line), uptake after incubation with gentamicin loaded MBICs-FITC

for 2 h (solid line without shading), and uptake after incubation with gentamicin loaded MBICs-FITC for 3 h (solid line with shading).

In addition, confocal microscopy visually revealed an efficient uptake of the MBICs by the macrophages. As macrophages have some auto-fluorescence, it was important to visualize the cells incubated with media alone (negative control). Figure 3.13A (negative control) shows the absence of any fluorescence in the cells. On the other hand, figure 3.13B shows the presence of fluorescence inside the cells indicating the uptake and intracellular localization of MBICs. Staining with nuclear stain and lysosomal stain shows that MBICs resided in endosomes/lysosomes and also in the cytoplasm within macrophages (blue arrow shows the fusion between lysosomes and MBICs, yellow arrow indicate the MBICs in the cytoplasm of the macrophages). (figure 3.13C)

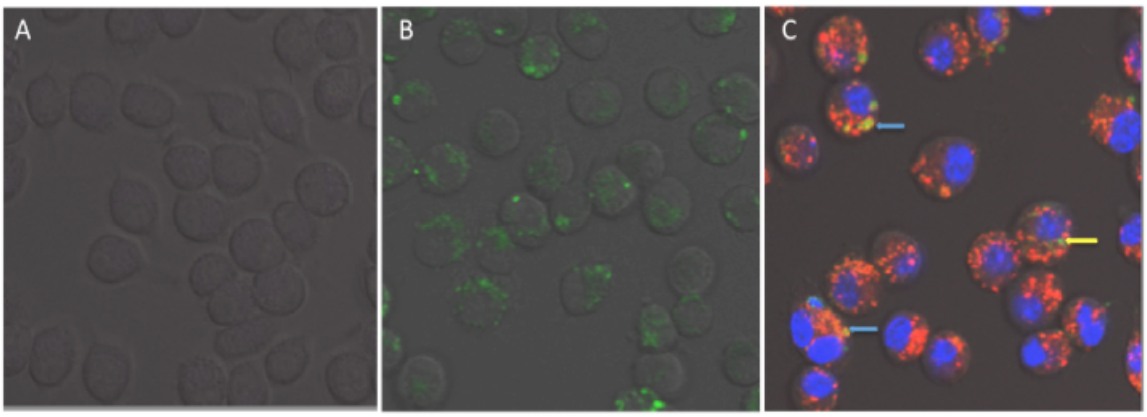

Figure 3.13 Confocal images showing the uptake and intracellular localization of MBICs.

Together, the ICP, flow cytometry and confocal microscopy experiments show that the macrophages take up these types of complexes over a range of incubation concentrations and complex sizes.

3.3.8 Minimum inhibitory concentrations (MICs) and minimum bactericidal concentrations (MBCs)

The minimum inhibitory concentration of the drug is defined as the concentration of drug needed to prevent a clear bacterial suspension containing 10^5 CFUs/mL from becoming turbid (indicating multiplication of bacteria) after incubation in growth media. The minimum bactericidal concentration of the drug is the concentration that kills the bacteria (density from 10^5 to 10^2 CFUs mL^{-1}, our limits of detection). Our results clearly show that there was no difference in the bioactivity of gentamicin after encapsulation in the MBICs. This establishes that the encapsulation process to load the antibiotic into the MBICs does not significantly alter the drug's bioactivity against pathogens. As expected, the empty MBICs did not show any bactericidal activity as 32 mg mL^{-1} was the highest concentration used in the assay, so the activity of the drug-loaded MBICs can be attributed solely to the gentamicin.

Drug or Particles	MIC (μg mL^{-1})	MBC (μg mL^{-1})
Free gentamicin	0.5	0.5
Gentamicin-loaded MBICs	1.6 (0.5 μg mL^{-1} of gentamicin)	1.6 (0.5 μg mL^{-1} of gentamicin)
MBICs (without gentamicin)	≥ 32	≥ 32

Table 3.2 Minimum Inhibitory Concentrations (MIC)

3.3.9 In vitro efficacy against intracellular brucellosis

Efficacy of the gentamicin-loaded MBICs to reduce intracellular Brucella was studied in J774A.1 murine cells and compared to free drug. The cells were infected with

Brucella, and any extracellular Brucella were eliminated with free gentamicin and discarded, then the macrophages infected with only the intracellular Brucella were incubated with either MBICs, free gentamicin, or gentamicin-loaded MBICs for 24 hours. A reduction of 2.10 log CFUs, corresponding to >99% killing of the intracellular bacteria, was achieved with gentamicin-loaded MBICs relative to the control without any treatment (Figure 3.14). This reduction was significantly higher than the reduction by free drug (0.45 logs). Thus, it is hypothesized that the MBICs can efficiently carry gentamicin into the J774.1A cells and release the drug within the cells, resulting in higher antibacterial activities.

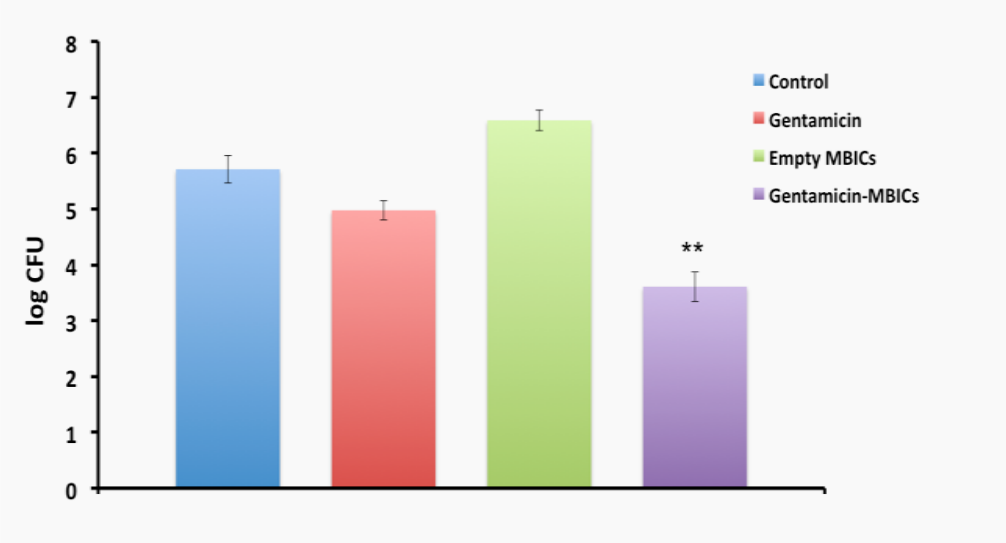

Figure 3.14 In vitro killing of intracellular Brucella in J774.1A murine macrophages: the bacterial colony forming unit (CFU) is expressed on a log scale. The results were averages of three replicates.

3.4 Conclusions

In conclusion, we have developed magnetic block ionomer complexes *(MBICs)* based on assembly of PEO-*b*-PAA ionomers with magnetite nanoparticles. High

concentrations of cationic antibiotic gentamicin were efficiently encapsulated into *MBICs*. The resultant polymer-magnetite-drug nanoparticles have excellent colloidal stability and high relaxivities. In addition, these nanoparticles were efficiently taken up by macrophages and appeared to enhance intracellular antimicrobial activities of gentamicin. These results suggest that these complexes could be used to enable simultaneous treatment and imaging.

3.5 References

1) Corbel, M. J. *Emerg Infect Dis* **1997,** *3*, 2113.

2) Pappas, G.; Panagopoulou, P.; Christou, L. *Cell Mol Life Sci* **2006,** *63*, 2229.

3) Seleem, M. N.; Boyle, S. M.; Sriranganathan, N. *Vet Microbiol* **2008,** *129*, 1.

4) Roop, R. M.; Bellaire, B. H.; Valderas, M. W. *Mol Microbiol* **2004,** *52*, 621.

5) Kohler, S.; Michaux-Charachon, S.; Porte, F. *Trends Microbiol* **2003,** *11*, 215.

6) Hall, W. H. *Rev Infect Dis* **1990,** *12*, 1060.

7) A. Shilnyy, E. Munnier, K. Herve, M. Souce, R. Benoit, S. Cohen-Jonathan, P. Limelette, M-L. Saboungi, P. Dubois, I. Chourpa *J. Phys. Chem. C*, **2010**, 114, 5850.

8) M. Kamat, K. El-Boubbou, D. C. Zhu, T. Lansdell, X. Lu, W. Li, X. Huang, *Bioconjugate Chem*, **2010**, 21, 2128.

9) A. Singh, F. Dilnawaz, S. Mewar, U. Sharma, N. R. Jagannathan, S. K. Sahoo, *Applied Materials and Interfaces*, **2011**, 3, 842.

10) M. Talelli, C. J. F. Rijcken, T. Lammers, P. R. Seevinck, G. Storm, C. F. van Nostrum, W. E. Hennick, *Langmuir*, 2009, 25, 2060.

11) M. Das, D. Bandyopadhyay, D. Mishra, S. Datir, P. Dhak, S. Jain, T. K. Maiti, A.

Basak, P. Pramanik, *Bioconjugate Chemistry*, 2011, 22, 1181.

12) S. Mohapatra, S. K. Mallick, T. K. Maiti, S. K. Ghosh, P. Pramanik, *Nanotechnology*, 2007, 18, 385102.

13) M. Das, D. Mishra, T. K. Maiti, A. Basak, P. Pramanik, *Nanotechnology*, 2008, 19, 415101.

(14) Goff, J. D.; Huffstetler, P. P.; Miles, W. C.; Pothayee, N.; Reinholz, C. M.; Ball, S.; Davis, R. M.; Riffle, J. S. *Chem Mater* **2009,** *21*, 4784.

(15) Pinna, N.; Grancharov, S.; Beato, P.; Bonville, P.; Antonietti, M.; Niederberger, M. *Chem Mater* **2005,** *17*, 3044.

(16) Virto, M. R.; Elorza, B.; Torrado, S.; Elorza Mde, L.; Frutos, G. *Biomaterials* **2007,** *28*, 877.

(17) Zhang, X.; Wyss, U. P.; Pichora, D.; Goosen, M. F. A., *J Pharm Pharmacol* **1994,** 46, 718.

(18) Hou, S.; Chaikof, E. L.; Taton, D.; Gnanou, Y. *Macromolecules* **2003,** *36*, 3874.

(19) Jun, Y.-W.; Huh, Y.-M.; Choi, J.-S.; Lee, J.-H.; Song, H.-T.; KimKim; Yoon, S.; Kim, K.S.; Chin, J.-S.; Suh, J.-S.; Cheon, J. *J Am Chem Soc* **2005,** *127*, 5732.

(20) Carroll, M. R. J.; Woodward, R. C.; House, M. J.; Teoh, W. Y.; Amal, R.; Hunley, T. L.; St. Pierre, T. G. *Nanotechnology* **2010**, 21, 035103(7pp).

(21) Nasongkla, N.; Bey, E.; Ren, J.; Ai, H.; Khemtong, C.; Guthi, J. S.; Chin, S.-F.; Sherry, A. D.; Boothman, D. A.; Gao, J. *Nano Lett* **2006,** *6*, 2427.

(22) Kim, B.-S.; Taton, T. A. *Langmuir* **2006,** *23*, 2198.

(23) Yang, J.; Lee, C.-H.; Ko, H.-J.; Suh, J.-S.; Yoon, H.-G.; Lee, K.; Huh, Y.-M.; Haam, S. *Angew Chem Int Ed* **2007,** *46*, 8836.

(24) Ranjan, A.; Pothayee, N.; Vadala, T. P.; Seleem, M. N.; Restis, E.; Sriranganathan, N.; Riffle, J. S.; Kasimanickam, R., *Antimicrob Agents Chemother* **2010,** *54*, 3524.

(25) Rohrer, M.; Bauer, H.; Mintorovitch, J.; Requardt, M.; Weinmann, H. J. *Invest Radiol* **2005,** *40*, 715.

(26) Balasubramaniam, S.; Pothayee, N.; Lin, Y.; Davis, R. M.; Rifle, J. S.; House, M.; Woodward, R. C.; St. Pierre, T. G. *Chem Mater* **2011,** *23*, 3348.

(27) Ranjan, A.; Pothayee, N.; Seleem, M.; Jain, N.; Sriranganathan, N.; Riffle, J.; Kasimanickam, R. *J Nanopart Res* **2010,** *12*, 905.

Chapter 4

Magnetic Nanoclusters with Hydrophilic Spacing for Dual Drug Delivery and Sensitive Magnetic Resonance Imaging

N. Pothayee, S. Balasubramaniam, N. Pothayee, N. Jain, N. Hu, Y. Lin, R. M. Davis, N. Sriranganathan, A. P. Koretsky and J. S. Riffle, *Journal of Materials Chemistry B*, 2013, 1, 1142-1149. DOI: 10.1039/c2tb00275b. Reproduced by permisssion of The Royal Society of Chemistry

4.1 Introduction

Magnetite nanoparticles are of interest as contrast-enhancement agents for T_2-weighted MRI due to their high magnetization, low toxicities and surface properties that allow for coatings to be applied so that the particles can be dispersed under physiological conditions.[1-5] The contrast is generated through dephasing of the magnetic moment of water protons near these complexes in the transverse plane, and higher rates of relaxation correlate with improved signal in the images.

In the past decade, multifunctional magnetite nanocarriers that integrate therapeutic agents into one system have attracted considerable interest because they may enable monitoring of biodistribution via MRI together with treatment.[1-3,6-7] However, the concept is challenging because the contrast agents can disperse broadly *in vivo*. Thus, in order to provide good contrast, the contrast agents must have high sensitivity or must accumulate at sufficient concentrations in close proximity. Another emerging application of magnetic particles is for cell-based therapies where cells can be labeled with magnetite and potentially monitored with T_2- and T_2*-weighted MRI *in vivo* following transplantation.[8-12] However, it is desirable to monitor cell migration and differentiation, and again, a challenge is to improve detection sensitivity.[13-19] Therefore, particles and agents with high transverse relaxivities are needed to improve upon tracking efficiencies of labeled cells as well as monitoring biodistribution of encapsulated drugs.

Recent results strongly suggest that the nanoscale size of magnetite-polymer particles is important for obtaining high transverse relaxivity.[20-25] We previously reported magnetite nanoparticles coated with copolyethers and showed that they could be aggregated slightly by tuning the hydrophobic versus hydrophilic compositions of the copolymers. Small increases in intensity average hydrodynamic diameter (from approximately 50 to 75 nm) were associated with transverse relaxivities that increased from approximately 150 to 240 s^{-1} mM Fe^{-1}. This was encouraging, and the best relaxivities obtained using that approach were about a factor of 1.7 better than commercial materials such as Feridex (as reported herein).[23] We also introduced the concept that a hydrophilic space between magnetic nanoparticles in a cluster may be important for increasing relaxivities, and developed a model which predicted that ~100 nm between particles in an aggregate would be optimal.[22,26] To test the model, functionalized ferritin protein was crosslinked to produce ~1.2 nm between the proteins. Transverse relaxivities increased by ~70% even with the small spacing over the non-crosslinked analogue, but the relaxivities of ferritin are low and this only produced a maximum relaxivity of ~16 s^{-1} mM Fe^{-1}. Related materials that contained magnetite clusters in hydrophobic cores have also been reported.[27] Altogether, both theoretical and experimental investigations of relationships among the properties of polymer coatings, sizes of aggregates, and relaxivities of the complexes have been initiated, but the optimal structure-relaxivity parameters remain far from defined.

Previously, we have prepared magnetite-polymer nanoparticles by adsorbing poly(ethylene oxide-*b*-acrylate) (PEO-*b*-PAA) onto magnetite.[28] A portion of the PAA block of the copolymer complexed with the metal oxide surfaces to form a core, while the

PEO component extended into aqueous media to form a corona. Realizing the need to enhance detection sensitivity of the nanocarriers, this chapter describes Magnetic Block Ionomer Clusters (*MBIClusters*) with controlled sizes and with significant hydrophilic space between the magnetite particles within the clusters. Amine groups at the tips of the H_2N-PEO corona were crosslinked through reaction with a poly(ethylene oxide) diacrylate oligomer to yield *MBIClusters*. These *MBIClusters* with hydrophilic intracluster spacing exhibit transverse relaxivities (r_2's) that increase from 190 to 604 s^{-1} $mMFe^{-1}$ measured at 1.4 T and 37 °C as their average size is increased. The *MBIClusters* were loaded with up to ~38 wt% of the multi-cationic drug gentamicin. Their prominent longditudinal and transverse relaxivities together with high capacities for encapsulating cationic therapeutic agents makes these highly promising as future MRI probes.

4.2 Experimental

4.2.1 Materials

Benzyl alcohol (>98%), diethyl ether, iron (III) acetylacetonate ($Fe(acac)_3$), oleic acid (90%, technical grade), triethylamine (>99.5%), pentamethyldiethylenetriamine (PMDETA), bromoisobutyryl bromide, gentamicin sulfate and poly(ethylene glycol) diacrylate (PEGDA, 700 g mol^{-1}) were purchased from Aldrich and used as received. 3-Hydroxypropyldimethylvinylsilane and *N*-(*t*-butoxycarbonyl)-2-aminoethanethiol were synthesized following previously-reported procedures.[31-32] *t*-Butyl acrylate (*t*BA, 99%) and Celite® (filter aid standard super-cel) were purchased from Alfa Aesar. *t*BA was distilled from calcium hydride before polymerization. Toluene (anhydrous), tetrahydrofuran (HPLC grade), dichloromethane (HPLC grade), hexane (HPLC grade), and acetone were purchased from Fisher Scientific and used as received. Dialysis tubing

was obtained from Spectra/Por. Phosphate buffered saline (PBS) was obtained from Mediatech, Inc.

4.2.2 Characterization

Dynamic Light Scattering (DLS) measurements were conducted with a Malvern Zetasizer NanoZS particle analyzer (Malvern Instruments Ltd) at a wavelength of 633 nm from a 4.0 mW, solid-state He-Ne laser at a scattering angle of 173° and at 25.0 ± 0.1 ˚C. The samples were dispersed in DI water at a concentration of 0.1 mg mL^{-1}, and the dispersion was sonicated for 5 min in a 75T VWR Ultrasonicator (120 W, 45 kHz). Then 1 mL of the dispersion was transferred into a polystyrene cuvette for analysis.

Thermogravimetric analyses (TGA) were carried out on the samples using a TA Instruments TGA Q500 to determine the fraction of each complex that was comprised of magnetite. Each sample (10-15 mg) was first held at 110 ºC for 10 min to drive off any excess moisture. The sample was equilibrated at 100 ºC, then the temperature was ramped at 10 °C min^{-1} to a maximum of 700 ºC in a nitrogen atmosphere. The mass remaining was recorded throughout the experiment. The mass remaining at 700 °C was taken as the fraction of magnetite in the complexes. The experiments were conducted in triplicate.

Transmission electron microscopy (TEM) was performed on a Philips EM-420 field emission gun TEM operating at an acceleration voltage of 120 kV. Samples were prepared by casting a drop of a dilute aqueous solution of the *MBICs* or *MBIClusters* onto amorphous carbon-coated copper grids. Images were acquired at a magnification of 96,000X.

A 7T MPMS SQuID magnetometer (Quantum Design) was used to determine

magnetic properties. Hysteresis loops were generated for the magnetite nanoparticles at 300K. Inductively coupled plasma-atomic emission spectroscopy (ICP-AES) was performed with a SPECTRO ARCOS 165 ICP spectrometer (SPECTRO Analytical Instruments, Germany). The particles were digested to release free iron by reacting them with concentrated nitric acid at a concentration of 0.02 mg mL^{-1} for 5 days at 25 °C. They were diluted to 0.002 mg mL^{-1} with DI water prior to measurement.

4.2.3 Synthesis of *tert*-butoxycarbonylamine-functional PEO (*tBoc*-HN-PEO)

Ethylene oxide was initiated with 3-hydroxypropyldimethylvinylsilane (3-HPMVS). Ethylene oxide (14.6 g, 0.332 mol) was distilled from a lecture bottle into a 300-mL Parr reactor cooled with a 2-propanol-dry ice bath. An initiator and catalyst solution consisting of 3-HPMVS (1.08 g, 7.5 mmol), THF (10 mL), and a double metal zinc hexacyanocobaltate catalyst (13 mg) was prepared in a flame-dried, 50-mL round-bottom flask and stirred at 25 °C for 24 h. The initiator-catalyst solution was added to the Parr reactor via syringe. The cooling bath was removed, and the reaction mixture was heated to 90 °C. The reaction began after ~15 min as evidenced by an exotherm from 90 to 180 °C and a pressure increase from 110 to 280 psi. After the exotherm subsided, the temperature and the pressure dropped to 95 °C and 60 psi, then the reaction was stirred for an additional 12 h. The reactor was purged with N_2 for 1 h and then opened, and its contents were diluted with 100 mL of dichloromethane. The mixture was filtered through celite using dichloromethane as the eluent (2x) to remove the catalyst. The dichloromethane was evaporated and the dimethylvinylsilyl-functional PEO was dried at 50 °C under vacuum overnight. The M_n was calculated to be 2800 g mol^{-1} by ^1H NMR. *tBoc*-HN-PEO-OH was obtained via an ene-thiol addition of N-(*tert*-butoxycarbonyl)-2-

amino-ethanethiol across the vinylsilane double bond. Dimethylvinylsilyl-functional PEO (2 g, 0.7 mmol), N-(*tert*-butoxycarbonyl)-2-amino-ethanethiol (0.43 g, 2.4 mmol) and AIBN (98.5 mg, 0.6 mmol) were dissolved in deoxygenated DMF (7 mL) in a 100-mL round-bottom flask. The reaction was conducted at 80 °C for 24 h with stirring, then cooled to room temperature. Dichloromethane (70 mL) was added, and the mixture was washed with DI water (4x). The dichloromethane was evaporated and the *tBoc*-HN-PEO was dried at 50 °C under vacuum.

4.2.4 Synthesis of an amine-functional poly(ethylene oxide-b-acrylic acid) copolymer (H_2N-PEO-PAA) by ATRP

tBoc-NH-PEO was functionalized with bromoisobutyryl bromide, then the protected amine-functional polymer was used as a macroinitiator for preparing *tboc*-NH-PEO-*b*-P*t*BA using a similar procedure to that described for the mPEO-*b*-P*t*BA. Removal of the t-butyl ester groups and the *tboc* group was achieved by dissolving the *tboc*-NH-PEO-*b*-PtBA (2.0 g, 1.09 x 10^{-2} eq of *t*-butyl ester groups) in 50 mL of dichloromethane. Trifluoroacetic acid (5 mL, 6.50 x 10^{-2} mol) was added and the reaction was stirred at 25 °C for 24 h. The polymer was precipitated in hexane and dried under vacuum, then dissolved in THF and dialyzed against 4 L of DI water through a cellulose acetate membrane (MWCO 3,500 g mol^{-1}) for 24 h. The H_2N-PEO-*b*-PAA had a PEO M_n of ~3,500 g mol^{-1} and PAA M_n of ~6,800 g mol^{-1} as measured by ^1H NMR.

4.2.5 Synthesis of magnetic iron oxide nanoparticles

The nanoparticles were prepared using a procedure adapted from Pinna et al.[28] $Fe(acac)_3$ (2.14 g, 8.4 mmol) and benzyl alcohol (45 mL, 0.43 mol) were charged to a 250-mL, three-neck, round-bottom flask equipped with a water condenser and placed in a

Belmont metal bath with an overhead stirrer with thermostatic (±1 °C) control. The solution was dehydrated at 110 °C for 1 h under a N_2 stream. The temperature was increased in 25 °C increments and held at each step temperature for 1 h, until it reached the reflux temperature of benzyl alcohol at 205 °C, then the temperature was maintained for 40 h. The reaction was cooled to room temperature and the particles were collected by centrifugation (4000 rpm, 30 min). The magnetite nanoparticles were washed 3 times with acetone (100 mL each), then were dispersed in chloroform (20 mL) containing oleic acid (0.3 g). The solvent was removed under vacuum at room temperature, and the oleic acid-stabilized magnetite nanoparticles were washed 3 times with acetone (50 mL each) to remove excess oleic acid. The particles were dried under vacuum overnight at room temperature and stored as a dispersion in chloroform at a concentration of 20 mg mL^{-1} prior to use.

4.2.6 Preparation of magnetic block ionomer complexes (*MBICs)*

Block copolymers with molecular weights of 3.5K-6.8K and 3.5K-9.5K H_2N-PEO-*b*-PAA were prepared in our laboratories as described previously (see supporting information) by synthesizing a H_2N-PEO-Br macroinitiator and using it with ATRP to prepare poly(*t*-butyl acrylate) blocks, then the *t*-butyl groups were removed.[31] The molecular weights and compositions of the copolymers were determined using size exclusion chromatography and ^1H NMR respectively (see supplemental data). Oleic acid-coated magnetite nanoparticles were synthesized as described previously.[31] The particles (50 mg) in chloroform were charged into a 50-mL round-bottom flask. H_2N-PEO-*b*-PAA (100.0 mg) was dissolved in DMF (10 mL) and added to the chloroform dispersion. The mixture was sonicated in a VWR 75T Ultrasonicator for 4 h under N_2, and then stirred at

RT for 24 h. The nanoparticles were precipitated in hexane (200 mL). A permanent magnet was utilized to collect the magnetite nanoparticles and free oleic acid was decanted with the supernatant. The particles were dried under vacuum, then dispersed in DI water (20 mL) with adjustment of the pH to 7 with 1 N NaOH and sonicated for 30 min. The particles were dialyzed against DI water (1 L) for 24 h in a 25,000 g mol^{-1} MWCO cellulose acetate dialysis bag to remove any free polymer. The dispersion was sterilized by filtration through a 0.2 μm Teflon filter. A black-brown solid product was obtained after freeze-drying with a yield of >85%.

4.2.7 Crosslinking the *MBICs* to form *MBIClusters*

The amine termini on the tips of the PEO coronas were crosslinked with PEGDA to form *MBIClusters*. The reactant concentrations were 10, 20 or 30 mg mL^{-1}. A stock solution of PEGDA (700 g mol^{-1}) was prepared by dissolving 250 mg of PEGDA in 10 mL of DI water, then a stoichiometric amount of the PEGDA solution was added to the *MBIC* dispersion. For example, to crosslink *MBICs* that contained 67 wt% of H_2N-PEO-*b*-PAA with block molecular weights of 3.5K-6.8K at a total reactant concentration of 20 mg mL^{-1}, *MBICs* (100 mg, 7 x 10^{-6} eq of amine on H_2N-PEO-PAA) were dispersed in 5 mL of DI water, the mixture was sonicated for 5 min, then the pH was adjusted to 7.8 with 1 N aq NaOH. The PEGDA stock solution (100 μL, 7 x 10^{-6} eq of acrylate) was added dropwise to the *MBIC* dispersion with stirring at room temperature over ~5 min. The mixture was stirred at 37 °C for 24 h, then dialyzed against DI water in a 25,000 g mol^{-1} MWCO dialysis bag for 24 h to remove any unreacted PEGDA. The product was recovered by freeze-drying.

4.2.8 Incorporation of gentamicin into *MBIClusters*

MBIClusters (40 mg, 2.18 x 10^{-4} eq COOH) were weighed into a 20-mL glass vial. Gentamicin sulfate solution in 10 mM phosphate buffer at pH 7.2 (45 mg gentamicin sulfate, 27 mg gentamicin, 5 mL) was added. The solution was sonicated for 5 min and transferred to a centrifugal filter unit equipped with a cellulose acetate membrane (MWCO of 10,000 g mol^{-1}). The free drug and salt solution were removed by centrifuging the dispersion at 3750 rpm for 1 h. This allowed the liquid to pass through the membrane into the bottom of the centrifugation unit, and the particles were collected on the membrane. They were removed from the membrane by redispersing them in a small amount of DI water (10 mL), and then the dispersion was freeze-dried to obtain gentamicin-loaded *MBIClusters*.

The amount of gentamicin in the *MBIClusters* was measured by reacting the primary amines in the gentamicin-loaded *MBIClusters* with phthalaldehyde and mercaptoethanol in borate buffer at pH 9.7.[47] The fluorescence emission intensity was measured in a fluorimeter (Biotek, USA) using an excitation wavelength of 340 nm and an emission wavelength of 450 nm. All samples including a series of standard solutions of gentamicin were transferred into 48-well plates and their fluorescence emission was measured. The concentration of gentamicin was calculated from a standardized calibration curve.

4.2.9 Release study of gentamicin from *MBIClusters*

To determine the release of gentamicin from the *MBIClusters* in PBS, 10 mg of gentamicin-loaded *MBIClusters* (equivalent to 3.8 mg gentamicin) were dispersed in 2 mL of PBS and placed in a 3,500 MWCO dialysis cassette (Fisher Scientific). The

cassette was placed in a 250-mL beaker and 150 mL of PBS (pH7.4) as the receptor medium was added to the beaker. The beaker was covered with Parafilm and maintained at 37 °C in a temperature-controlled Environ shaker agitated at 50 RPM. Aliquots of 3 mL were taken from the receptor medium and placed in separate scintillation vials at each time point. Each time, 3 mL of fresh PBS was added to the beaker to retain constant volume. The gentamicin in each aliquot was derivatized with a phthalaldehyde-mercaptoethanol assay solution as described above and the fluorescence intensity was measured at 450 nm. The amount of free drug (the control) that passed through the dialysis membrane was compared to the drug released at each time point using a standardized curve.

4.2.10 Relaxivity measurements

The proton transverse relaxation times (T_2) and longitudinal relaxation times (T_1) were measured on a Model mq-20 or mq-60 NMR Analyzer (Bruker Minispec) at a magnetic field strength of either 0.47 (ω_o = 20 MHz) or 1.4 T (ω_o = 60 MHz) and at 25 or 37.5 °C. T_2 was obtained from fitting a monoexponential decay curve to signal data generated by a Carr-Purcell-Meiboom-Gill (CPMG) spin-echo pulse sequence with an echo spacing of 1 ms and a repetition time of 6000 ms. T_1's were obtained from fitting a monoexponential recovery curve to signal data generated with an inversion recovery (IR) pulse sequence using ten logarithmically spaced inversion times between 50 and 10,000 ms. Samples were diluted in DI water in the concentration range of 0.01-0.001 wt% and 500 μL of each concentration was transferred into a 7.5 mm NMR tube and equilibrated for 15 min prior to measurements. To measure relaxivities at high fields, T_1 and T_2 relaxation times of five samples at different concentrations were measured on 4.7 T/40-

cm, 7 T/21-cm, and 11.7 T/31-cm horizontal bore small animal MRI scanners (Bruker, MA). The images were fitted with a 3-parameter function to calculate T_1 and T_2 values using the Bruker TopSpin built-in image-processing program. The relaxivities were calculated from the least-squares fit of the relaxation rate ($1/T_2$ or $1/T_1$) as a function of iron concentration (mM Fe). Fe concentrations were determined by inductively coupled plasma-atomic emission spectroscopy (ICP-AES, Varian Vista Axial CCD) as described above.

4.2.11 Phantom and *in vivo* MRI

Phantom MR images were measured to demonstrate that the enhanced r_2 relaxivities of the *MBIClusters* led to superior images relative to those of the non-crosslinked *MBICs*. *MBICs* (55 nm intensity average diameter) and *MBIClusters* (174 nm intensity average diameter) were dispersed in DI water at Fe concentrations ranging from 0 to 200 μM Fe. The dispersions were transferred to 1.5 mL Eppendorf tubes and mounted in a 1.5 wt% agarose gel in a glass container. MRI was performed on a 4.7 T small animal MRI scanner with a 40-cm horizontal bore (Bruker). T_2-weighted MR images were acquired with a spin-echo sequence with repetition time (TR) = 2,400 ms, echo time (TE) = 63 ms, flip angle = 180°, matrix size = 128 x 128 and slice thickness = 1.00 mm. T_1-weighted MR images were acquired with a FLASH sequence with TR = 150 ms, TE = 2.7 ms and FA angle = 90°. Six adult male B6 mice (25-30 g) were used to obtain images of the biodistribution of particles. All animal work was perfomed according to the guidelines of the Animal Care and Use Committee and the Animal Health and Care Section of the National Institute of Neurological Disorders and Stroke, National Institutes of Health (Bethesda, MD). For tail vein injection, the animals were

initially anesthetized with 4% isoflurane in 3:3:2 air:nitrogen:oxygen, and kept on 1.5-2.5% isoflurane during the infusions. For MRI scans, the mice were placed in a custom made plastic holder. The anesthesia was maintained at 1.5-2.0% using a nose cone and rectal temperature was maintained at 37 ± 1 °C by a heated water bath. No abnormalities were observed after injection in any of the mice. MRI's were acquired on a 7T/21cm horizontal bore Bruker Biospec System. The images were acquired using a Fast Low Angle SHot (FLASH) sequence synchronized to respiratory motion. The echo time (TE) was 10 ms, the repetition time (TR) was ~300 ms and the excitation flip angle was 30°. Each set consisted of 16 slices with no gap and a FOV of 3.84 x 2.56 x 1.2 cm, matrix 128 x 192 x 16.

4.3 Results and Discussion

4.3.1 Synthesis of *MBIClusters*

H_2N-PEO-*b*-PAA block copolymers were synthesized through controlled radical polymerization of *t*-butyl acrylate initiated by a protected aminofunctional PEO macroinitiator.[31] The *t*-butyl esters and the *tBoc* protecting group on the amine terminus were subsequently removed to yield diblock H_2N-PEO-*b*-PAA copolymers. Two copolymers with number average molecular weights of 3.5K-6.8K and 3.5K-9.5K H_2N-PEO-*b*-PAA were utilized. Magnetite nanoparticles were synthesized by reducing $Fe(acac)_3$ in benzyl alcohol. Each H_2N-PEO-*b*-PAA was coated onto the magnetite through ligand adsorption of a portion of the carboxylates on the PAA block. A targeted composition of 33:67 wt:wt magnetite:polymer was utilized that allowed for carboxylate adsorption onto the nanoparticles and also for a significant fraction of the carboxylates to remain free for subsequent salt formation with charged drugs. TGA indicated that the

compositions were ~34 wt% magnetite and ~66 wt% polymer in close agreement with the targeted composition.

When dispersed in water, core-shell nanoparticles formed that had PAA-magnetite hydrophilic cores and PEO coronas with amine tips on their outer peripheries. Clusters were formed from these complexes by crosslinking the amines on the corona tips with acrylates on poly(ethylene oxide) diacrylate wherein the magnetite nanoparticles were separated by the hydrophilic polymer around each precursor (Figure 4.1).

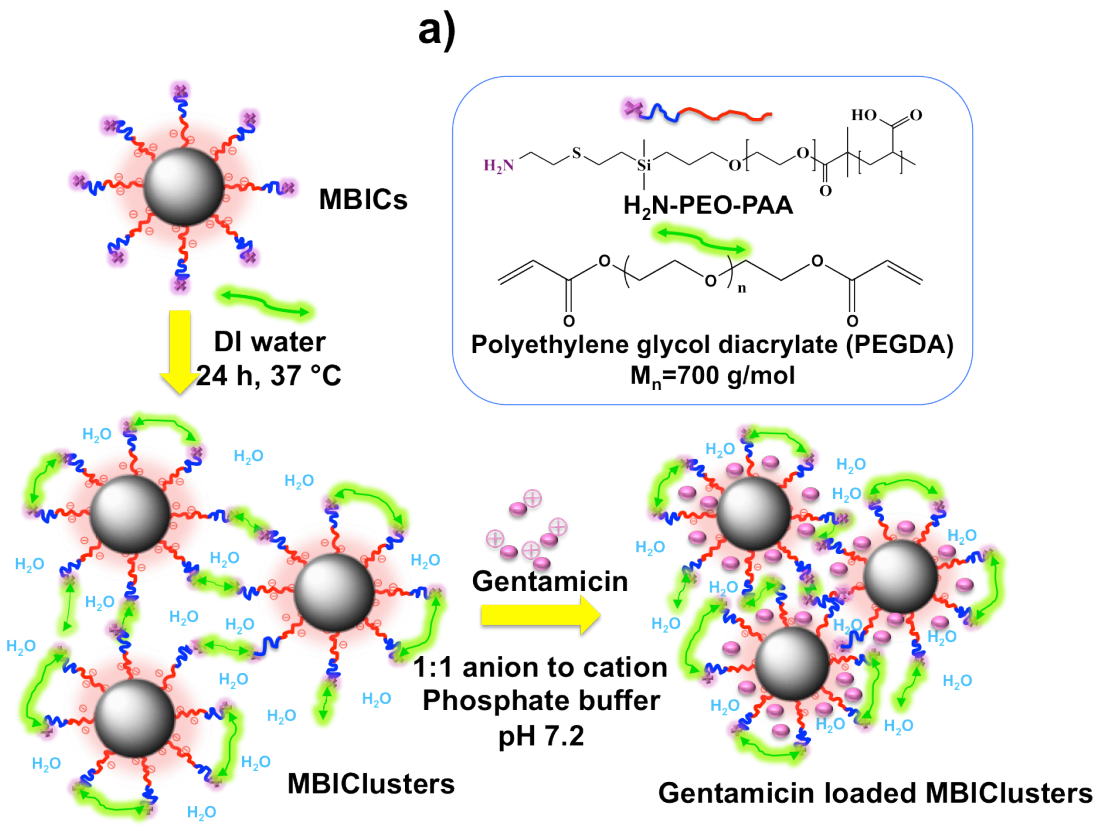

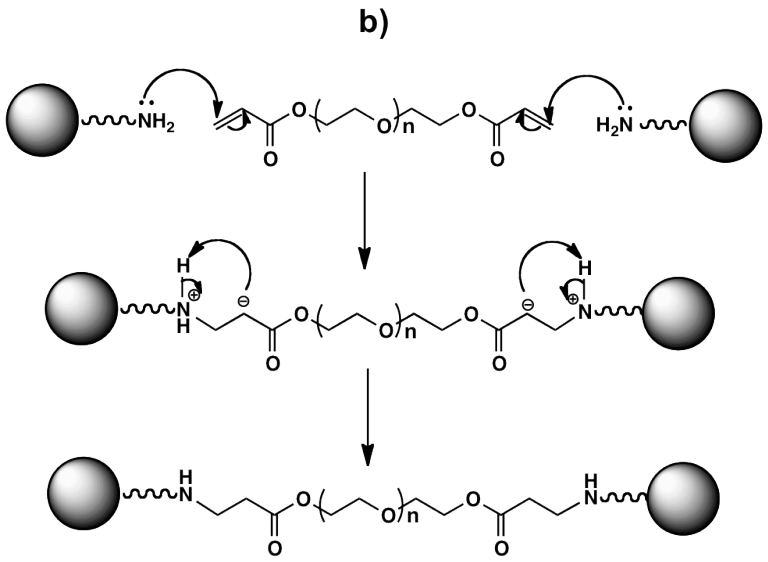

Figure 4.1 (a) Synthesis of *MBIClusters* containing magnetite contrast agents with hydrophilic spacing in the cores and subsequent drug loading via electrostatic interactions of complementary charged molecules. (b) chemistry of the crosslinking reaction to form *MBIClusters*

To distinguish the precursor magnetite-polymer nanoparticles from the clusters, the precursors will be designated as Magnetic Block Ionomer Complexes (*MBICs*), while the clusters will be called Magnetic Block Ionomer Clusters (*MBIClusters*).

The cluster sizes were controlled by adjusting the reactant concentrations in the crosslinking step (Table 4.1). In each case, a 1:1 ratio of amines to acrylate groups was utilized. The hydrophilic, oligomeric, crosslinking reagent reacted with amines on the coronas in water to form both inter- and intra-particle links. As the concentration in the crosslinking reaction was increased, inter-particle crosslinking became more pronounced, thus increasing the average cluster sizes. TGA confirmed that the composition of the *MBIClusters* was 32 wt% magnetite and 68 wt% polymer (including the crosslinking reagent), as expected.

Sample	Crosslinking concentration (mg mL^{-1})	Block ionomer (H_2N-PEO-PAA)	Intensity average diameter (nm)	Z average diameter (nm)	PDI
MBICs	-	2.8K-7.2K	55±2	45±1	0.19
		3.5K-9.5K	50±2	42±1	0.23
MBIClusters	10	2.8K-7.2K	119±6	97±3	0.24
		3.5K-9.5K	105±2	83±2	0.20
	20	2.8K-7.2K	143±5	135±1	0.21
		3.5K-9.5K	139±4	110±1	0.22
	30	2.8K-7.2K	181±2	161±2	0.12
		3.5K-9.5K	174±2	155±1	0.11

Table 4.1 Intensity and z-average diameters of MBICs and MBIClusters as a function of reactant concentration in the crosslinking step

TEM images of the non-crosslinked particles suggested that they formed small aggregates in water (Figure 4.2a). It was reasoned that this was likely a result of interparticle interactions among cationic ammonium groups on the particle coronas with anionic carboxylates on a neighboring particle. It is noteworthy that analogous non-crosslinked complexes without amine groups on the coronas formed discrete particles. Figure 4.2b shows the nanoscale *MBIClusters* after the crosslinking reaction. In addition to the clusters, some of the precursor small aggregates still remain.

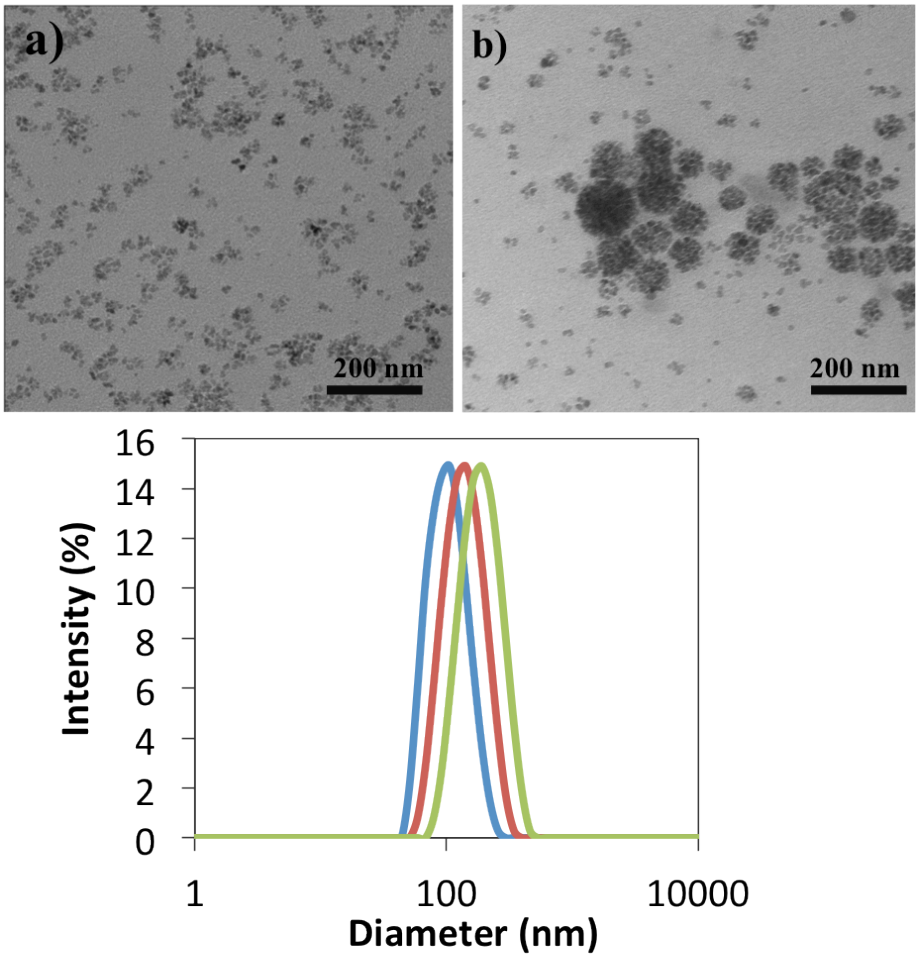

Figure 4.2 TEM images (top) of a) *MBICs*, D_i of 50 nm, and b) *MBIClusters*, D_i of 105 nm, and (bottom) DLS curves of intensity-average sizes of *MBIClusters*

Colloidal stability under physiological conditions is one of the most important issues when considering biological applications of nanomaterials.[29] The *MBIClusters* had excellent colloidal stability in both DI water and phosphate buffered saline (PBS) for up to 7 days (Figure 4.3). This suggests that they will be sufficiently stable under physiological conditions to be suitable drug carriers.

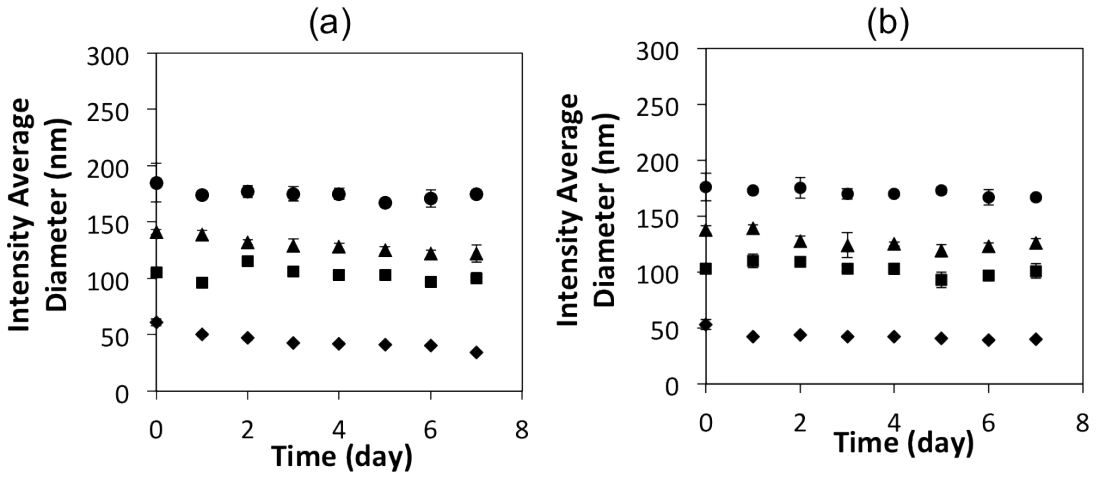

Figure 4.3 Stability in a) DI water (pH 7.0), and b) PBS (0.14 M NaCl, pH 7.4) of *MBICs,* D_i = 50 nm (Diamonds), *MBIClusters,* D_i = 105 nm (squares), D_i = 139 nm (triangles), D_i =174 nm (circles)

The magnetic properties of the bare magnetite nanoparticles were characterized via SQuID analysis. Hysteresis loops revealed that the nanoparticles were superparamagnetic at 300 K with a saturation magnetization of 67 $Am^2\ kg^{-1}$ of magnetite (Figure 4.4).

This value corresponds to ~92 $Am^2\ kg^{-1}$ of Fe and is consistent with the mass magnetization values reported for similar sized Fe_3O_4 nanoparticles.[30]

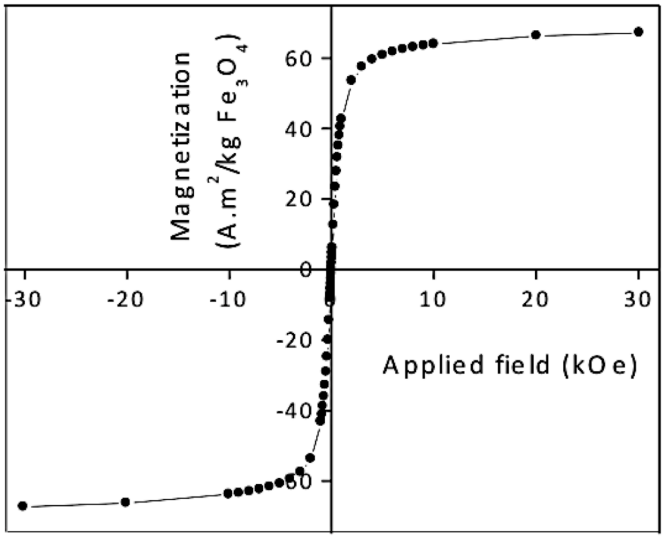

Figure 4.4 Hysteresis loop of bare magnetite nanoparticles at 300 K

4.3.2 Relaxivities of *MBIClusters*

To validate the potential for these *MBIClusters* as T_2 contrast agents, the proton transverse relaxivities (r_2*'s*) were measured at the clinically-relevant field strength of 1.4 T and physiological temperature. While the non-crosslinked precursor *MBICs* had r_2*'s* of 68-93 s^{-1} mM Fe^{-1}, r_2*'s* of the clusters were significantly higher and increased with size (Table 4.2). For example, *MBIClusters* with the 3.5K-9.5K H_2N-PEO-*b*-PAA had r_2*'s* increasing from 255 to 444 and 534 s^{-1} mM Fe^{-1} as the cluster size was increased from 105 to 139 and 174 nm, respectively. Thus, control over the cluster sizes from ~50-180 nm in intensity average diameter afforded control over r_2*'s* covering almost an order of magnitude.

Sample	Intensity average diameter (nm)	r_1 (s^{-1} mM Fe^{-1})	r_2 (s^{-1} mM Fe^{-1})
MBICs	55±2	18	68
	50±2	14	93
MBIClusters	119±6	30	194
	105±2	40	255
	143±5	34	410
	139±4	69	444
	181±2	43	604
	174±2	75	534

Table 4.2 NMR relaxivities of *MBICs* and *MBIClusters* at 1.4 T, 37 °C

The very high r_2 values are likely due to the ability of water to diffuse through the intra-cluster hydrophilic spaces between magnetite nanoparticles.[22,31] Vuong et al. have recently developed an empirical equation based on the classical motional-averaging model to predict the transverse relaxivities of hybrid magnetic nanoparticles such as controlled clusters.[32] It was shown that the normalized r_2's of magnetic particles over a range of sizes, morphologies and magnetizations followed a universal scaling law varying with the square of the particle hydrodynamic diameter. We used the volume fractions of magnetite in all of the dried *MBICs* and *MBIClusters* (from TGA) in the hydrodynamic size range of 50-180 nm (Table 4.2) and the volumetric magnetizations (M_v at 1.4 T) to normalize the observed r_2's according to [$r_2' = (r_2 \times \phi_{intra})/M_v^2$] and plotted them versus $(D_{MBICluster})^2$ (Figure 4.5). The magnetite volume fraction within the cluster, ϕ_{intra}, is based on the TGA analyses but does not account for water included in the clusters. At present, we have no ready method for measuring the magnetite volume fraction in the hydrated

clusters. The plot of r_2' versus the square of the hydrodynamic diameters was a straight line with a slope of 2.2×10^{-12}, a factor of 5 smaller than the prefactor in Vuong et al. (from figure 1 in that reference). The difference in the prefactor could be attributed, in part, to effects of hydration in the clusters. Specifically, if ϕ_{intra} increased with the cluster diameter $D_{MBICluster}$, this could account for the smaller value of the slope that we find (relative to Vuong et al.) since $(r_2 \times \phi_{intra})/M_v^2 = (r_2/(\phi_{intra} \times M^2)$ where M is the magnetization of magnetite at 1.4 T. Other variables may also affect r_2 such as the diffusion coefficient of water in the cluster and the spacing between magnetite particles in the cluster. These effects can be captured in part by recent Monte Carlo computer simulations for r_2 in hydrophilic clusters.[22,26,31,33]

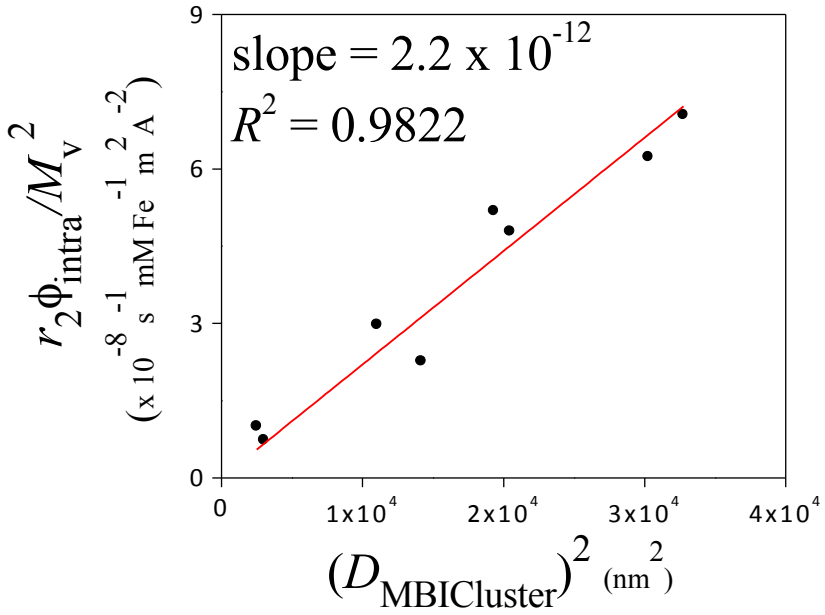

Figure 4.5 Relationship between transverse relaxivities normalized by the volume fractions of magnetite in the dried *MBICs* and *MBIClusters* and the hydrodynamic diameters

Interestingly, even for the single *MBICs*, if one considers that only the surface iron on the magnetite nanoparticles is accessible to water, it appears that r_1*'s* of iron oxide nanoparticles can be substantially higher than for gadolinium chelates. At 0.47 T and room temperature, r_1 relaxivities of the *MBICs* and Feridex (a commercial dextran-magnetite control) were ~40 and 22 s^{-1} mM Fe^{-1}, values that are in line with those reported in the literature for iron oxide nanoparticles.[34-36] By controlled clustering of *MBICs* to form *MBIClusters*, further increases in r_1*'s* were observed. At 1.4 T and 37 °C, the relaxivity of *MBIClusters* with an intensity average diameter of 139 nm was 69 s^{-1} mM Fe^{-1}. Although the numbers are remarkably high, such r_1 values are not unheard of. For example, specialty materials such as gadonanotubes in which clusters of gadolinium ions were trapped within defects of short single-walled carbon nanotubes, and also trimetallic gadolinium nitrides encapsulated within fullerenes have been reported to have very high r_1*'s*.[37-38] Possible explanations for the marked fast r_1*'s* of the *MBIClusters* is likely partly attributable to the hydrophilic spacing between each *MBIC* within the clusters that results in a larger volume fraction of Fe atoms accessible to water molecules relative to aggregated nanoparticle clusters. However, it is not yet fully understood why these r_1 values are so high.

The r_1*'s* of both the *MBIClusters* and precursor *MBICs* were field-dependent, decreasing as expected with increasing field strength (Figure 4.6).[34,39] The sharp decrease of r_1 with increasing field suggests that rotational correlation times of these particles also play a role in enhancing the relaxivities. In contrast, r_2 values for these agents remained essentially constant with field strength and this is likely at least partially attributable to the magnetic moments of the particles being almost saturated even at the lowest field

investigated (0.47 T).

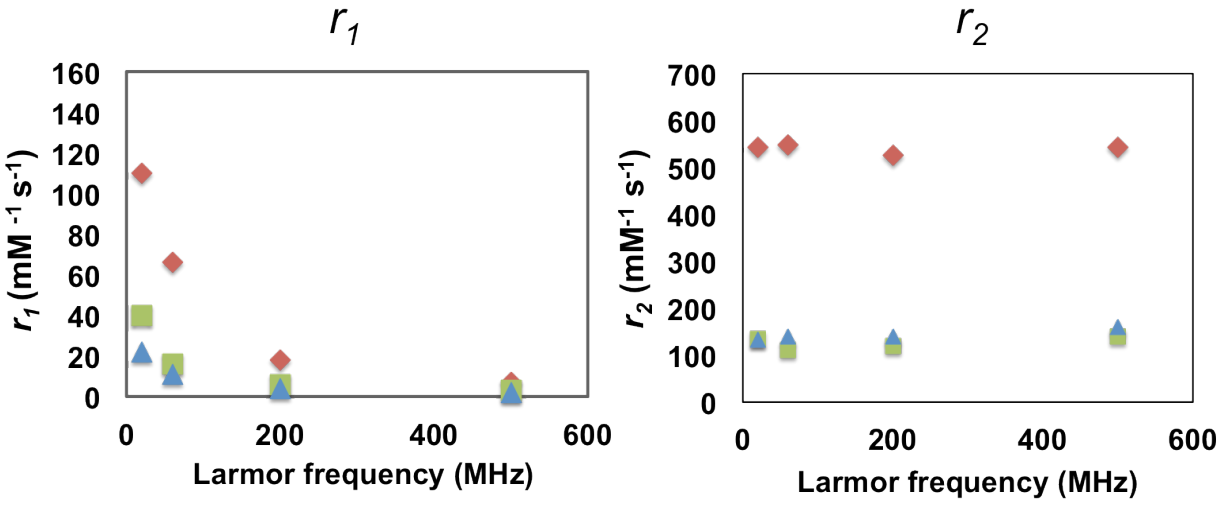

Figure 4.6 Relaxivities, r_1*'s* and r_2*'s,* of *MBIClusters,* D_i = 174 nm (diamonds), *MBICs* (squares), and Feridex (triangles) as a function of field strength at room temperature

4.3.3 Phantom and *in vivo* MRI

The feasibility of the *MBIClusters* to be potent negative MRI contrast agents was demonstrated in phantom images measured at 4.7 T. Figure 7 shows that the hypointense contrast signals obtained from aqueous dispersions of the *MBIClusters* were more pronounced relative to dispersions of the non-crosslinked precursors. With the clusters, significant contrast was already observed at an Fe concentration of 12.5 μM, and complete signal losses were observed at Fe concentrations >50 μM. In contrast, a similar dark hypointense image was only detected in the *MBICs* dispersion at an Fe concentration of 200 μM, consistent with the lower r_2's. Positive contrast signals generated by the *MBIClusters* and *MBICs* were also observed in T_1-weighted MRI. As observed for the T_2-weighted images, the clusters led to more T_1-relaxation enhancement

compared to the smaller *MBICs*. There is an increasing interest in developing MRI contrast agents that exert both positive and negative signals so that the two images can be compared. The *MBIClusters*, with prominent MRI relaxivities, may be useful as dual T_1/T_2 contrast agents at clinical field strengths where r_1*'s* of the clusters are still high.

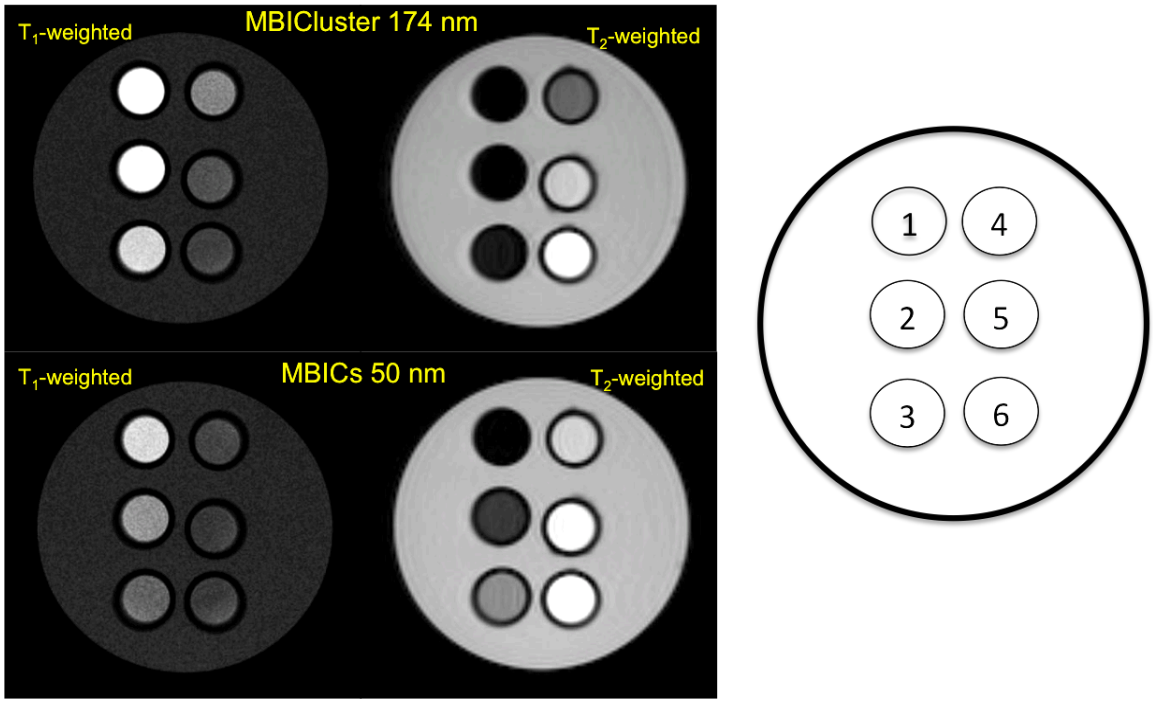

Figure 4.7 MR phantom images at 4.7 T of the *MBICs* and *MBIClusters* with intensity-average diameters of 50 and 174 nm respectively. Concentrations of Fe in each tube were 1) 200, 2) 100, 3) 50, 4) 25, 5) 12.5 and 6) 0 μM.

In an *in vivo* demonstration of T_2 contrast with the clusters, mice were intravenously injected with *MBIClusters*, *MBICs* or Feridex at Fe doses of 0.28 mg per kg. Serial 2D FLASH T_2*-weighted MRI was performed pre-injection and 10 and 50 minutes after injection. It is clear that administration of the *MBIClusters* at 0.28 mg/kg generated an enhanced hypointense signal in the livers compared to either the *MBICs* or Feridex (Figure 4.8). To quantify the comparison, liver signal intensities were normalized

against muscle signals and the amounts of signal drop were calculated by dividing the normalized signal intensities by the pre-injection intensity. Figure 9 shows that injection of a low dose of *MBIClusters* resulted in 81-84% signal drop while injection of the same dose of *MBICs* and Feridex caused 38-48% and 39-45% signal drop, respectively. The decrease in signal intensity occurred within the first few minutes after injection, thus suggesting rapid uptake of particles by the livers, probably due to endocytosis by Kupffer cells. It was reasoned that the prominent signal drops caused by the *MBIClusters* are at least partially attributable to the high r_2 values. However, it is also possible that the size distributions of these clusters lead to more efficient liver uptake, thus resulting in higher iron accumulation relative to the smaller *MBICs* or Feridex. Further investigation into the dose-dependent contrast signals, and quantification of the tissue iron content of these clusters will enable a better understanding of the *in vivo* relaxivities. However, it is clear that the *MBIClusters* are potent MRI contrast agents *in vivo* as well as *in vitro*.

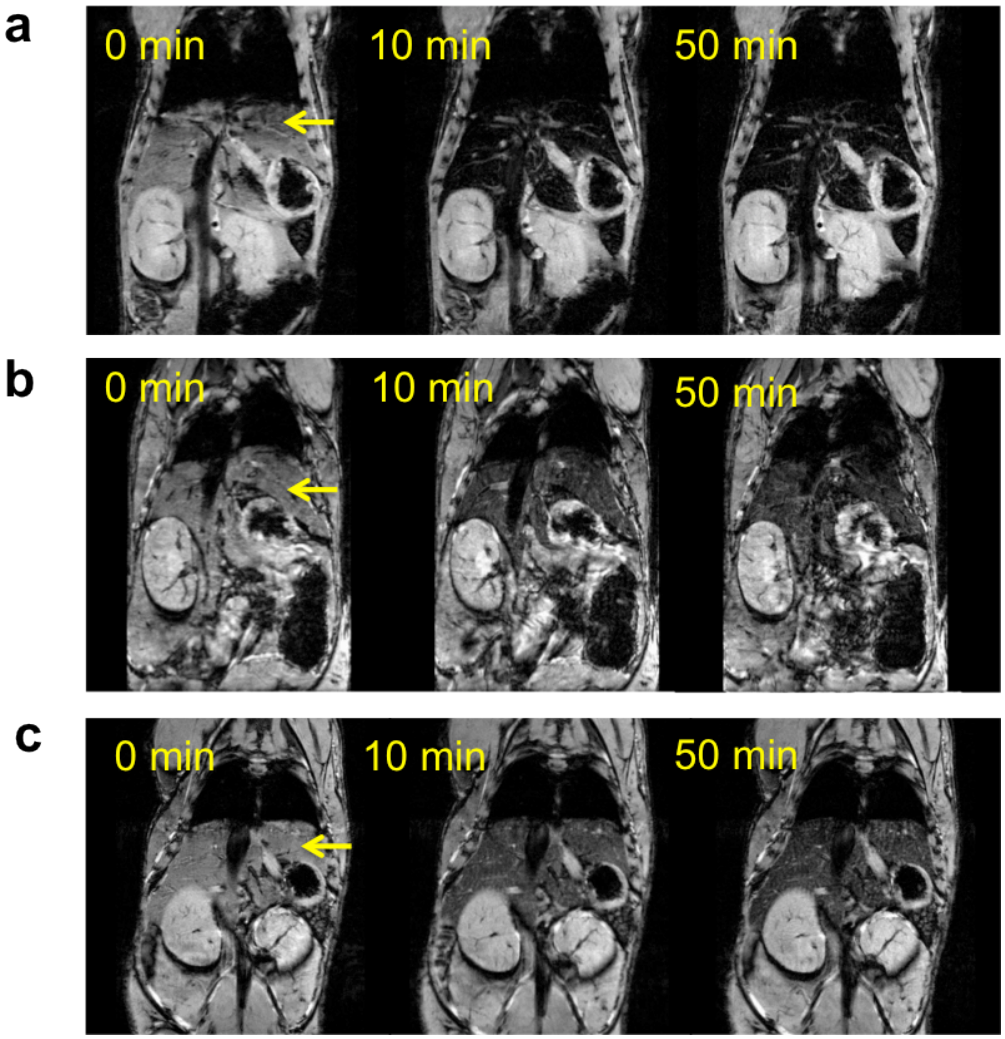

Figure 4.8 *In vivo* MR images of mice before and after i.v. injection of a) *MBIClusters*, b) Feridex and c) *MBICs* at an Fe dose of 0.28 mg/kg (arrow indicates liver)

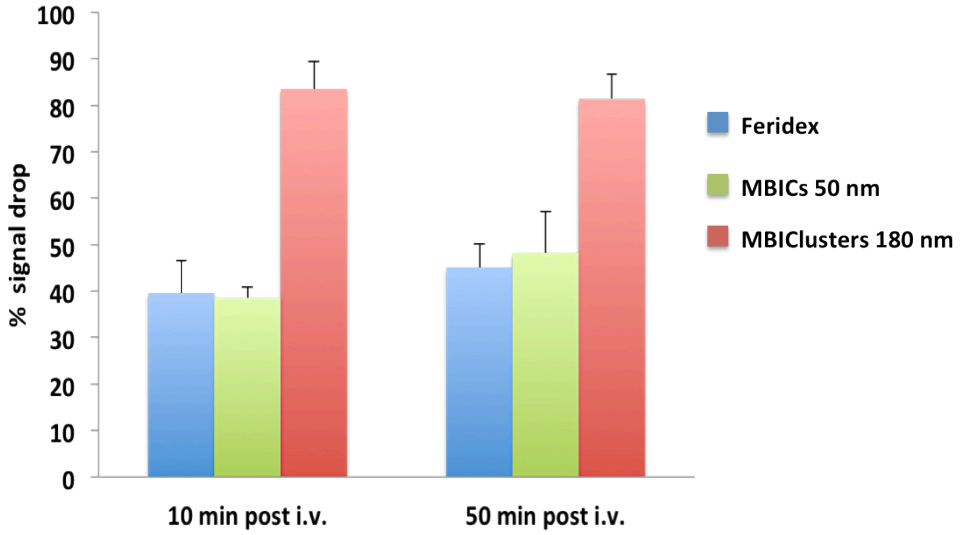

Figure 4.9 Comparison of % signal drop in mouse livers after i.v. administration of contrast agents.

4.3.4 *MBIClusters* as potential nanocarriers for delivering cationic drugs

Gentamicin, an aminoglycoside antibiotic, was selected as a model drug for these studies due to its highly polar and positively-charged structure to demonstrate that the *MBIClusters* may be suitable as imageable depot systems for therapeutic agents. Simple mixing of the drug solution with the clusters in phosphate buffer was sufficient to incorporate the drug molecules into the anionic cores (Figure 4.1). The amount of charged gentamicin was based on a 1:1 equivalence ratio of cations to anions assuming that all of the anions were free to complex with the drug (and that none were deactivated through adsorption on the magnetite). The fluorescence assay showed that 95% of the charged gentamicin had been encapsulated in the clusters, corresponding to a high drug content of 38 wt%. This remarkable loading of gentamicin is attributed to cooperative

interactions between the multi-cationic drug (5 ammonium ions in its molecular structure) and the anionic polymeric cores.

Upon gentamicin encapsulation, the physicochemical properties of the *MBIClusters* changed. The intensity average diameters decreased from 174 to 150 nm as the polyelectrolyte polymers formed complexes with the drug. Moreover, the zeta potentials of the gentamicin-loaded clusters dramatically decreased from -56 to -2 mV, indicating that the multi-cationic drug had effectively localized the charges in the cluster cores. The r_2*'s* and r_1*'s* of the clusters remained high but almost constant with versus without the hydrophilic drug (Figure 4.10), even though the cluster size decreased upon drug incorporation.

Gentamicin release profiles were measured by placing the nanoplexes in a cellulose acetate dialysis cassette with a MWCO of 3500 g $mole^{-1}$ in PBS and sampling the receptive media over time. The gentamicin in the receptive medium was derivatized with phthalaldehyde-mercaptoethanol and the fluorescence intensity of the derivative was measured at 450 nm and compared to the calibration curve. The free drug control fully diffused through the membrane into the receptor medium within 9 hours. Release of the gentamicin from the *MBIClusters* was sustained significantly longer. Approximately 20 wt% of the encapsulated gentamicin was released within 10 hours, and 38 wt % was released by 48 hours (figure 4.11). It also appears that the release rate of gentamicin from *MBIClusters* was slightly slower than that from single particle, suggesting that crosslinking might play role in the release behavior of gentamicin.

The fact that high concentrations of drug molecules did not detract from the MRI relaxivities together with the sustained drug release reinforces the promise of using

hydrophilic *MBIClusters* for dual delivery and imaging. These novel nanocarriers can also potentially efficient vehicles for loading other cationic drugs into the formulation.

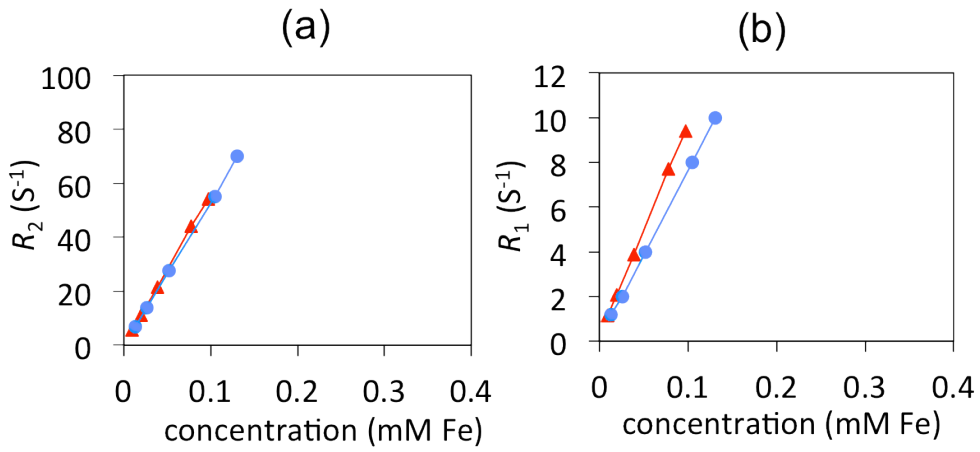

Figure 4.10 a) Transverse relaxivities (r_2) of *MBIClusters* (534 $s^{-1}mMFe^{-1}$, circles) versus *gentamicin loaded MBIClusters* (555 $s^{-1}mMFe^{-1}$, triangles) b) longitudinal relaxivities (r_1) of *MBIClusters* (75 $s^{-1}mMFe^{-1}$, circles) versus *gentamicin loaded-MBIClusters* (95 $s^{-1}mMFe^{-1}$, triangles).

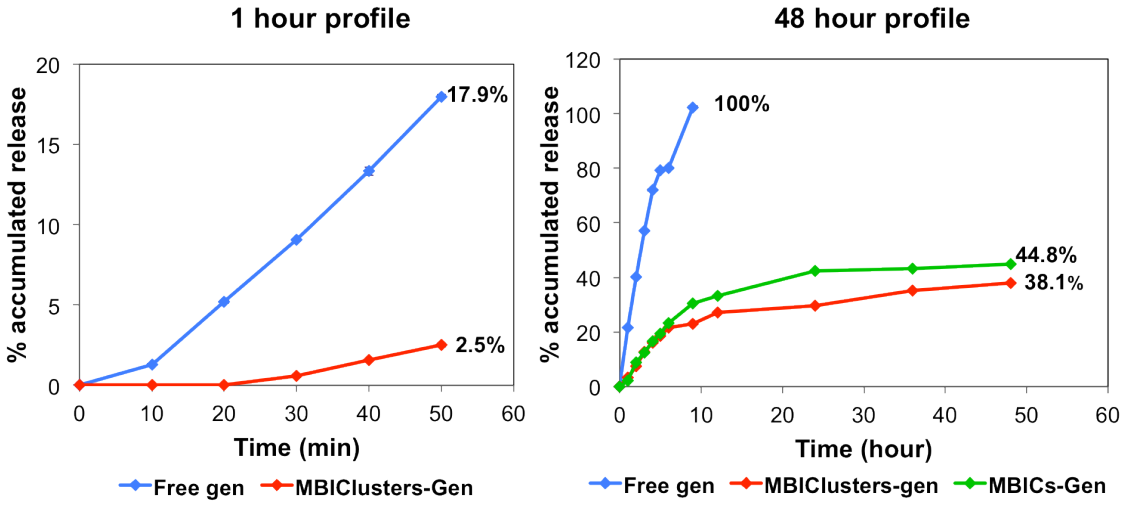

Figure 4.11 Release profile of gentamicin from MBIClusters at pH 7.4 37 °C

4.4 Conclusions

A series of *MBIClusters* with hydrophilic polymer spacing between magnetite nanoparticles within the clusters have been prepared, and they have extremely high MRI sensitivity. The average cluster sizes were controlled by adjustments to the reactant concentrations in the crosslinking (clustering) step, and their sizes directly relate to high relaxivities. MRI scans focused on the livers of mice demonstrate that these *MBIClusters* are significantly sensitive contrast agents. We posit that the hydrophilic space within these clusters plays a strong role in enhancing field gradients to diffusing water molecules, thus leading to the large increases in relaxivities. Owing to their charged, nanogel-like network, we demonstrated that these clusters could be effective nanocarriers for oppositely charged cargo. The prominences in MRI relaxivities and high drug encapsulation efficiency warrant further exploration in using these *MBIClusters* as potential dual ultrasensitive contrast agents for molecular imaging combined with therapeutic capacities.

4.5 References

1. M. Kamat, K. El-Boubbou, D.C. Zhu, T. Lansdell, X. Lu, W. Li, X. Huang, *Bioconjugate Chem.,* 2010, **21***,* 2128.
2. S. Mohapatra, S.K. Mallick, T.K. Maiti, S.K. Ghosh, P. Pramanik, *Nanotechnology,* 2007, **18**, 385102.
3. A. Singh, F. Dilnawaz, S. Mewar, U. Sharma, N.R. Jagannathan, S.K. Sahoo, *Appl. Mater. Interfaces,* 2011, **3***,* 842.
4. H. Sadek, S. Latif, R. Collins, M.G. Garry, D.J. Garry, *Regen. Med.,* 2008, **3**(6)*,* 807.

5. M. Talelli, C.J.F. Rijcken, T. Lammers, P.R. Seevinck, G. Storm, C.F. van Nostrum, W.E. Hennick, *Langmuir,* 2009, **25**, 2060.

6. M. Das, D. Mishra, T.K. Maiti, A. Basak, P. Pramanik, *Nanotechnology,* 2008, **19**, 415101.

7. A. Shilnyy, E. Munnier, K. Herve, M. Souce, R. Benoit, S. Cohen-Jonathan, P. Limelette, M.-L. Saboungi, P. Dubois, I. Chourpa, *J. Phys. Chem. C,* 2010, **114***,* 5850.

8. T. Arai, T. Kofidis, J.W.M. Bulte, J. de Bruin, R.D. Venook, G.J. Berry, M.V. McConnell, T. Quertermous, R.C. Robbins, P.C. Yang, *Magn. Reson. Med.*, 2006, **55**, 203.

9. M.E. Cohen, N. Muja, N. Fainstein, J.W.M. Bulte, T. Ben-Hur, *J. Neurosci. Res.,* 2010, **88**, 936.

10. I.J.M. de Vries, W.J. Lesterhuis, J.O. Barentsz, P. Verdijk, J.H. van Krieken, O.C. Boerman, W.J.G. Oyen, J.J. Bonenkamp, J.B. Boezeman, G.J. Adema, J.W.M. Bulte, T.W.J. Scheenen, C.J.A. Punt, A. Heerschap, C.G. Figdor, *Nat. Biotechnol.,* 2005, **23**(11)*,* 1407.

11. E.M. Shapiro, K. Sharer, S. Skrtic, A.P. Koretsky, *Magn. Reson. Med.,* 2006, **55**, 242.

12. E.M. Shapiro, S. Skrtic, A.P. Koretsky, *Magn. Reson. Med.,* 2005, **53**, 329.

13. J.W.M. Bulte, D.L. Kraitchman, *Curr. Pharm. Biotechno.,* 2004, **5**, 567.

14. P. Foster-Gareau, C. Heyn, A. Alejski, B.K. Rutt, *Magn. Reson. Med.,* 2003, **49**, 968.

15. K.A. Hinds, J.M. Hill, E.M. Shapiro, M.O. Laukkanen, A.C. Silva, C.A. Combs, T.R. Varney, R.S. Balaban, A.P. Koretsky, C.E. Dunbar, *Blood,* 2003, **102**, 867.

16. E.M. Shapiro, S. Skrtic, K. Sharer, J.M. Hill, C.E. Dunbar, A.P. Koretsky, *P. Natl Acad. Sci. USA,* 2004, **101**(30)*,* 10901.

17. A. Stroh, C. Faber, T. Neuberger, P. Lorenz, K. Sieland, P.M. Jakob, A. Webb, H. Pilgrimm, R. Schober, E.E. Pohl, C. Zimmer, *NeuroImage,* 2005, **24**, 635.

18. L. Wang, K.-G. Neoh, E.-T. Kang, B. Shuter, S.-C. Wang, *Biomaterials,* 2010, **31**, 3502.

19. Y. Zhang, S.J. Dodd, K.S. Hendrich, M. Williams, C. Ho, *Kidney Int.,* 2000, **58**, 1300.

20. H. Ai, C. Flask, B. Weinberg, X. Shuai, M.D. Pagel, D. Farrell, J. Duerk, J. Gao, *Adv. Mater.,* 2005, **17**, 1949.

21. S. Balasubramaniam, N. Pothayee, Y. Lin, R.M. Davis, J.S. Riffle, M. House, R.C. Woodward, T.G. St. Pierre, *Chem. Mater.,* 2011, **23**(14)*,* 3348.

22. K.M. Bennett, E.M. Shapiro, C.H. Sotak, A.P. Koretsky, *Biophys. J.,* 2008, **95**, 342.

23. M.R.J. Carroll, P. Huffstetler, W. Miles, J.D. Goff, R.M. Davis, J.S. Riffle, M. House, R.C. Woodward, T.G. St. Pierre, *Nanotechnology,* 2011, **22**, 325702.

24. M.R.J. Carroll, R.C. Woodward, M.J. House, W.Y. Teoh, R. Amal, T.L. Hanley, T.G. St. Pierre, *Nanotechnology,* 2010, **21**(3), 1-035107.

25. Z.R. Stephen, F.M. Kievit, M. Zhang, *Mater. Today,* 2011, **14**(7-8), 330.

26. Y. Matsumoto, A. Jasanoff, *Magn. Reson. Imaging,* 2008, **26**, 994.

27. C.W. Kessinger, O. Togao, C. Khemtong, G. Huang, M. Takahashi, J. Gao, *Theranostics,* 2011, **1**, 263.

28. Nikorn Pothayee, Nipon Pothayee, N. Jain, N. Hu, S. Balasubramaniam, L.M. Johnson, R.M. Davis, N. Sriranganathan, J.S. Riffle, *Chem. Mater.,* 2012, **24**(11)*,* 2056.

29. J.D. Goff, P.P. Huffstetler, W.C. Miles, N. Pothayee, C.M. Reinholz, S. Ball, R.M. Davis, J.S. Riffle, *Chem. Mater.,* 2009, **21**, 4784.

30. Y.-W. Jun, Y.-M. Huh, J.-S. Choi, J.-H. Lee, H.-T. Song, S. Kim, S. Yoon, K.-S. Kim, J.-S. Shin, J.-S. Suh, J. Cheon, *J. Am. Chem. Soc.,* 2005, **127**(16), 5732.

31. C. Paquet, H.W. de Haan, D.M. Leek, H.-Y. Lin, B. Xiang, G. Tian, A. Kell, B. Simard, *ACS Nano.,* 2011, **5**(4), 3104.

32. Q.L. Vuong, J.-F. Berret, J. Fresnais, Y. Gossuin, O. Sandre, *Adv. Healthcare Mater.,* 2012, **1**(4), 502.

33. Q.L. Vuong, P. Gillis, Y. Gossuin, *J. Magn. Reson.,* 2011, **212**, 139.

34. A. Bjornerud, L. Johansson, *NMR Biomed.,* 2004, **17**, 465.

35. Y.X.J. Wang, S.M. Hussain, G.P. Krestin, *Eur. Radiol.,* 2001, **11**, 2319.

36. R. Weissleder, A. Bogdanov, E.A. Neuwelt, M. Papisov, *Adv. Drug Deliv. Rev.,* 1995, **16**, 321.

37. B. Sitharaman, K.R. Kissell, K.B. Hartman, L.A. Tran, A. Baikalov, I. Russakova, Y. Sun, H.A. Khant, S.J. Ludtke, W. Chiu, S. Laus, E. Toth, L. Helm, A.E. Merbach, L.J. Wilson, *Chem. Commun.,* 2005, **31**, 3915.

38. J. Zhang, P.P. Fatouros, C. Shu, J. Reid, L.S. Owens, T. Cai, H.W. Gibson, G.L. Long, F.D. Corwin, Z.-J. Chen, H.C. Dorn, *Bioconj. Chem.,* 2010, **21**(4), 610.

39. K.E. Kellar, D.K. Fujii, W.H. Gunther, K. Briley-Saebo, A. Bjornerud, M. Spiller, S.H. Koening, *J. Magn. Reson. Imaging,* 2000, **11**(5), 488.

Chapter 5

Structure-property relationships of polycarboxylate, polyaminobisphosphonate and their complexes with manganese (*MaGICs*) for potential MRI positive contrast agent

N. Pothayee, N. Pothayee, N. Hu, R. Zhang, A. P. Koretsky and J. S. Riffle, *Journal of Materials Chemistry B*, 2013, submitted. Reproduced by permisssion of The Royal Society of Chemistry

5.1 Introduction

T1 Contrast agents are known to enhance MR imaging contrast by accelerating longitudinal (T1) relaxation of water protons and they generate a bright contrast signal in tissue. The most commonly used MRI T1 contrast agents are paramagnetic gadolinium (Gd^{3+})-based chelates. However, several cases of nephrogenic systemic fibrosis (NSF) have been reported in patients where Gd-based contrast agents have been used.[1-4] Therefore, over the past few years, there has been increased interest in development of non-gadolinium MRI contrast agents. Significant attention has been paid to manganese as an alternative. Several types of Mn-based contrast agents have been reported and can be classified into two broad categories including small molecule agents and nanoparticulate agents. Small molecule agents have mainly been based on Mn chelates with polycarboxylic acid ligands and porphyrin derivatives, while nanoparticulate agents were purely inorganic or included polymeric components. [5-9]

Polymeric Mn-based nanoparticles have been explored and some of these have exhibited excellent relaxivities.[10-17] Rongved and Klaveness were among the first to investigate complexes of water-soluble biopolymers with manganese.[11] They mixed Mn^{2+} salts with the biopolymers, some of which had carboxylic acid groups or chelating agents. While no stability data was provided in terms of displacement of manganese from these polymers, the authors postulated that specific binding groups on the polymers

would be necessary for in vivo applications. They reported that the r_1 relaxivity of the manganese that was complexed to the polymer through polymer-bound chelating groups was three fold higher than that of GdDTPA. Later on, Zhang and coworkers reacted modified dextran with a Mn (III) porphyrin complex. The resulting macromolecule exhibited a better r_1 relaxivity than GdDTPA and was reported to selectively target tumors in vivo.[12] More recently, Huang and co-workers coupled MnDTPA to chitosan oligosaccharides through an amide link. The complex exhibited high stability in aqueous solution without the release of free Mn^{2+}, together with a higher relaxivity than GdDTPA in both water and aqueous bovine serum albumin.[13]

It has been reported that block copolymers comprised of a polyelectrolyte block and a nonionic water-soluble block can bind electrostatically with molecules of opposite charge to form block ionomer complexes (BICs).[18-27] The polyelectrolyte block and the charged cargo formed the cores of such complexes while the nonionic block protruded outward into aqueous media to provide a polymer sheath that dispersed the complexes. Several multivalent metal ions have been shown to induce formation of nanostructured complexes with various classes of polyelectrolytes in aqueous solution.[28-30] However, direct self-assembly of paramagnetic ions with ion-containg block or graft copolymers and their relaxometric properties have not been studied.

This chapter describes the direct formation of novel manganese-graft ionomer complexes (*MaGICs*) as potential MRI contrast agents. Different types of graft copolymers including polycarboxylate-g-PEO and polyaminobisphosphonate-g-PEO were utilized to fabricate *MaGICs* through spontaneous self-organization with Mn^{2+} in aqueous solution. This approach has several advantages. First, the non ionic PEO grafts

provide steric colloidal stability that is insensitive to pH. Secondly, residual anions on the polymer backbone provide a means for binding a variety of drugs. The relaxometric properties and applicability of each type of *MaGIC* as an effective contrast agent was investigated and compared to that of commercial contrast agents.

5.2 Experimental

5.2.1 Materials

Methanol (99.9%), hexane (99.9%), chloroform (99.9%), magnesium sulfate (anhydrous, 98%), diethyl ether (anhydrous, 99.8%), dichloromethane (99.8%, HPLC grade), and dialysis tubing (Spectra/Por, 3,500 MWCO), all from Fisher Scientific, were used as received. *N,N*-Dimethylformamide (DMF, anhydrous, 99.8%), methanol (anhydrous, 99.8%), sodium sulfate (anhydrous, 99%), 3-amino-1-propanol (>99%), 6-amino-1-hexanol (>99%), triethylamine (>99.5%), sodium hydroxide (97%), poly(ethylene oxide) methyl ether (M_n= 5,085 g mol^{-1}), 2,2'-azobisisobutyronitrile (AIBN, 98%), sodium chloride (>99.5%), acryloyl chloride (97%), methacryloyl chloride (97%), bromotrimethylsilane (TMSBr, 97.0%) and manganese (II) chloride tetrahydrate ($MnCl_2.4H_2O$, 99%) were purchased from Sigma-Aldrich. Diethyl vinylphosphonate (Epsilon-Chimie, >98%) and dichloromethane (EMD Chemicals, anhydrous, 99.8%) were used as received. *tert*-Butyl acrylate (*t*BA) was purchased from Alfa Aesar and distilled from calcium hydride before polymerization. Deionized water was obtained through a MilliQ A10 synthesis water purification system (EMD Millipore, MA). Phosphate buffered saline (PBS) was obtained from Mediatech Inc. (VA, USA).

5.2.2 Characterization

^{1}H NMR spectral analyses were performed on a Varian Unity 400 NMR, a JEOL Eclipse Plus 500 NMR or a Bruker Advance II-500 NMR operating at 399.95 MHz, 500 MHz or 500 MHz, respectively. ^{31}P NMR spectral analyses were obtained on a Varian Inova 400 NMR operating at 161.91 MHz. Parameters utilized for the ^{31}P NMR were a 45° pulse and 1 s relaxation delay with 128 scans. All spectra of the monomers and phosphonate polymers were obtained in $CDCl_3$. Spectra of the phosphonic acid polymers were obtained in D_2O by adjusting the pH to 7.4 with NaOD.

DLS measurements were conducted with a Malvern Zetasizer NanoZS particle analyzer (Malvern Instruments Ltd) at a wavelength of 633 nm from a 4.0 mW, solid-state He-Ne laser at a scattering angle of 173° and at 25 ± 0.1 ˚C. Intensity, volume and number average diameters were calculated with the Zetasizer Nano 4.2 software utilizing an algorithm based upon Mie theory that transforms time-varying intensities to particle diameters. For DLS analysis, the dialyzed complexes were dispersed in DI water at a concentration of 1.0 mg mL^{-1}, and the dispersion was sonicated for 1 min in a 75T VWR Ultrasonicator (120 W, 45 kHz) for analysis.

The amount of incorporated Mn^{2+} in the complexes was quantified using ICP-AES performed on a SPECTRO ACROS ICP 165 (Spectro Analytical Instruments, Germany).

5.2.3 Synthesis of hydroxyhexyl (and propyl) ammonium bisdiethylphosphonate

6-Amino-1-hexanol (10.0 g, 0.085 mol), diethyl vinylphosphonate (28.0 g, 0.17 mol), and 200 mL of deionized water were charged to a 250-mL round-bottom flask equipped with magnetic stir bar and sealed with a septum. The reaction was placed in an

oil bath and maintained at 60 °C for 24 h. The reaction mixture was extracted with dichloromethane (5 x 50 mL) at room temperature and dried over anhydrous magnesium sulfate, then the solvent was evaporated to afford hydroxyhexylammonium bisdiethylphosphonate. Hydroxypropyl ammonium bisdiethylphosphonate was synthesized using an analogous procedure.[31]

5.2.4 Synthesis of an ammonium bisdiethylphosphonate methacrylate monomer

Hydroxyhexyl ammonium bisdiethylphosphonate (17 g, 38 mmol), triethylamine (7.5 g, 72 mmol), and 200 mL of anhydrous dichloromethane were charged to a flame-dried, 250-mL round-bottom flask equipped with a magnetic stir bar and placed in an ice bath. Methacryloyl chloride (7.7 g, 72 mmol) was added drop-wise. The flask was removed from the ice bath and the reaction was stirred for 24 h at room temperature. The reaction mixture was washed with aq 0.2 N sodium hydroxide (3 x 50 mL) followed by saturated NaCl solution (2 x 50 mL) and DI water (2 x 20). The organic phase was dried over anhydrous sodium sulfate. The solvent was evaporated and the product was dried under vacuum at room temperature overnight. The hydroxyhexyl ammonium bisdiethylphosphonate methacrylate monomer was dissolved in dichloromethane (20 mL) and stored at 4 °C. Hydroxypropyl ammonium bisdiethylphosphonate methacrylate monomer was synthesized in a similar manner.

5.2.5 Synthesis of acrylate-functional PEO

Poly(ethylene oxide) methyl ether (20 g, M_n = 5,000 g mol^{-1}, 4.0 mmol) was dried under vacuum at 50 °C overnight in a flame-dried 250-mL round bottom flask. Triethylamine (4.0 g, 40 mmol) and 100 mL of anhydrous dichloromethane were charged to the flask via syringe. Acryloyl chloride (3.6 g, 40 mmol) was added dropwise to the

flask via syringe. The reaction mixture was stirred at room temperature overnight. The mixture was diluted with chloroform and washed with an aqueous solution of sodium hydroxide (0.1 N, 3 x 50 mL). The organic phase was washed with water (2 x 50 mL), dried over anhydrous sodium sulfate and concentrated by evaporation. The concentrated mixture was precipitated in hexane, filtered and dried under vacuum at room temperature to afford a pale yellow acrylate-PEO powder.

5.2.6 Synthesis of a poly(ammonium bisdiethylphosphonate methacrylate)-g-PEO copolymer

The hexyl ammonium bisdiethylphosphonate methacrylate monomer (1.20 g, 2.3 mmol) and acrylate-PEO (0.6 g, 0.1 mmol) were charged to a flame-dried, 25-mL Schlenk flask equipped with a stir bar. Anhydrous DMF (4 mL) was added to the Schlenk flask and the reaction mixture was deoxygenated for 30 min. AIBN (0.02 g, 0.1 mmol) was dissolved in degassed DMF (5 mL) in a separate 20-mL vial. The freshly prepared AIBN solution (1 mL) was added to the Schlenk flask via syringe. After three freeze-pump-thaw cycles, the reaction mixture was heated at 70 °C for 7 h. The copolymer was precipitated in a cold mixture of 1:1 v:v anhydrous diethyl ether:hexane (2 x 400 mL). The resulting copolymer was vacuum dried at room temperature overnight to yield a 62:38 % wt/wt poly(hexyl ammonium bisdiethylphosphonate methacrylate)-g-PEO copolymer. A poly(propylammonium bisdiethylphosphonate methacrylate)-g-PEO copolymer was prepared using an analogous procedure.

5.2.7 Deprotection of the poly(ammonium bisdiethylphosphonate methacrylate)-g-PEO copolymers

A flame-dried, round-bottom flask equipped with a stir bar was charged with dry poly(hexylammonium bisdiethylphosphonate methacrylate)-*g*-PEO (1.0 g, 4.8 meq of phosphonate), TMSBr (2.2 g, 15 mmol) and 10 mL of anhydrous dichloromethane. The reaction was stirred at room temperature for 24 h. Dichloromethane and the excess TMSBr were removed by rotary evaporation at 75 °C and the copolymer was dried under vacuum at room temperature for 2 h. Anhydrous methanol (10 mL) was added to the flask via syringe. After 5 h the reaction mixture was precipitated in cold ether (400 mL) and filtered. The copolymer was dissolved in 10 mL of DI water and the pH was adjusted to 7.0. The solution was transferred into a 3,500 MWCO dialysis tube and dialyzed against 4 L of DI water for 48 h. The solution was freeze-dried to obtain the poly(hexyl ammonium bisphosphonic acid)-*g*-PEO.

5.2.8 Synthesis of a polyacrylic acid-g-PEO copolymer

tert-Butyl acrylate monomer (2.05 g, 16 mmol) and acrylate-PEO (1.15 g, 0.23 mmol) were charged to a flame-dried, 25-mL Schlenk flask equipped with a stir bar. Anhydrous toluene (14 mL) was added to the Schlenk flask and the reaction mixture was deoxygenated for 30 min. AIBN (150 mg g, 0.9 mmol) was dissolved in degassed toluene (5 mL) in a separate 20-mL vial. The freshly prepared AIBN solution (1 mL) was added to the Schlenk flask via syringe. After three freeze-pump-thaw cycles, the reaction mixture was heated at 70 °C for 24 h. The copolymer was precipitated in a cold mixture of 1:1 v:v anhydrous diethyl ether:hexane (2 x 400 mL) and the resulting copolymer was vacuum dried at room temperature overnight. The *t*-butyl ester groups were removed by

dissolving P(*t*BA)-g-PEO (0.8 g, 0.6 x 10^{-2} eq of *t*-butyl ester groups) in 30 mL of dichloromethane. Trifluoroacetic acid (3.5 mL, 4.6 x 10^{-2} mol) was added and the reaction mixture was stirred at room temperature for 24 h. The copolymer was precipitated into hexane and dried under vacuum at room temperature. The copolymer was dissolved in a 9:1 v:v THF:water mixture and dialyzed against 4 L of DI water through a cellulose acetate membrane (MWCO 3,500 g mol^{-1}) for 24 h. The final product was recovered by freeze-drying.

5.2.9 Synthesis of Manganese (II)-Graft Ionomer Complexes (*MaGICs*)

To fabricate *MaGICs*, graft copolymer solution (10.0 mg/mL in DI water) was filtered through a 1.0-μm syringe-driven filter unit (PTFE, Millipore) and subsequently added to a 20-mL vial equipped with magnetic stir bar. The graft copolymer solution was adjusted to pH 7.4 with 1.0 N NaOH. Manganese (II) chloride tetrahydrate solution (20.0 mg/mL in DI water) was added slowly into the polymer solution under stirring. The initial molar ratio of manganese to phosphorus (Mn:P) was kept at 1:1 (cloudy mixture) or 1:2 (clear mixture). The mixture was stirred at room temperature for 5 h and then transferred into a dialysis cassette (MWCO = 3,500 $gmol^{-1}$) and dialyzed against 2 L of DI water for 2 days, with two changes of water daily. The final complexes were recovered by freeze-drying.

5.2.10 Relaxivities of *MaGICs*

The proton longitudinal relaxation times (T1) and transverse relaxation times (T2) were measured on a Model mq-60 NMR Analyzer (Bruker Minispec) at a magnetic field strength of 1.4 T (ω_o = 60 MHz) and at 37.5 °C. T1's were obtained from fitting a monoexponential recovery curve to signal data generated with an inversion recovery (IR)

pulse sequence using ten logarithmically spaced inversion times between 50 and 10,000 ms. T2 was obtained from fitting a monoexponential decay curve to signal data generated by a Carr-Purcell-Meiboom-Gill (CPMG) spin-echo pulse sequence with an echo spacing of 1 ms and a repetition time of 6000 ms. Samples were diluted in DI water in the concentration range of 0.5-0.05 mg/mL and 500 μL of each concentration was transferred into a 7.5 mm NMR tube and equilibrated at 37 °C for 15 min prior to measurements. The relaxivities were calculated from the least-squares fit of the relaxation rate (or $1/T_1$ or $1/T_2$) as a function of manganese concentration (mM Mn). Mn concentrations were determined by inductively coupled plasma-atomic emission spectroscopy (ICP-AES).

5.2.11 Stability of *MaGICs* against Ca^{2+} ion displacement

A solution of *MaGICs in* 2.5 mM or 10.0 mM $CaCl_2$ solution (0.5 mg/mL) was prepared and stirred at room temperature for 1 or 24 h. In the first set of experiments, the solution was diluted with $CaCl_2$ solution to the concentration range of 0.5-0.05 mg/mL, then 500 μL of each concentration was transferred into a 7.5 mm NMR tube and equilibrated at 37 °C for 15 min prior to relaxivity measurements. In the second set of experiments, the solution mixtures were transferred to a centrifugal cellulose acetate membrane tube (MWCO 3,500) and centrifuged for 1 h. The filtrate was collected and the amount of Mn^{2+} was quantified by ICP-AES. Both relaxivity values and amount of released Mn^{2+} were compared with the values that were obtained from a similar protocol but without $CaCl_2$.

5.2.12 In vitro release of Mn ion

To determine the release of Mn from the complexes in physiological media, the required quantity of *MaGICs* (equivalent to ca. 500 μg Mn) were dispersed in 2 mL of PBS and placed in a 3500 MWCO dialysis cassette. The cassette was placed in a 250-mL beaker and 150 mL of PBS (pH 7.4) as the receptor medium was added to the beaker. The beaker was covered with Parafilm and maintained at 37 °C. Aliquots of 10 mL were taken from the receptor medium and placed in separate scintillation vials at each time point. At each time, 10 mL of fresh medium was added to the beaker to retain a constant volume. The Mn in each aliquot was measured by ICP-AES. A comparative release study was performed on $MnCl_2$ using a similar procedure.

5.2.13 Cellular cytotoxicity assessment

MTS assays were utilized to measure cytotoxicity of the free polymers and *MaGICs*. AML mouse hepatocyte cells were seeded into a 96-well plate at a density of 5,000 cells/well. Either free polymers, *MaGICs* or $MnCl_2$ were suspended in PBS and added at varying concentrations. After 24-hours of incubation, MTS assays were performed according to the manufacturer protocol.[32]

5.2.14 Phantom MRI

Solutions of *MaGICs,* MnDPDP, or GdDPTA in DI water were prepared with varying concentrations of Mn^{2+} or Gd^{3+} from 25 to 200 μM. Then 200 uL of each dispersion was transferred to a 96-well plate to prepare the phantom samples. MRI was performed on a 7 T small animal MRI scanner with a 40-cm horizontal bore (Bruker). T1-weighted MR images were acquired with a FLASH sequence with TR = 300 ms, TE = 4.1 ms, FA angle = 90°. The values reported are the averages of 2 samples. Regions of

interest (ROI) were drawn and signal intensities from each phantom image was obtained using PARAVISION Software (Bruker). Relative contrast signal enhancements from each agent were calculated by comparing signal intensities that were generated from the agents with that of DI water.

5.3 Results and Discussion

5.3.1 Synthesis of ammonium bisdiethylphosphonate methacrylate monomers and poly(ammonium bisdiethylphosphonate methacrylate)-g-PEO copolymers

We have previously reported a facile and mild method for synthesizing ammonium bisdiethylphosphonate acrylate and methacrylate monomers through a double aza-Michael addition of 3-aminopropanol across the double bond of bisdiethylphosphonate, followed by acylation with acryloyl or methacryloyl chloride.[31] Conventional free radical copolymerizations of the bisphosphonate containing monomers with acrylate-functional PEO macromonomers were conducted. It was found that copolymerizations with the methacrylate-functional ammonium phosphonate monomer incorporated the macromonomer efficiently while use of the acrylate-functional phosphonates produced heterogeneous blends of graft copolymers and homopolymers. These zwitterionic copolymers formed aggregates in water, likely due to electrostatic interchain attractions.

In this study, bisphosphonate methacrylate monomers with 3 and 6 methylenes between the methacrylate and the nitrogen were investigated to understand the effect of the alkyl chain length on polymer properties and hydrolytic stability. To prepare the bisphosphonate monomers, an aminoalcohol was simply reacted with diethyl vinylphosphonate in water to afford 6-hydroxyhexanol ammonium bisdiethylphosphonate

without the need for a catalyst. Subsequently, ammonium bisdiethylphosphonate-containing monomers were obtained by esterification of the hydroxyhexyl ammonium bisdiethylphosphonate with methacryloyl chloride (Figure 5.1). The chemical structures of the monomers were confirmed by ^{1}H NMR (Figure 5.2).

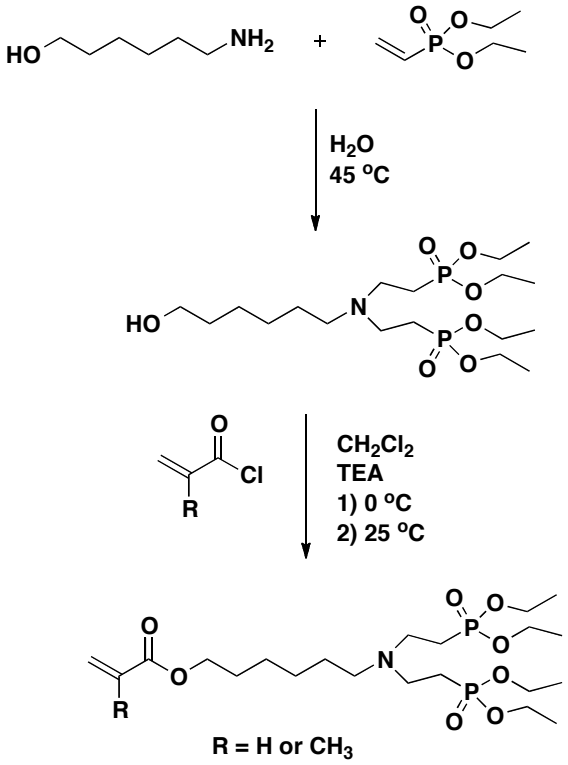

Figure 5.1 Synthesis of hexyl ammonium bisdiethylphosphonate methacrylate monomer

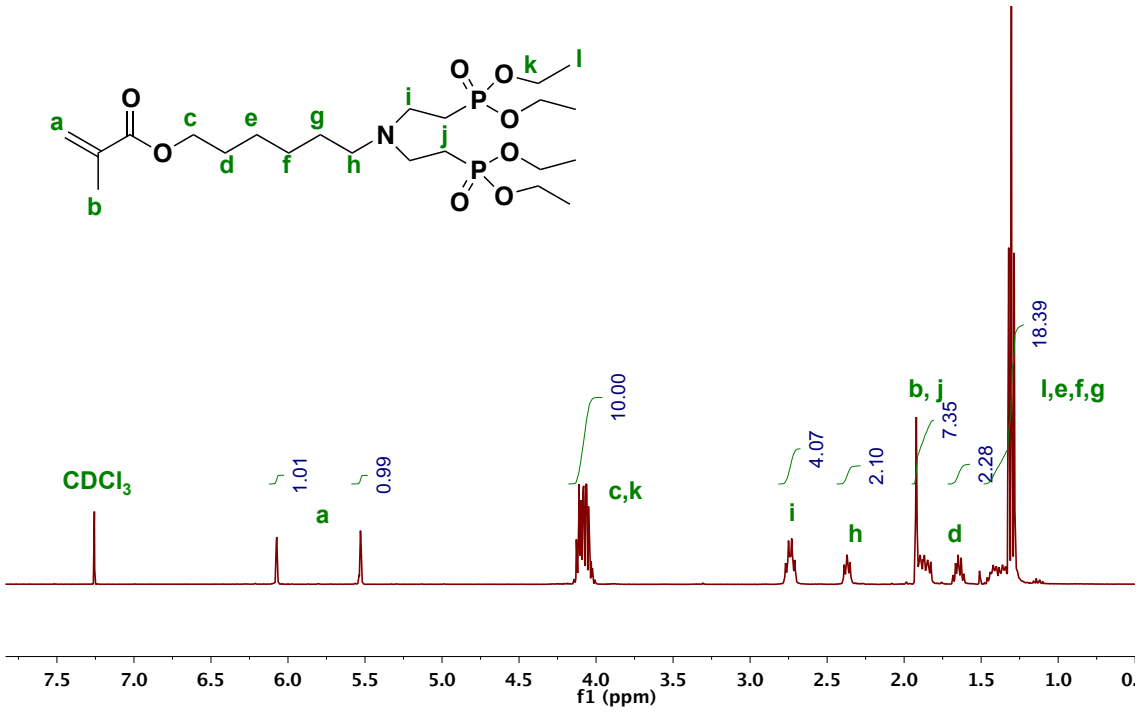

Figure 5.2 ^{1}H NMR spectrum of hexyl ammonium bisdiethylphosphonate methacrylate monomer

Ammonium bisdiethylphosphonate methacrylate monomers were then copolymerized with acrylate-PEO macromonomers through conventional free radical polymerization to yield graft copolymers with methacrylate-phosphonate backbones and PEO grafts (Figure 5.3) with the composition of 62:38 wt:wt poly(ammonium bisdiethylphosphonate acrylate):PEO as measured by ^{1}H NMR. The diethyl phosphonate pendent groups on the copolymers were then removed by using an excess of TMSBr in anhydrous dichloromethane to form trimethylsilyl phosphonates, then the trimethylsilyl groups were reacted with methanol to form poly(ammonium bisphosphonic acid methacrylate)-*g*-PEO copolymers.

^{1}H NMR confirmed quantitative removal of the ethyl groups without cleavage of the esters between the polymer backbone and the pendent groups. The signals at 1.2 and

4.0 ppm characterized the methyl and methylene groups in the bisdiethylphosphonates (Figure 5.4, top). The decrease of these signals (Figure 5.4, bottom) compared to the PEO repeat unit protons at 3.6 ppm indicated quantitative removal of the ethyl groups without loss of the pendent ammonium bisphosphonates. Before deprotection, the integration at 4.1 ppm was 161 relative to the PEO, this corresponds to 10 protons per repeat unit. Therefore, the integration of 161 corresponds to 16 repeat units of aminobisphosphonate. After deprotection, the integration at 4.1 ppm reduced to 30, corresponding to 2 protons remaining in the bisphosphonate unit, thus this represents 15 repeat units of aminobisphosphonate. The close agreement of the number of repeat units confirmed that the ester bonds were retained after deprotection. In addition, only a single peak in the ^{31}P NMR spectra was observed for each of the protected (Figure 5.5, top) and deprotected (Figure 5.5, bottom) copolymers. The single ^{31}P resonance shifted from 32 to 19 ppm after deprotection which was similar to data obtained in our previous study with polymer end groups.[33]

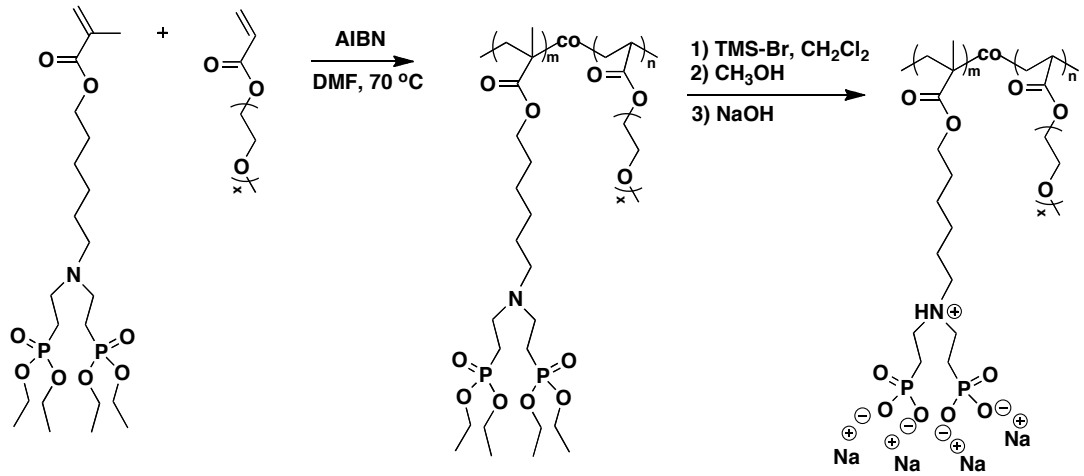

Figure 5.3 Synthesis of poly(ammonium bisdiethylphosphonate methacrylate)-g-PEO copolymers

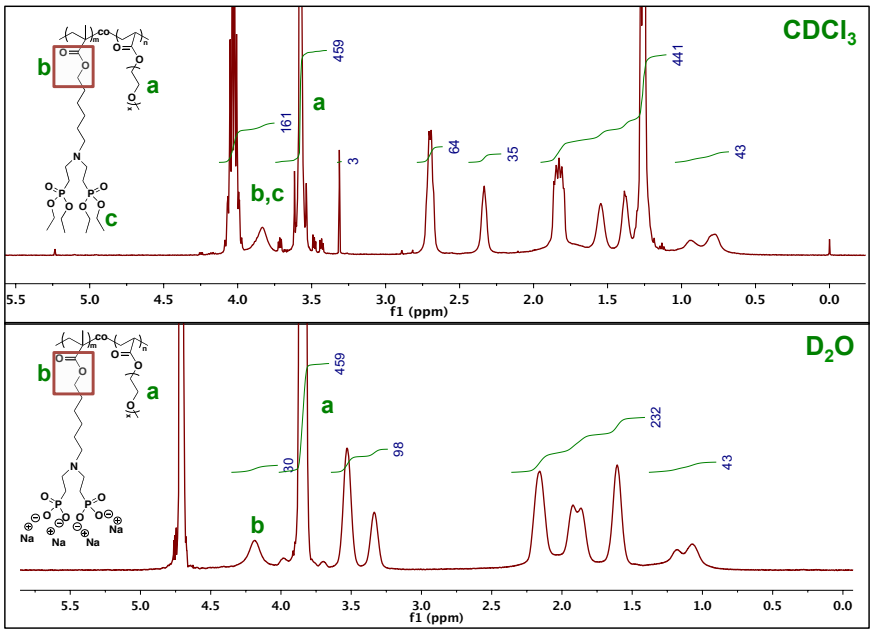

Figure 5.4 ^{1}H NMR spectra show quantitative deprotection of poly(ammonium bisdiethylphosphonate methacrylate)-g-PEO copolymers.

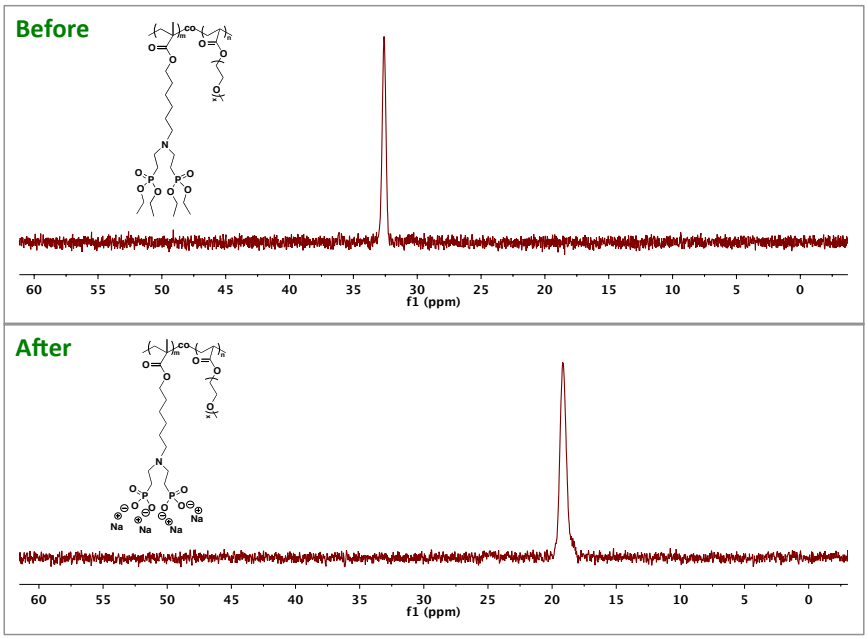

Figure 5.5 ^{31}P NMR spectra of protected poly(ammonium bisdiethylphosphonate methacrylate)-*g*-PEO and deprotected poly(ammonium bisphosphonate methacrylate)-*g*-PEO copolymers in DMSO-d_6

5.3.2 Synthesis and characterization of *MaGICs*

Block copolymers comprised of a carboxylate polyelectrolyte block and a PEO as a nonionic water-soluble block have been shown to bind electrostatically with cationic drugs or ions such as calcium to form block ionomer complexes (BICs). The carboxylate containing block and the cations were designed to form the cores of such complexes while the nonionic PEO block protruded outward into water to provide a polymer sheath that dispersed the complexes. However, the stability and characteristics of such complexes are disturbed by high ionic strength solutions with added salts due to shielding effects of ionic species on the Coulombic interactions. Therefore, approaches such as cross-linking the shell and the core have been reported to overcome this issue. In this case, the structures of the micelles become locked and can efficiently prevent any dissociation due to a fluctuating environment. [18-27]

Previously, Bronich et al. explored the use of ionic complexation of polyethylene oxide-b-polymethacrylic acid with Ca^{2+} to form micelles that were loaded with chemotherapeutic agents such as doxorubicin and cis-platin.[18-21] However, these polyion complexes were not stable enough in high ionic strength solution or physiological media. Therefore, the cores of these complexes were covalently crosslinked with dicystamine to enhance their stability.

In the present study, we investigated self-assembly between Mn^{2+} ions and the new graft copolymers containing ammonium bisphosphonate groups and compared these complexes with analogous polyacrylate-g-PEO (Figure 5.6). Fabrication of *MaGICs* was performed by simply mixing different feed ratios of Mn^{2+} salts with graft copolymer solutions. Ionic complexes formed spontaneously through electrostatic interactions and

possibly also chelation between Mn^{2+} cations and the polymers (Figure 5.7). ICP-AES revealed the amount of manganese in these complexes and the molar ratios of phosphorus or carbon to Mn in final complexes were calculated to be 2.0 and 3.3 (Table 5.1). The hydrodynamic intensity average diameters of the *MaGICs* as measured by DLS ranges from 56-130 nm.

To evaluate the colloidal stabilities of *MaGICs* under simulated physiological conditions, their hydrodynamic sizes in PBS containing 0.14 M NaCl were recorded as a function of time over 24 hours. Sizes of the aminobisphosphonate containing *MaGICs* (*Propyl and Hexyl MaGICs*) remained constant in PBS (Figure 5.8). This indicates that the particles were stable and did not dissociate in physiological conditions even without the additional crosslinking. On the other, the hydrodynamic sizes of complexes made from the carboxylate-containing graft copolymer (*Carboxyl MaGICs*) gradually increased over time, showing signs of both aggregation and sedimentation. The results clearly suggest that the amino bisphosphonate containing *MaGICs* should be sufficiently stable under physiological conditions, and therefore may be suitable for use as contrast agents or drug carriers.

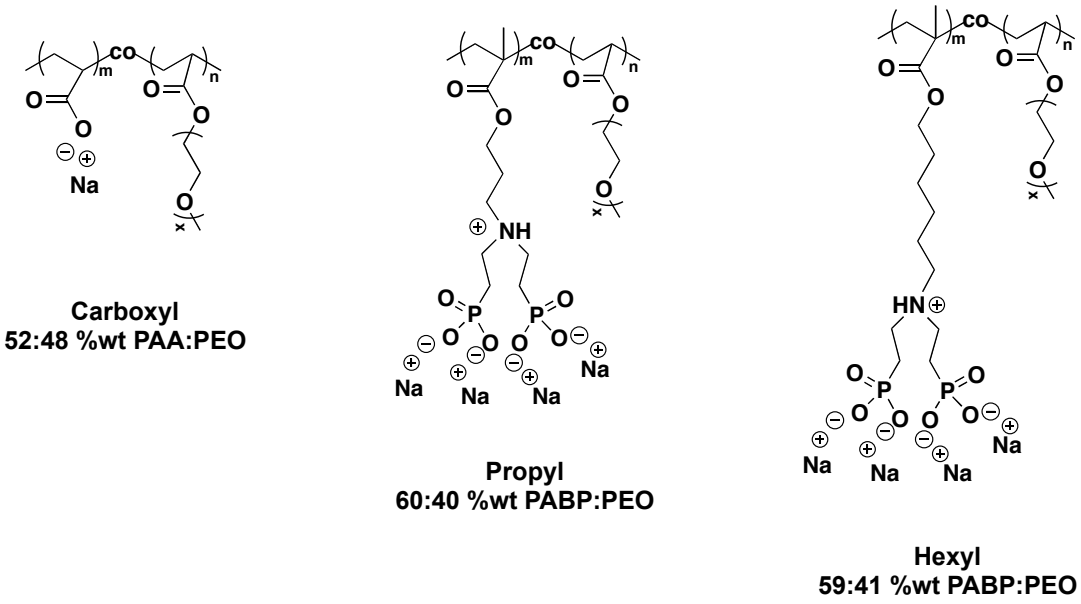

Figure 5.6 Types of graft copolymer used to fabricate *MaGICs*. In all cases, the M_n of PEO = 5,000 g mol^{-1}

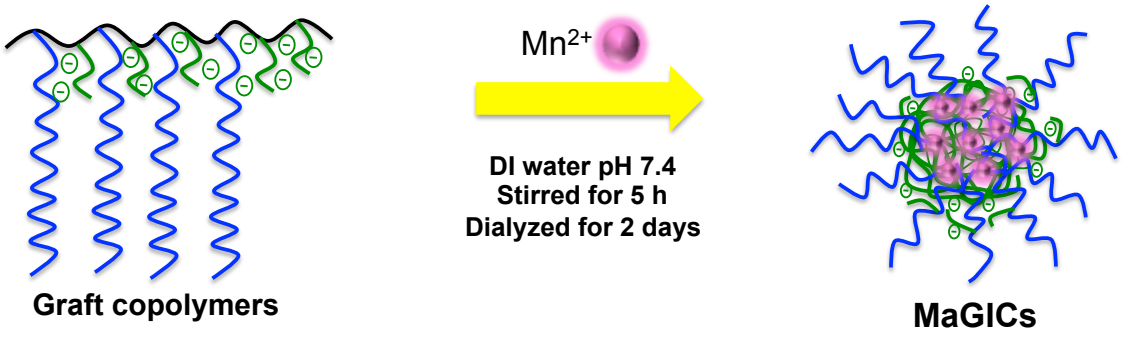

Figure 5.7 Schematic illustration of nanocomplex formation

Sample	Charged Mn (wt%)	Mn (wt%)	Mole of P/Mn or C/Mn	Intensity average diameter (nm)	PDI	Zeta Potential (mv)
Carboxyl MaGICs 2.0	21.7	10.6	2.0	130.2	0.25	-21.7
Propyl MaGICs 2.0	11.3	7.5	2.0	81.5	0.20	-19.0
Hexyl MaGICs 2.0	9.8	5.9	2.0	69.9	0.20	-18.7
Carboxyl MaGICs 3.3	10.8	7.5	3.3	113.6	0.23	-36.3
Propyl MaGICs 3.3	5.9	4.7	3.3	64.2	0.20	-37.5
Hexyl MaGICs 3.3	5.2	3.7	3.3	56.2	0.20	-37.3

Table 5.1 Physico-chemical properties of *MaGICs*

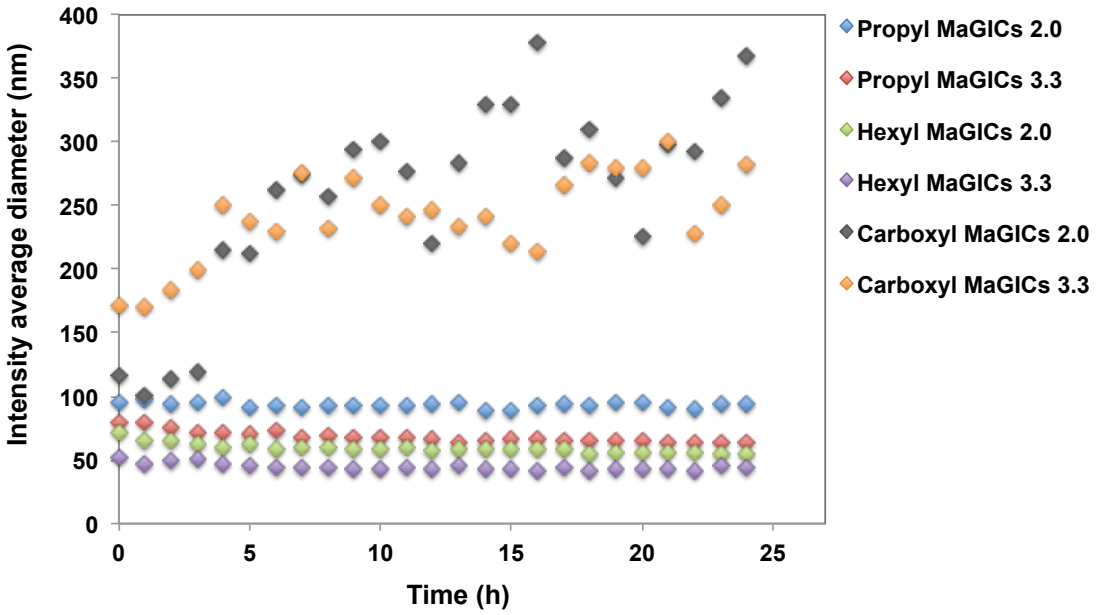

Figure 5.8 Stability of *MaGICs* in PBS, pH 7.4.

5.3.3 NMR Relaxivities of *MaGICs*

To determine the feasibility of *MaGICs* to be potent positive MRI contrast agents, the proton longitudinal relaxivities (r_1's) and transverse relaxivities (r_2's) were measured in water at the clinically-relevant field strength of 1.4 T and physiological temperature (37 °C). Table 5.2 shows relaxivities of *MaGICs* compared to $MnCl_2$ and a commercial positive contrast agent, MnDPDP. Most of the *MaGICs* exhibited 2-20 fold higher r_1's compared to those of $MnCl_2$ and MnDPDP (Table 5.2). Although it is not clear why relaxivities significantly increased upon complexation, one possible explanation is that the ionic and hydrophilic environment within the nanocomplexes facilitates the water-exchange and diffusion rates leading to efficient relaxation. With the same phosphorus to manganese ratio, the *Propyl MaGICs* had higher relaxivites followed by the *Hexyl MaGICs*. In terms of relaxivities, all of the ammonium bisphosphonate *MaGICs* appear to be attractive for use as MRI agents. While the carboxylate complexes had very high

relaxivities, they were colloidally unstable in the presence of salts, and thus likely would not be suitable for in vivo applications.

Sample	Mole of P/Mn or C/Mn	r_1	r_2/r_1	Size (nm)
$MnCl_2$	-	5.6	11.9	-
Carboxyl MaGICs	2.0	17.6	1.6	130.2
Propyl MaGICs	2.0	9.9	1.7	81.5
Hexyl MaGICs	2.0	4.2	2.1	69.9
Carboxyl MaGICs	3.3	40.9	1.6	113.6
Propyl MaGICs	3.3	25.7	1.6	64.2
Hexyl MaGICs	3.3	16.9	1.7	56.2
Mn-DPDP*	-	2.3	1.7	-

Table 5.2 Relaxivities of *MaGICs* in comparison with $MnCl_2$ and commercial positive contrast agent at 1.4T, 37 °C (unit = s^{-1} mM Mn^{-1})

5.3.4 Release profiles of Mn^{2+} ion from *MaGICs*

Small amounts of Mn ions are essential to human health. However, prolonged overexposure to free Mn ions has been found to cause some neurotoxicity.[7-9] Therefore, a fundamental issue for Mn ions as well as other metals as contrast agents is their complex stability because this is a critical property that reflects the potential release of free Mn ions.

To determine the stability of manganese in the nanocomplexes containing bisphosphonate groups, the release behavior of Mn^{2+} from *Propyl* and *Hexyl MaGICs* was explored at pH 7.4 and compared to those from *Carboxyl MaGICs*. Either $MnCl_2$ or

a *MaGIC* was dispersed in buffer and placed in a dialysis cassette. The cassettes were fully submerged in a beaker containing a 75-fold volume of receptor medium to ensure sink conditions. The release of Mn ions into the receptor medium was measured at respective time points by ICP-AES. As shown in figure 5.6, the control $MnCl_2$ fully diffused through the membrane into the receptor medium within 9 hours. The release rate of Mn from *Carboxyl MaGICs* was slower than the $MnCl_2$ control, but yet still fast considering that half of the Mn was released by 24 hours. On other hand, *Propyl* and *Hexyl MaGICs* drastically reduced the release of Mn reaching only 7 and 0 % respectively. This result confirms that interactions between Mn and aminobisphosphonate groups are much stronger than that of carboxylate groups.

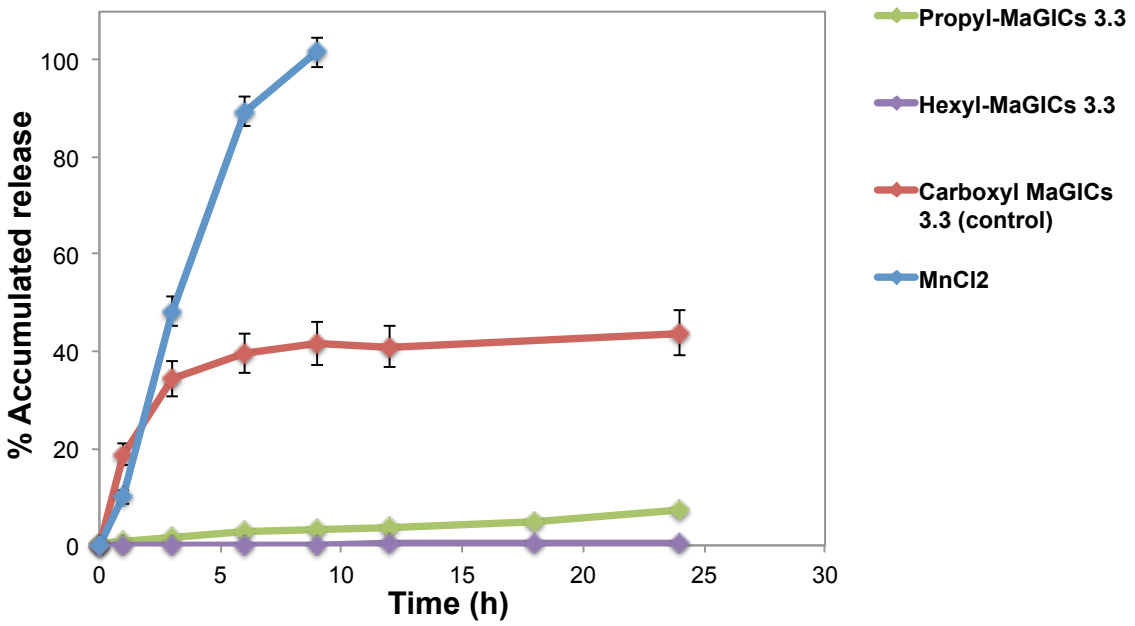

Figure 5.9 In vitro release profiles of Mn^{2+} in PBS, pH 7.4 at 37 °C

5.3.5 Hydrolytic stability of propyl aminobisphosphonate vs hexyl aminobisphonate graft copolymer

From the release results, we hypothesized that the 7% release of Mn from the *Propyl MaGICs* might be caused by partial hydrolysis of the ester bonds of the propyl aminobisphosphonate copolymer. The hydrolytic stabilities of propyl and hexyl aminobisphosphonate copolymers were compared under the conditions that were used for the manganese release study. Each copolymer was dispersed in PBS, pH 7.4 and stirred at 37 °C for 24 hours. The polymers were then freeze dried and characterized by ^{1}H NMR. Before the hydrolysis study, the integration at 4.1 ppm corresponding to 2 methylene protons next to the ester bonds of the propyl aminobisphosphonate copolymer was 36 relative to one PEO graft (figure 5.10). Therefore, the integration of 36 corresponds to 18 repeat units of propyl aminobisphosphonate. After the hydrolysis study, the integration at 4.1 ppm reduced to 27, thus indicating that approximately 5 repeat units of propyl aminobisphosphonate had been hydrolyzed. By contrast, the integration at 4.1 ppm remained the same for the hexyl aminobisphosphonate copolymer, indicating its hydrolytic stability (Figure 5.11). This can be at least partially attributed to the more hydrophobic nature of the hexyl aminobisphosphonate copolymer. The combined results from this investigation of manganese release and hydrolytic stability suggests that the manganese released from the *Propyl MaGICs* may have been due to ester hydrolysis instead of dissociation of manganese from the complex.

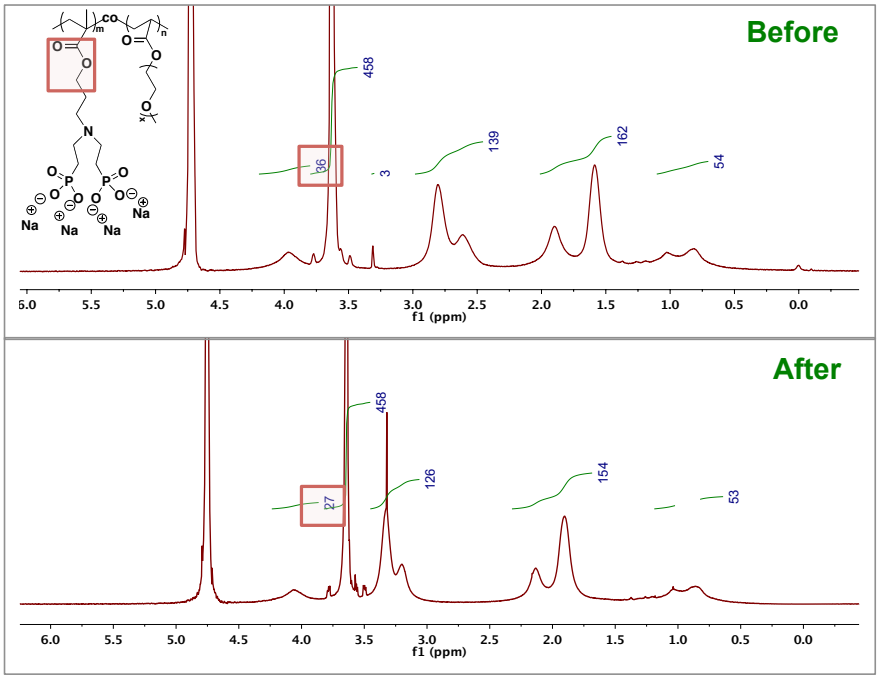

Figure 5.10 ^{1}H NMR spectra show the hydrolysis of propyl aminobisphosphoante copolymer

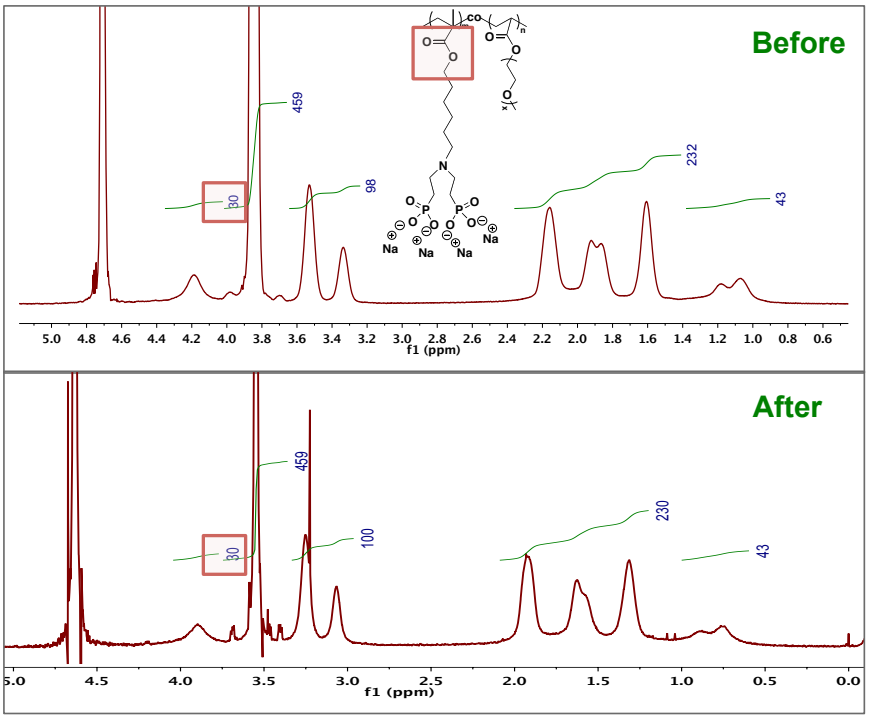

Figure 5.11 ^{1}H NMR spectra show the hydrolytic stability of hexyl aminobisphosphoante copolymer

5.3.6 Stability of *MaGICs* against Ca^{2+} ion displacement

Since free manganese ions exhibit some toxicities in vivo, it is of interest to confirm whether calcium ions would ion exchange with manganese ions to eliminate free manganese ions. The stability of *MaGICs* against Ca^{2+} displacement was explored by two methods. First, *MaGICs* were dispersed in either 2.5 or 10.0 mM $CaCl_2$ solution or DI water, and the solutions were stirred at room temperature for 1 or 24 hours. The relaxivities of *MaGICs* in the presence of $CaCl_2$ were then compared with those without $CaCl_2$. It was found that the relaxivities of *MaGICs* did not change significantly in any of the cases (Figure 5.12).

Secondly, to quantitatively measure any Mn^{2+} that was released, the *MaGICs*/$CaCl_2$ solution were treated as describe above, then transferred to centrifugal membrane tubes (MWCO 3,500) and centrifuged for 1 hour. Any Mn in the solutions that passed through the membrane was quantified by ICP-AES. The Mn in the solution containing $CaCl_2$ was compared with those without $CaCl_2$. No significant amount of Mn ion was detected in any of the solutions, (Table 5.3) showing that Ca^{2+} did not displace Mn^{2+} ion from the *MaGICs.* The results from both experiments suggest that *MaGICs* are stable against Ca^{2+} ion even above the physiological concentration of Ca^{2+}.

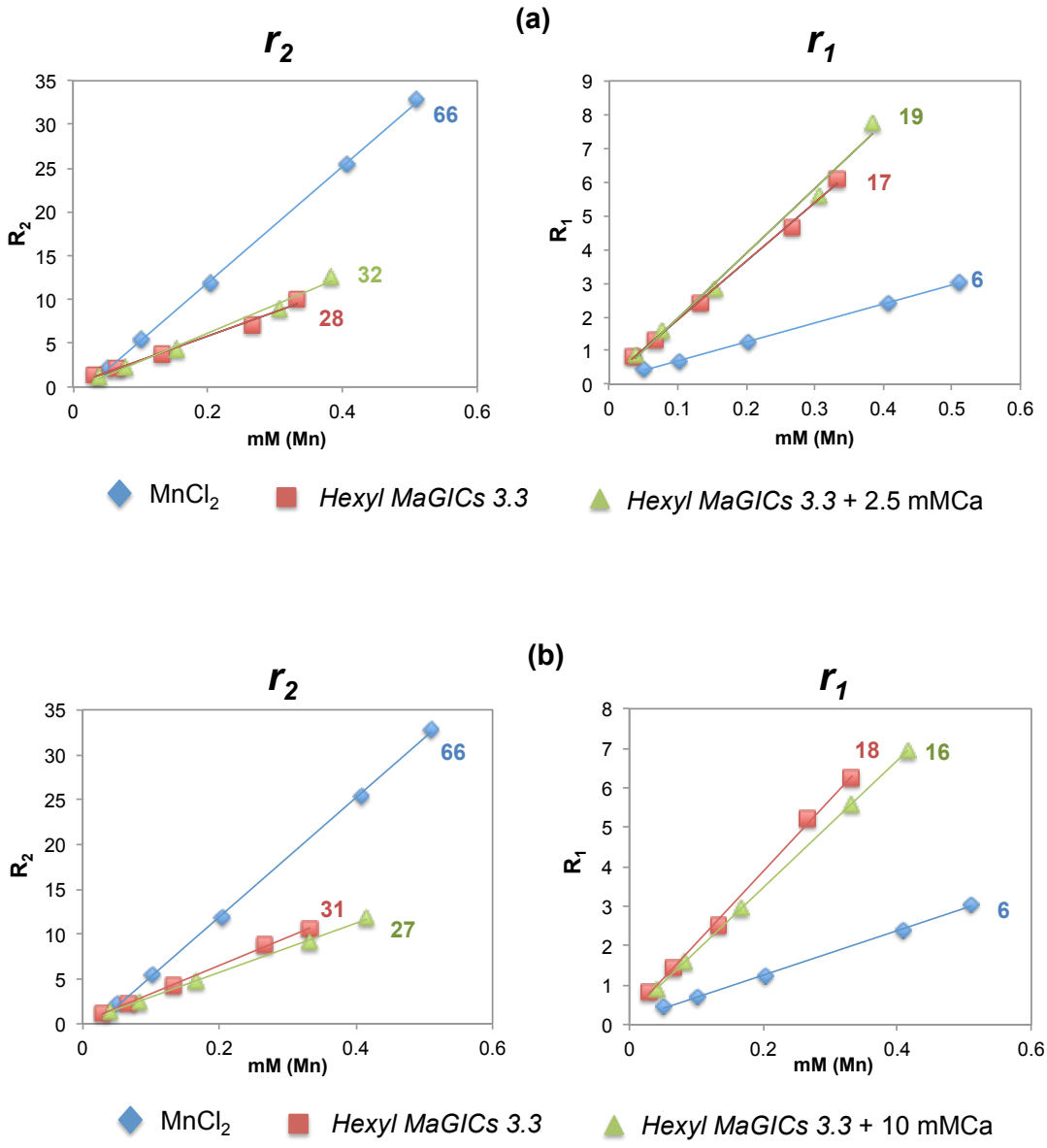

Figure 5.12 Relaxivities of *Hexyl MaGICs 3.3* before and after incubating with (a) 2.5 mM Ca solution for 1 h, and (b) 10.0 mM Ca solution for 24 h.

Sample	Ca concentration (mM)	Time (h)	% Release of Mn
Propyl MaGICs 3.3	0	1	0
Propyl MaGICs 3.3	0	24	0
Propyl MaGICs 3.3	2.5	1	0
Propyl MaGICs 3.3	10.0	24	0.13
Hexyl MaGICs 3.3	0	1	0
Hexyl MaGICs 3.3	0	24	0
Hexyl MaGICs 3.3	2.5	1	0
Hexyl MaGICs 3.3	10.0	24	0

Table 5.3 % Release of Mn from *MaGICs* after incubation with different concentrations of $CaCl_2$ for 1 and 24 h

5.3.7 MTS proliferation assay for cell viability

The potential toxicity of free polymers and *MaGICs* was assessed by in vitro cell proliferation MTS assays. Treatment of AML-12 cells with free polymers did not appear to cause any toxicity to the cells even at high concentrations (Figure 5.13). In the case of $MnCl_2$, cellular toxicity in AML12 cells was shown to be dependent on Mn concentration. Significant cell death with survival less than 20% was observed only with cells treated with $MnCl_2$ at 500 μM Mn. Neither *Propyl MaGICs* nor *Hexyl MaGICs* caused any significant decrease in cell survival (Figure 5.14). This can be explained by the fact that the *Propyl* and *Hexyl MaGICs* retain Mn^{2+} well and therefore mitigate cellular toxicity of free Mn^{2+} in the AML-12 cells.

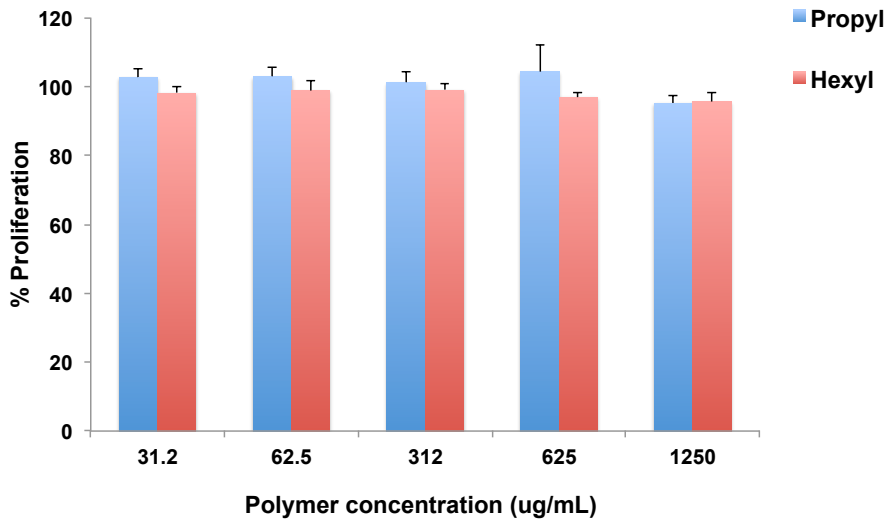

Figure 5.13 Cell viability of AML12 cells after 24 h incubation with various concentrations of free polymers; Propyl= poly(propyl ammonium bisdiethylphosphonate methacrylate)-g-PEO copolymer, Hexyl = poly(hexyl ammonium bisdiethylphosphonate methacrylate)-g-PEO copolymer.

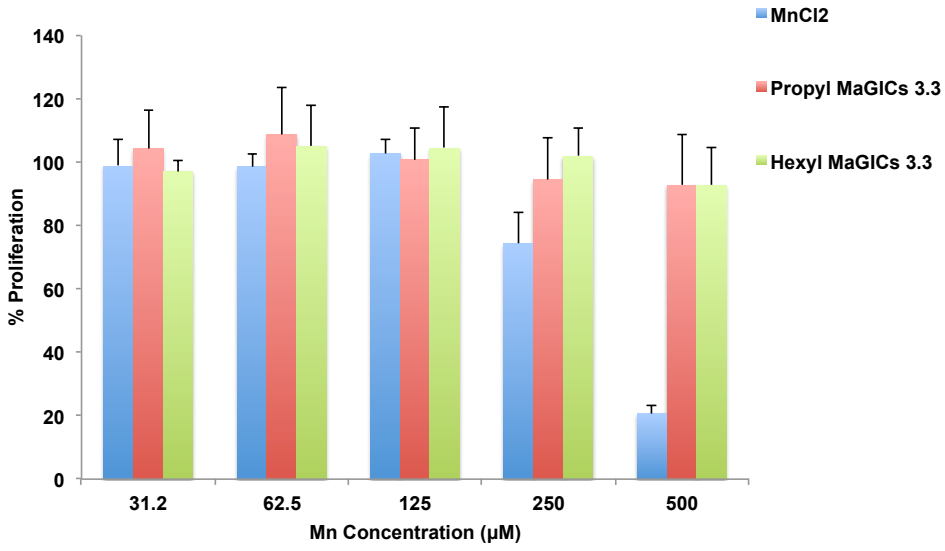

Figure 5.14 Cell viability of AML12 cells after 24 hours incubation with various concentrations of $MnCl_2$, *Propyl MaGICs 3.3* and *Hexyl MaGICs 3.3*

5.3.8 Phantom MRI

To investigate the potential of *MaGICs* as effective positive MRI contrast agents, phantom MR images were acquired using a 7.0 T MRI scanner. As shown in figure 5.15, the bright contrast signals obtained from aqueous dispersions of the *MaGICs* were more prominent relative to those of the commercial positive contrast agents MnDPDP and GdDPTA. Relative signal contrast enhancement was calculated by comparing signal intensities from the dispersions containing contrast agents to that of DI water. As shown in figure 5.16, the enhancements from *Propyl* and *Hexyl MaGICs 3.3* were superior to GdDTPA and MnDPDP. Even at the low concentration of 25 μM Mn^{2+} ion, contrast enhancements of ~ 50 % were already achieved. Comparing enhancement across the concentration range, both types of *MaGICs 3.3* were approximately 100% and 200% better than GdDTPA and MnDPDP respectively. *MaGICs 2.0*, though with less prominent contrast enhancement, still performed as well as the commercial agents. These results point out that the *MaGICs* are indeed promising for use as sensitive macromolecular MRI contrast agents.

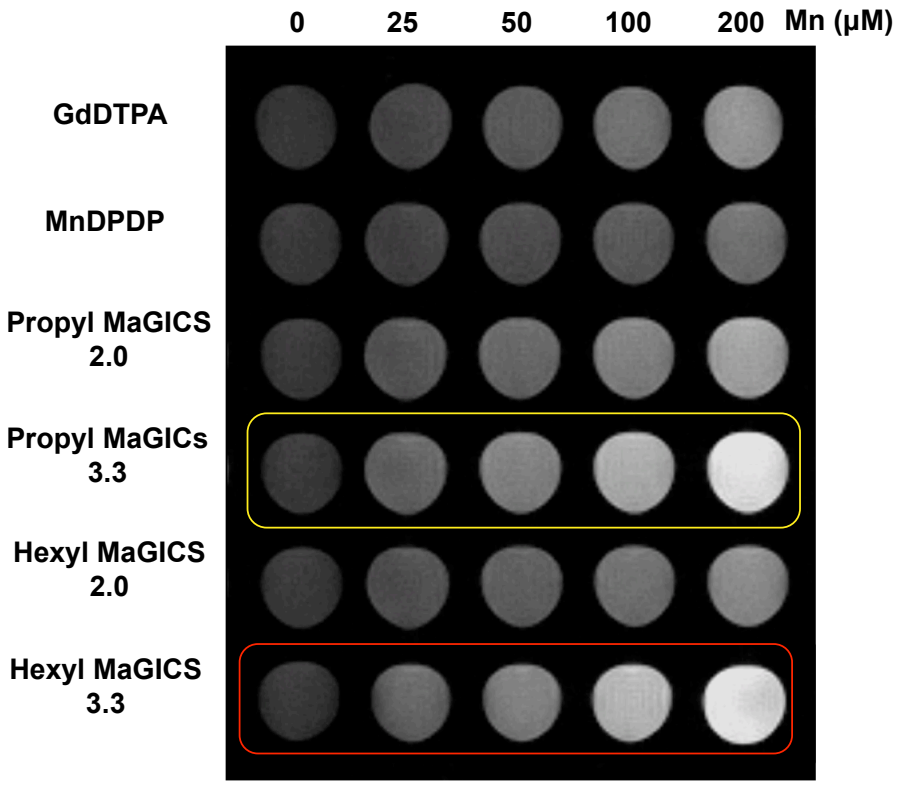

Figure 5.15 MR phantom images at 7.0 T of the *MaGICs,* MnDPDP and GdDTPA at various concentration of Mn^{2+} and Gd^{3+}.

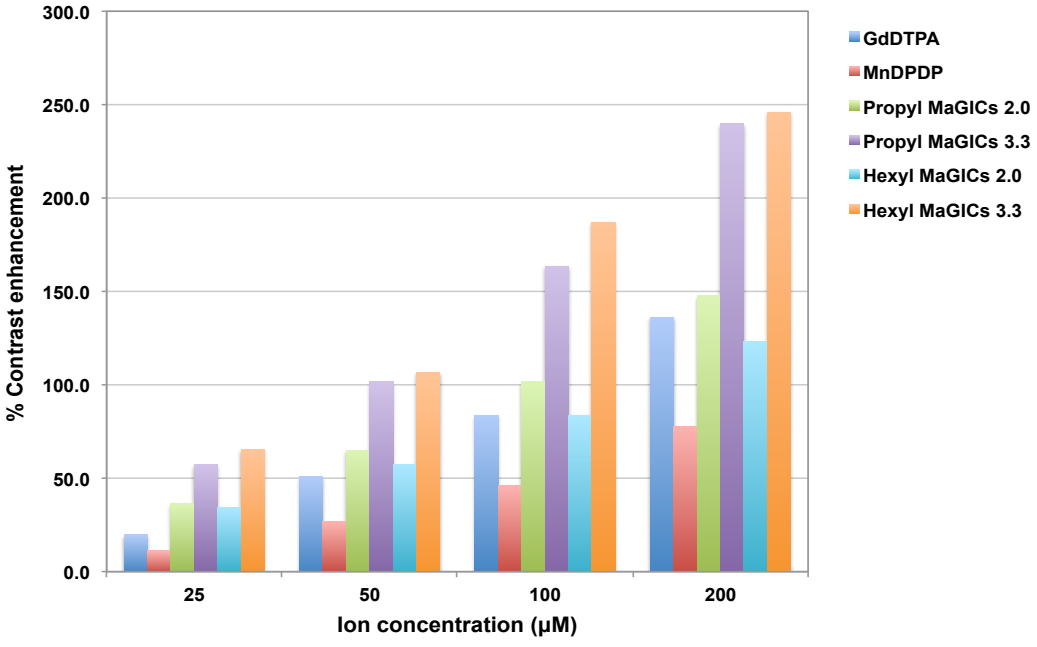

Figure 5.16 Comparison of % contrast enhancement

5.4 Conclusion

Overall, we have reported the formation of novel manganese graft ionomer complexes (*MaGICs*) for MRI positive contrast agents. The aminobisphosphonate containing *MaGICs* exhibited better complexation stability with manganese and better colloidal stability in simulated physiological media than carboxylate containing *MaGICs*. The complexes displayed high water solubility and did not reveal any in vitro toxicity against mouse hepatocytes. The relaxometric properties of the *MaGICs* were found to be superior to those of free manganese ions and commercial positive contrast agents, indicating the potential for these complexes as sensitive MRI contrast agents.

5.5 References

1. K. W.-Y. Chan, W.-T. Wong, *Coordination Chemistry Reviews*, 2007, **251**, 2428.
2. M. A. Sieber, T. Steger-Hartmann, P. Lengsfeld, H. Pietsch, *Journal of Magnetic Resonance Imaging*, 2009, **30**, 1268.
3. M. R. Prince, H. L. Zhang, J. C. Prowda, M. E. Grossman, D. N. Silvers, *Radiographics*, 2009, **29**, 1565.
4. J.-M. Idee, M. Port, A. Dencausse, E. Lancelot, C. Corot, *Radiologic Clinics of North America*, 2009, **47**, 855.
5. D. Pan, S. D. Caruthers, A. Senpan, A. H. Schmieder, S. A. Wickline, G. M. Lanza, *Wiley Interdisciplinary Reviews: Nanomedicine and Nanobiotechnology*, 2011, **3**, 162.
6. M. H. Mendona-Dias, E. Gaggelli, P. C. Lauterbur, *Seminars in Nuclear Medicine*, 1983, **13**, 364.

7. D. Pan, A. H. Schmieder, S. A. Wickline, G. M. Lanza, *Tetrahedron*, 2011, **67**, 8431.

8. P. C. Lauterbur, M. H. Dias, A. M. Rudin, P. L. Dutton, J. S. Leigh, e. A. Scarpa, *Frontiers of Biological Energetics*, 1987.

9. Z. Zhen, J. Xie, *Theranostics*, 2012, **2**, 45.

10. M. Kueny-Stotz, A. Garofalo, D. Felder-Flesch, *European Journal of Inorganic Chemistry*, 2012, **2012**, 1987.

11. P. l. Rongved, J. Klaveness, *Carbohydrate Research*, 1991, **214**, 315.

12. Z. Zhang, R. He, K. Yan, Q.-n. Guo, Y.-g. Lu, X.-x. Wang, H. Lei, Z.-y. Li, *Bioorganic & Medicinal Chemistry Letters*, 2009, **19**, 6675.

13. Y. Huang, X. Zhang, Q. Zhang, X. Dai, J. Wu, *Magnetic Resonance Imaging*, 2011, **29**, 554.

14. S. Aime, M. Botta, E. Gianolio, E. Terreno, *Angewandte Chemie*, 2000, **112**, 763.

15. A. Bertin, J. Steibel, A.-I. Michou-Gallani, J.-L. Gallani, D. Felder-Flesch, *Bioconjugate Chemistry*, 2009, **20**, 760.

16. A. Bertin, A.-I. Michou-Gallani, J.-L. Gallani, D. Felder-Flesch, *Toxicology in Vitro*, 2010, **24**, 1386.

17. M. Tan, X. Wu, E.-K. Jeong, Q. Chen, D. L. Parker, Z.-R. Lu, *Molecular Pharmaceutics*, 2010, **7**, 936.

18. A. V. Kabanov, T. K. Bronich, V. A. Kabanov, K. Yu, A. Eisenberg, *Macromolecules*, 1996, **29**, 6797.

19. T. K. Bronich, A. M. Popov, A. Eisenberg, V. A. Kabanov, A. V. Kabanov, *Langmuir*, 1999, **16**, 481.

20. T. K. Bronich, A. Nehls, A. Eisenberg, V. A. Kabanov, A. V. Kabanov, *Colloids and Surfaces B: Biointerfaces*, 1999, **16**, 243.

21. T. K. Bronich, A. V. Kabanov, V. A. Kabanov, K. Yu, A. Eisenberg, *Macromolecules*, 1997, **30**, 3519.

22. K. Kataoka, A. Harada, K. Yasugi, T. Matsumoto, S. Katayose, *Macromolecules*, 1996, **29**, 8556.

23. A. Harada, K. Kataoka, *Macromolecules*, 1995, **28**, 5294.

24. I. K. Voets, A. de Keizer, M. A. Cohen Stuart, *Advances in Colloid and Interface Science*, 2009, **147-148**, 300.

25. K. T. Oh, T. K. Bronich, L. Bromberg, T. A. Hatton, A. V. Kabanov, *Journal of Controlled Release*, 2006, **115**, 9.

26. L. Bromberg, M. Temchenko, T. A. Hatton, *Langmuir*, 2002, **18**, 4944.

27. L. Bromberg, *Journal of Controlled Release*, 2008, **128**, 99.

28. N. Sanson, F. d. r. Bouyer, M. Destarac, M. In, C. Garardin, *Langmuir*, 2012, **28**, 3773.

29. L. An, Y. Wang, X. Liu, N. Ma, H. Du, M. Jin, Y. Liu, L. Zhang, Y. Xu, P. Huang, Z. Sun, *Chemical and Pharmaceutical Bulletin*, 2011, **59**, 559.

30. M. S. Islam, W. S. Choi, Y. B. Lee, H.-J. Lee, *Journal of Materials Chemistry A*, 2013, **1**, 3565.

31. N. Hu, L. M. Johnson, N. Pothayee, N. Pothayee, Y. Lin, R. M. Davis, J. S. Riffle, *Polymer*, 2013, **54**, 3188.

32. http://www.promega.com/resources/protocols/technical-bulletins/0/celltiter-96-aqueous-nonradioactive-cell-proliferation-assay-protocol/.

33. N. Pothayee, S. Balasubramaniam, R. M. Davis, J. S. Riffle, M. R. J. Carroll, R. C. Woodward, T. G. St. Pierre, *Polymer*, 2011, **52**, 1356.

Chapter 6

Anticancer Drugs Loaded *MaGICs* for Dual MR Imaging and Chemotherapeutic Agent Delivery

N. Pothayee, N. Pothayee, N. Hu, R. Zhang, A. P. Koretsky and J. S. Riffle, *Journal of Materials Chemistry B*, 2013, submitted. Reproduced by permission of The Royal Society of Chemistry

6.1 Introduction

Cancer is a major public health burden and remains one of the world's most devastating diseases. Current treatments for cancer include surgical intervention, radiation and chemotherapeutic treatment. Although chemotherapeutic drugs have potent activity, they present major disadvantages including short plasma circulation half-lives, long elimination times, drug resistance, and nonspecific cell-cytotoxicity leading to severe side effects.[1-3]

To overcome these issues, chemotherapeutic drugs have been packaged or encapsulated into polymeric nanocarriers, which can prolong circulation half-life and decrease non-specific uptake into normal tissue.[4-11] Various anticancer drugs have been successfully loaded into polymeric nanoparticles with high loading efficiency. For example, Bronich and Kabanov et al. loaded both doxorubicin and cisplatin into crosslinked micelles of polymethacrylic acid-b-polyethylene oxide block copolymers.[4-6] The drug-loaded micelles efficiently released the drugs in physiological and acidic environments. They also exhibited cytotoxicity against cancer cells in vitro. Kataoka et al. conjugated doxorubicin with PEO-*b*-polyaspartic acid copolymers.[7-11] The drug-loaded micelles had prolonged circulation in blood compartments due to reduced uptake into the reticuloendothelial system (RES). Although the blood circulation time of anticancer drugs can be improved by polymeric nanocarriers, the distribution and accumulation of anticancer drugs in vivo are still largely unknown due to the lack of real-

time imaging capability to monitor their distribution *in vivo*. Therefore, nanocarriers that possess both chemotherapeutic and imaging functions are highly desirable. Such agents could allow control of the therapeutic efficacy in different individuals and ultimately lead to simultaneous diagnosis and treatment in clinical applications.

In chapter 5, we described the formation of manganese graft ionomer complexes (*MaGICs*) that contain Mn ions and polyaminobisphosphonate-*g*-PEO and these were shown to have good colloidal stability and MR imaging capability. In this chapter, we further report the possibility of using *MaGICs* for dual imaging and anticancer drug delivery. Chemotherapeutic drugs including doxorubicin, cisplatin and carboplatin were encapsulated into *MaGICs*. Their release behavior depends on pH of the medium, drug structures and payload. The anticancer drug-loaded *MaGICs* show excellent in vitro efficacy against the MCF-7 breast adenocarcinoma cell line as well as MRI contrast enhancement.

6.2 Experimental

6.2.1 Materials

Manganese (II) chloride tetrahydrate ($MnCl_2.4H_2O$, 99%), calcium (II) chloride anhydrous ($CaCl_2$, 99%), cis-diamineplatinum(II)dichloride (99%), carboplatin, sodium hydroxide solution (NaOH, 1.0 N), and hydrochloric acid (HCl, 1.0 N) were purchased from Sigma-Aldrich. Doxorubicin hydrochloride (99%) was purchased from Chemie Tek , USA. Deionized water was obtained through the MilliQ A10 water purification system (EMD Millipore, MA). Phosphate buffered saline (PBS) was obtained from Mediatech Inc. (VA, USA). Acetate buffer solution (ABS) was purchased from Fluka analytical. Dimethyl sulfoxide (HPLC grade) was obtained from Fisher Scientific and used as

received. Slide-A-Lyser dialysis cassettes (MWCO 3,500) were obtained from Thermo scientific. Centrifugal filter units (MWCO 10,000) were obtained from EMD Millipore. The poly(ammonium bisdiethylphosphonate methacrylate)-g-PEO copolymer was synthesized and characterized in a similar procedure to that reported in chapter 5. Breast adenocarcinoma (MCF-7) cells were received from the National Cancer Institute (NCI) (Frederick, MD).

6.2.2 Characterization

DLS measurements were conducted with a Malvern Zeta sizer NanoZS particle analyzer (Malvern Instruments Ltd) at a wavelength of 633 nm from a 4.0 mW, solid-state He-Ne laser at a scattering angle of 173° and at 25 ± 0.1 ˚C. Intensity, volume and number average diameters were calculated with the Zetasizer Nano 4.2. For DLS analysis, the dialyzed complexes were dispersed in DI water at a concentration of 0.5 mg mL^{-1}, and the dispersion was sonicated for 2 min in a 75T VWR Ultrasonicator (120 W, 45 kHz), then filtered through a 1.0 μm, Teflon^{TM} filter directly into a polystyrene cuvette for analysis.

UV-Vis spectroscopy was performed with an Evolution 300 Thermo Scientific UV-Visible spectrometer by measuring the absorbance of doxorubicin solutions at λ_{max}= 488 nm. The doxorubicin loaded complexes were dispersed in PBS at a concentration of 1.0 mg mL^{-1}, and the dispersion was sonicated for 2 min in a 75T VWR Ultrasonicator (120 W, 45 kHz), then transferred into a quartz cuvette for analysis.

The amount of bound platinum in the complexes was quantified using ICP-AES performed on a SPECTRO ACROS ICP 165 (Spectro Analytical Instruments, Germany).

6.2.3 Synthesis of Manganese(II)-Graft Ionomer Complexes (*MaGICs*)

To fabricate *MaGICs*, the graft copolymer solution (10.0 mg mL^{-1} in DI water) was filtered through a 1.0-μm syringe-driven filter unit (PTFE, Millipore) and added to a 20-mL vial equipped with magnetic stir bar. The pH of the solution was adjusted to 7.4 with 1.0 N NaOH. Manganese (II) chloride tetrahydrate solution (20.0 mg mL^{-1} in DI water) was added slowly to the polymer solution with stirring. The initial molar ratio of manganese to phosphorus (Mn:P) was kept at 1:2. The mixture was stirred at room temperature for 5 h and then transferred into a dialysis bag (MWCO = 3,500 $gmol^{-1}$) and dialyzed against 2 L of DI water for 2 days, with two changes of water daily. The final complexes were recovered by freeze-drying.

6.2.4 Synthesis and characterization of doxorubicin-loaded *MaGICs*

Doxorubicin-loaded *MaGICs* were prepared with various doxorubicin contents. For a targeted 20 wt % doxorubicin, 26.71 mg of doxorubicin hydrochloride was dissolved in phosphate buffer (3 mL, pH 7.4) and added dropwise to the *MaGICs* solution (100 mg in 3 mL phosphate buffer, pH 7.4). The mixture was sonicated for 5 min followed by stirring at room temperature for 3 h. The complex solution was transferred to a centrifugal filter unit equipped with a cellulose acetate membrane (MWCO of 10,000 g mol^{-1}) and centrifuged at 4000 rpm for 1 h to remove free drug and salt. The filtrates were discarded and the particles were removed from the membrane unit by re-dispersing them in 5 mL of DI water, and then the dispersion was freeze-dried to obtain doxorubicin loaded *MaGICs.*

Doxorubicin content was determined by using a UV-Vis spectroscopy calibration curve. To construct the calibration curve for assaying doxorubicin, doxorubicin

hydrochloride (3.2 mg, 3 mg doxorubicin) was dissolved in PBS (3 mL) in a scintillation vial and sonicated for 2 min to make a stock solution of doxorubicin with a concentration of 1 mg mL^{-1}. From this, a series of dilutions was performed to yield doxorubicin concentrations of 100, 50, 25, 12.5, 6.25 μg mL^{-1}. Aliquots of each solution (1 mL) were transferred to a quartz cuvette and the absorption at 488 nm was measured. The calibration curve was constructed by plotting the absorbance versus doxorubicin concentration.

To quantify the doxorubicin content in *MaGICs*, 5.0 mg of complexes were dispersed in 5 mL of PBS and sonicated for 1 min. The solution (1 mL) was transferred to a quartz cuvette and the absorption at 488 nm was measured. The *MaGICs* alone did not absorb at this wavelength.

6.2.5 Synthesis and characterization of cisplatin-loaded *MaGICs*

Cisplatin loading was performed at different feed weight ratios of platinum to *MaGICs* of 5, 10 and 20 wt %. For a targeted 20 wt % platinum, 38.50 mg of cis-diamineplatinum (II) chloride was dispersed in 0.5 mL of DMSO and added dropwise to the *MaGICs* solution (100 mg in 4.5 mL phosphate buffer) with stirring. The solution was sonicated for 5 min followed by stirring at room temperature for 12 h. Unincorporated drugs and DMSO were removed by dialysis against DI water (4 L, 24 h). The external medium was renewed one time in the course of dialysis. Then the solution was freeze-dried to obtain cisplatin-loaded *MaGICs.* The percent of loaded cisplatin in the *MaGICs* was quantified by ICP-AES.

6.2.6 Synthesis and characterization of carboplatin-loaded *MaGICs*

Carboplatin-loaded *MaGICs* were prepared with platinum contents at 5, 10, and 20 wt % relative to *MaGICs*. To prepare complexes with a targeted content of 20 wt %, 24 mg of carboplatin was dispersed in phosphate buffer (3 mL, pH 7.4) and added dropwise to the *MaGICs* solution (50 mg in 5 mL phosphate buffer, pH 7.4). The mixture was sonicated for 5 min followed by stirring at room temperature for 24 h. The complex solution was transferred to a centrifugal filter unit equipped with a cellulose acetate membrane (MWCO of 10,000 $gmol^{-1}$). Free drugs and salts were removed by centrifuging the dispersion at 4000 rpm for 1 h. This allowed the liquid to pass through the membrane into the bottom of the centrifugation unit, and the particles were collected on the membrane. They were removed from the membrane by re-dispersing them in 5 mL of DI water, and then the dispersion was freeze-dried to obtain carboplatin loaded *MaGICs*. The amount of loaded platinum was measured by ICP-AES.

6.2.7 Release study of doxorubicin from *MaGICs*

To determine the release of doxorubicin, drug-loaded *MaGICs* (equivalent to ca. 4000 μg doxorubicin) were dispersed in 3 mL of either phosphate buffered saline (PBS, pH 7.4) or acetate buffered saline (ABS, pH 4.5) and transferred to the dialysis cassette (3,500 MWCO g mol^{-1}). The cassette was placed in a 250-mL beaker containing 100 mL of either PBS or ABS as the receptor medium. The beaker was covered with Parafilm and maintained at 37 °C. At each prescribed time, a 2-mL aliquot was removed and fresh PBS or ABS was added to the beaker to retain constant volume. The aliquots were freeze-dried and re-dispersed in 1 mL of PBS. The doxorubicin content was determined by UV-

Vis spectroscopy by measuring the absorbance at λ_{max} = 488 nm. A similar procedure was performed with doxorubicin as the free drug control.

6.2.8 Release study of cisplatin or carboplatin from *MaGICs*

To determine the release of cisplatin or carboplatin, the required quantity of cisplatin or carboplatin-loaded *MaGICs* (equivalent to ca. 4000 μg Pt) was dispersed in either PBS pH 7.4 or ABS pH 4.5 and transferred to a dialysis cassette (MWCO 3,500 g mol^{-1}). The dialysis cassette was placed into a receptor medium containing 100 mL of either PBS or ABS pH. The beaker was covered with Parafilm and maintained at 37 °C. At prescribed times, 10-mL aliquots were removed from the receptor medium and placed in separate scintillation vials. Fresh PBS or ABS (10 mL) was added to the beaker to retain constant volume. The amount of Pt in each aliquot was quantified by ICP-AES.

6.2.9 Relaxivity measurements

The proton longitudinal relaxation times (T1) and transverse relaxation times (T2) were measured on a Model mq-60 NMR Analyzer (Bruker Minispec) at a magnetic field strength of 1.4 T (ω_o = 60 MHz) and at 37.5 °C. T1's were obtained from fitting a monoexponential recovery curve to signal data generated with an inversion recovery (IR) pulse sequence using ten logarithmically spaced inversion times between 50 and 10,000 ms. T2 was obtained from fitting a monoexponential decay curve to signal data generated by a Carr-Purcell-Meiboom-Gill (CPMG) spin-echo pulse sequence with an echo spacing of 1 ms and a repetition time of 6000 ms. Samples were diluted in DI water in the concentration range of 0.5-0.05 mg mL^{-1} and 500 μL of each concentration was transferred into a 7.5 mm NMR tube and equilibrated at 37 °C for 15 min prior to measurements. The relaxivities were calculated from the least-squares fit of the relaxation

rate (or 1/T1 or 1/T2) as a function of manganese concentration (mM Mn). Mn concentrations were determined by ICP-AES.

6.2.10 In vitro cellular toxicity against cancer cells

Cytotoxicity of anticancer drugs loaded *MaGICs* against MCF-7 breast cancer cells were assessed by MTT proliferative assay. Different amounts of drug-loaded *MaGICs* were prepared and resuspended in 0.1 mL DPBS using a sonicator bath for 5 min to ensure thorough redispersion of the complexes. These concentrated solutions were used as stock solutions to prepare various concentrations of drug-loaded complexes (on basis of free drugs). Serial dilutions were made with complete media (RPMI 1640, 2 mM glutamine supplemented with 10 % FBS). To perform the test, MCF-7 were seeded into a 96-well plate at density of 5000 cells/well and allowed to adhere and recovered for 24 h. The media were removed and 100 uL of each drug concentration was added to the wells. MCF-7 cells were exposed to drug-loaded *MaGICs* for 48 h at 37 °C under humidified 5% CO_2 incubator. 10 **µ**l of MTT indicator dye (5 mg/ml) was added to each well and the cells were incubated for 4 h at 37 °C under humidified 5 % CO_2 incubator. The medium was then removed, 100 uL of DMSO was added and the UV-Vis absorbance at 490 nm was read using a microplate reader, employing cell-free media as a blank. Antiproliferative effects of *MaGICs* were compared with those of free drugs using similar protocol and drug concentrations. The averaged proliferative values were expressed in percentages of the values obtained from cells that were not treated with either free drug or drug loaded-*MaGICs*. All results were obtained from triplicate independent runs.

6.3 Results and Discussion

6.3.1 Synthesis and characterization of anticancer drugs-loaded *MaGICs*

The aim of this work was to develop MR-active imageable Mn-based polymeric nanocarriers (*MaGICs*) that are suitable for delivering a wide range of chemotherapeutic agents. We envision that bisphosphonate anions can form robust ionic interactions with oppositely charged drugs. Three cancer drugs including doxoroubicin, cisplatin, and carboplatin (figure 6.1 and 6.2) were selected as candidates to investigate the hypothesis.

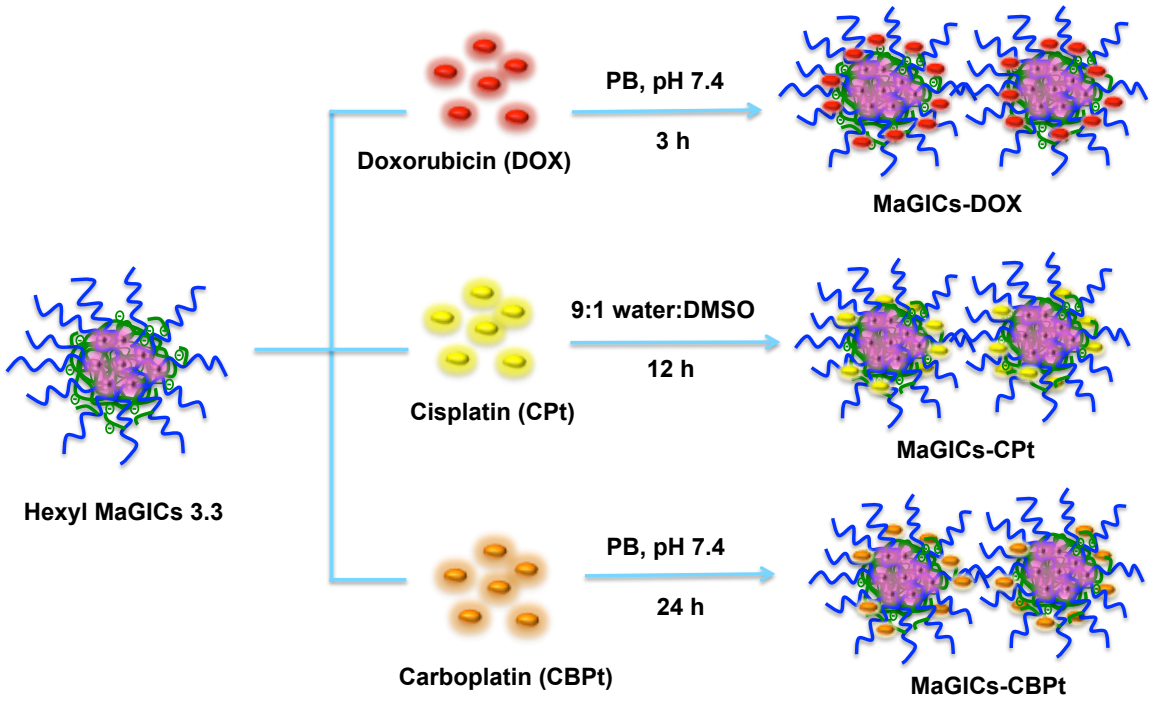

Figure 6.1 Synthesis of anticancer drugs loaded *MaGICs*

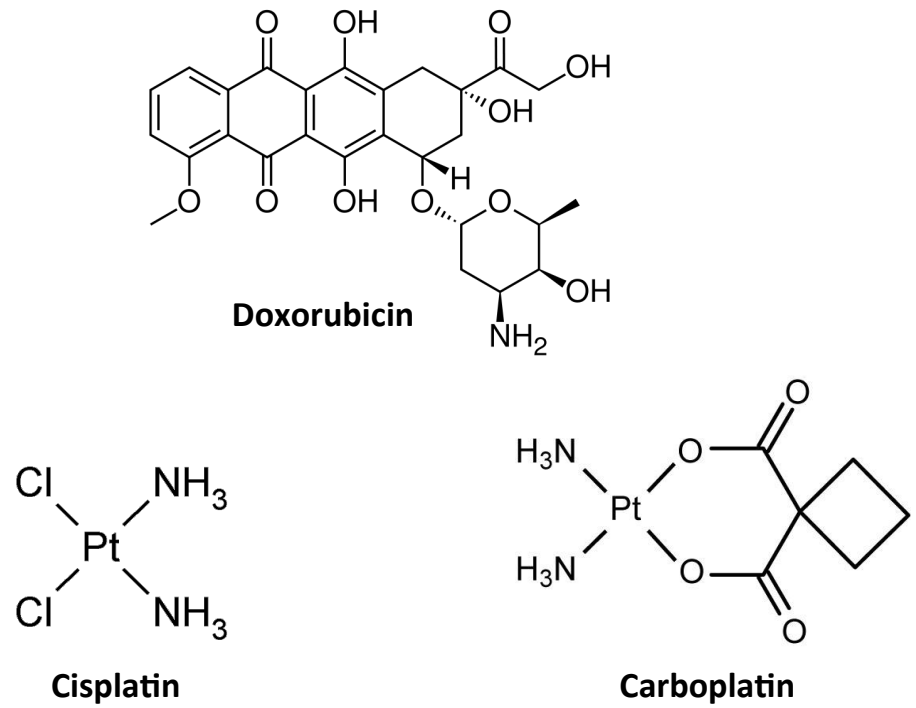

Figure 6.2 Structures of anticancer drug in this study

6.3.1.1 Doxorubicin-loaded *MaGICs*

Doxorubicin is a widely used anticancer chemotherapeutic belonging to a family of anthracyclines. Despite its potent activity, doxorubicin has a number of disadvantages including a short plasma circulation half-life, long elimination half-life, and nonspecific cell-cytotoxicity leading to severe side effects.[12, 13] In order to improve the selectivity of doxorubicin and thereby overcome systemic toxicities, tremendous efforts have been made to develop polymeric nanocarriers for this drug.[14-18]

Herein, the net anionic charge characteristics of the polyaminobisphosphonate segments of *MaGICs* enable efficient encapsulation of positively charged doxorubicin at pH 7.4. At this pH, it is expected that the ammonium bisphosphonate groups are mostly ionized with a net charge of approximately -3. It was observed that doxorubicin loading increased almost linearly with doxorubicin feed ratios (4.6 to 14.5 wt%). On the other

hand, encapsulation efficiency (% EE), which corresponds to the percentage of the charged doxorubicin that was encapsulated into the particles, decreased slightly with increasing doxorubicin feed percentage. This could be due to less availability of phosphonate anions with increasing encapsulation of doxorubicin molecules.

Upon doxorubicin encapsulation, the physicochemical properties of *MaGICs* were altered. As shown in Table 6.1, the intensity-average diameters of nanocomplexes increased proportionally with the % doxorubicin. In addition, the zeta potentials of the particles significantly decreased from -37.3 mV to near zero upon doxorubicin loading, indicating that the cationic drug had effectively bound to the *MaGICs*.

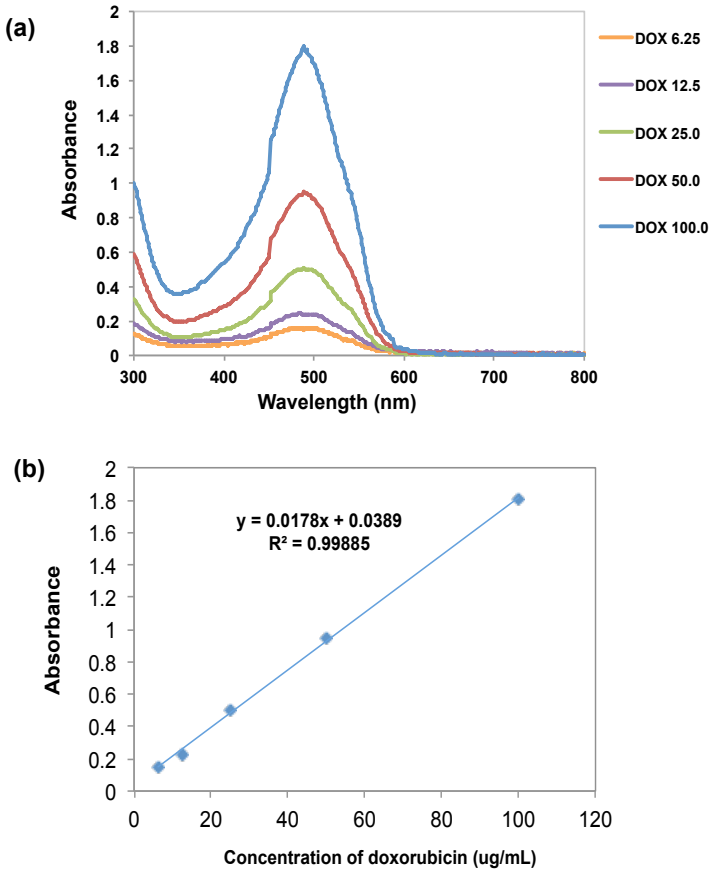

Figure 6.3 a) absorbance spectra of doxorubicin at various concentration in PBS and b) calibration curve of doxorubicin by absorbance measurement at 488 nm.

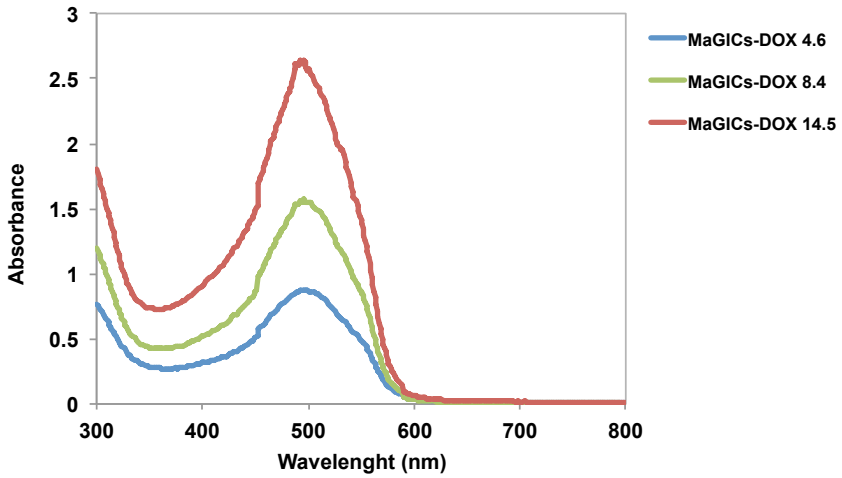

Figure 6.4 Absorbance spectra of doxorubicin loaded *MaGICs* in PBS

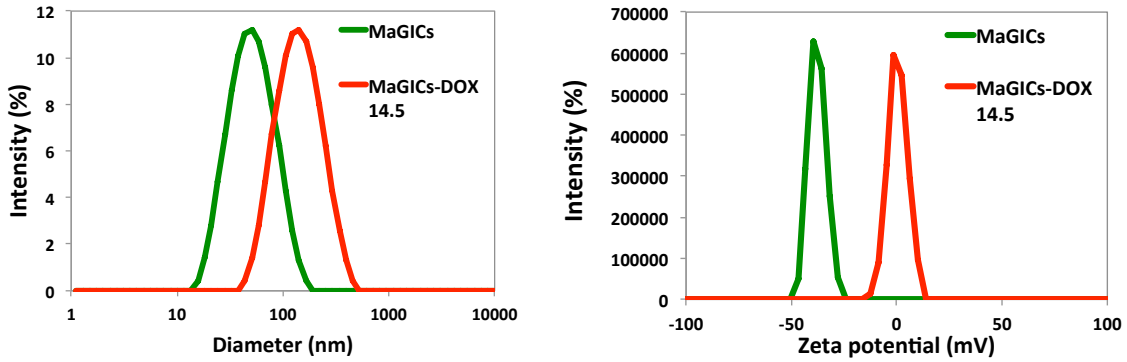

Figure 6.5 Intensity average diameter and zeta potential distributions of *MaGICs* and *MaGICs-DOX 14.5*

Sample	Charged DOX (wt%)	Found DOX (wt%)	%EE	Intensity average diameter (nm)	PDI	Zeta Potential (mV)
MaGICs	-	-	-	56.2	0.20	-37.3
MaGICs-DOX 4.6	5.0	4.6	92	107.7	0.19	-14.80
MaGICs-DOX 8.4	10.0	8.4	84	118.6	0.17	-6.40
MaGICs-DOX 14.5	20.0	14.5	73	123.2	0.17	-3.15

Table 6.1 Characteristics of Doxorubicin loaded *MaGICs*

6.3.1.2 Cisplatin-loaded *MaGICs*

cis-Dichlorodiamineplatinum (II) (Cisplatin, CPt) is a well-known platinum-based anticancer drug that remains one of the first line of chemotherapeutic drugs for treatment of various malignant tumors. However, its clinical use has a limitation due to significant toxic side effects including acute nephrotoxicity and chronic neurotoxicity.[19, 20] Cisplatin also has very short circulation times in the blood due to glomerular excretion.

It is known that two chloride ligands in cisplatin can be substituted by a variety of reactive groups such as carboxylates and amines.[8, 21-24] Several studies have reported on carboxylate-containing polymers as carriers for cisplatin. However, conjugation to homopolymers and alternating copolymers often results in poorly soluble and unstable drug-polymer conjugates.[21, 22] Therefore, carboxylate-containing PEO copolymers such as PEO-poly(aspartic acid) or PEO-poly(glutamic acid) block copolymers were employed to form soluble and stable drug loaded micelles.[8, 23, 24]

In this work, we found that aminophosphonate groups on the hexyl bisphosphosphonate polymers complexed with cisplatin, likely due to a combination of chelation and electrostatic bonds. The targeted encapsulation weights of Cisplatin in these polymer complexes were 5, 10, and 20 wt %. The cisplatin was dissolved in DMSO and slowly added into an aqueous solution of the polymer to form a clear dispersion without any sedimentation. Cisplatin-loaded *MaGICs* formed via substitution of the polymer displacing the chlorides. Attempts to use only water in the encapsulation process were unsuccessful due to the poor water solubility of cisplatin. After 12 hours of mixing to allow for complex formation, free cisplatin and DMSO were removed and the concentrations of encapsulated cisplatin were determined by ICP-AES. As shown in

Table 6.4, consistent with the observations upon doxorubicin loading, zeta potentials of the *MaGICs* also decreased with cisplatin loading. Binding of cisplatin to the *MaGICs* also led to an increase of particle size from ca. 50 nm to ca. 120-130 nm. Increases in particle sizes were most likely due to some condensation of multiple *MaGICs* into one complex.

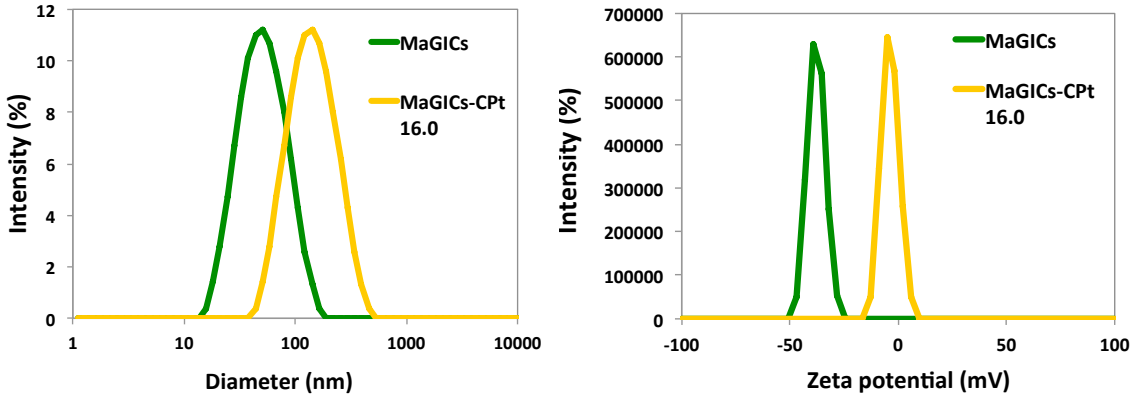

Figure 6.6 Intensity average diameter and zeta potential distributions of *MaGICs* and *MaGICs-CPt 14.5*

Sample	Charged Pt (wt%)	Found Pt (wt%)	% EE	Intensity average diameter (nm)	PDI	Zeta potential (mV)
MaGICs	-	-	-	56.2	0.20	-37.8
MaGICs-CPt 5.0	5.0	5.0	100	119.9	0.22	-19.8
MaGICs-CPt 9.7	10.0	9.7	97	122.5	0.19	-9.2
MaGICs-CPt 16.0	20.0	16.0	80	138.8	0.22	-8.1

Table 6.2 Characteristics of Cisplatin loaded *MaGICs*

6.3.1.3 Carboplatin-loaded *MaGICs*

Carboplatin (cis-diamine(1,1-cyclobutanedicarboxylato)-platinum, CBPt) a cisplatin analogue, is an anticancer drug with an activity profile similar to cisplatin and used predominantly to treat ovarian cancer. This second-generation platinum drug has

fewer side effects than cisplatin and is commonly used in combination therapies.[19] Carboplatin is more soluble in water with a solubility of 10.0 mg mL^{-1} compared to 2.5 mg mL^{-1} for cisplatin (25 °C).[25] Thus, employing water as a medium was sufficient for the loading protocol, but efficient complex formation required longer times. The coordination bonds between the cyclobutanedicarboxylate ligand and Pt ion in carboplatin are stronger than those of chloride ions in cisplatin. This may have caused a slower ligand exchange rate in the case of carboplatin and *MaGICs*. An attempt to react the carboplatin with *MaGICs* for 12 hours produced only 20 % drug encapsulation efficiency (EE). The mixture was allowed to react for 24 hours and 65-90 % EE was achieved. Similar to loading of doxorubicin and cisplatin, encapsulation of carboplatin lead to an increase of the intensity average diameters proportionally to feed ratios. The surface charges were also significantly reduced, indicating that the drug had been effectively encapsulated (Table 6.3).

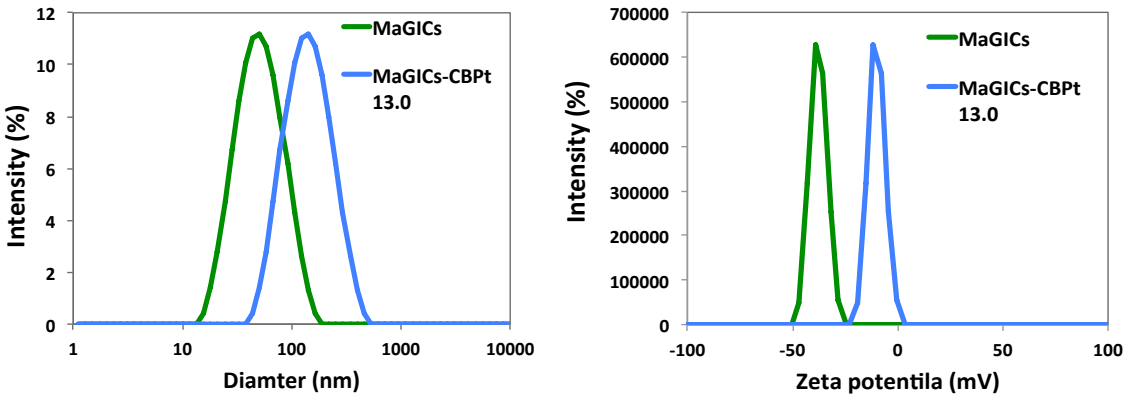

Figure 6.7 Intensity average diameter and zeta potential distributions of *MaGICs* and *MaGICs-CBPt 13.0*

Sample	Charged Pt (wt%)	Found Pt (wt%)	% EE	Intensity average diameter (nm)	PDI	Zeta potential (mV)
MaGICs	-	-	-	56.2	0.20	-37.8
MaGICs-CBPt 4.7	5.0	4.7	94	91.2	0.22	-32.1
MaGICs-CBPt 7.7	10.0	7.7	77	121.1	0.22	-22.4
MaGICs-CBPt 13.0	20.0	13.0	65	134.8	0.19	-10.2

Table 6.3 Characteristics of carboplatin loaded *MaGICs*

6.3.2 Effect of anticancer drugs on the relaxivities of *MaGICs*

Tremendous efforts have been made to incorporate drug molecules into MR-active nanocarriers for noninvasively visualizing biodistribution and tracking accumulation at targeted sites.[26-28] In order to possess dual functionality, it is imperative that the nanocarriers have prominent therapeutic efficacy as well as pronounced T1/T2-NMR relaxometric properties. However, drug molecules can alter the physical and surface characteristics of nanocarriers such as hydrodynamic size, charge, stability, magnetization, and hydrophilic-hydrophobic balance. Therefore, incorporation of considerable payloads into the carriers while retaining their MRI relaxivities is paramount. Recently, Tapan et al. have shown that loading of doxorubicin and paclitaxel slightly decreased both the T1 and T2 relaxivities of Pluronic stabilized magnetite nanoparticles even though the incorporated drugs did not change the hydrodynamic sizes of the particles.[29] It is possible that the drug molecules reduced access of water to the nanoparticles, thus leading to reduced relaxation rates. Our group has previously reported that encapsulation of the hydrophilic antibiotic gentamicin into magnetite-poly(ethylene oxide)-*b*-poly(acrylic acid) complexes increases hydrodynamic size of the particles and increases the T2 relaxivity.[30] So there is an interplay of various parameters when

considering effects of payload on the capacities of nanocarriers to retain their MRI relaxivities.

To evaluate the effect of each type of anticancer drug on the relaxivities of *MaGICs* that contained manganese ions as opposed to magnetite nanoparticles, the NMR relaxivities of drug loaded *MaGICs* were measured at 1.4 T and compared to that of *MaGICs* without drug. In the case of doxorubicin, we observed that the r_2*'s* and r_1*'s* of the *MaGICs* remained almost constant with versus without the doxorubicin even though there were increases in the nanocomplex sizes (Table 6.4). On the other hand, incorporation of cisplatin and carboplatin resulted in decreases in both r_2*'s* and r_1*'s* of the *MaGICs* by up to a factor of 2. (Table 6.5 and 6.6) This may be due to the poor water solubility of the cisplatin that reduces the interaction between water molecules and Mn ions in *MaGICs*, thus decreasing relaxivities of the complexes. Although the relaxivities of cisplatin- and carboplatin-loaded *MaGICs* are lower than *MaGICs* without drug, they are superior to those of the commercial manganese based contrast agent MnDPDP, Teslascan®.

Sample	r_2	r_1	r_2/r_1	Intensity average diameter (nm)
MaGICs	29.1	17.6	1.7	56.2
MaGICs-DOX 4.6	31.6	19.7	1.6	107.7
MaGICs-DOX 8.4	35.3	21.0	1.7	118.6
MaGICs-DOX 14.5	34.3	21.0	1.6	123.2

Table 6.4 Relaxivities of doxorubicin loaded *MaGICs* (unit = s^{-1} mM Mn^{-1})

Sample	r_2	r_1	r_2/r_1	Intensity average diameter (nm)
MaGICs	29.1	17.6	1.7	56.2
MaGICs-CPt 5.0	20.6	12.3	1.7	119.9
MaGICs-CPt 9.7	17.1	10.7	1.6	122.5
MaGICs-CPt 16.0	15.4	9.3	1.7	138.8

Table 6.5 Relaxivities of cisplatin loaded *MaGICs* (unit = s^{-1} mM Mn^{-1})

Sample	r_2	r_1	r_2/r_1	Intensity average diameter (nm)
MaGICs	29.1	17.6	1.7	56.2
MaGICs-CBPt 4.7	27.5	16.8	1.6	91.2
MaGICs-CBPt 7.7	24.8	15.0	1.6	121.1
MaGICs-CBPt 13.0	21.4	13.4	1.7	134.8

Table 6.6 Relaxivities of carboplatin loaded *MaGICs* (unit = s^{-1} mM Mn^{-1})

6.3.3 Release behavior of drugs from *MaGICs* at pH 7.4 and pH 4.5

It is common that drug-loaded polymeric nanocarriers tend to have a burst release when they are dispersed in physiological media.[31-33] The initial burst release rates could cause unwanted side effects or tissue irritation. It is thus often desirable to achieve slow drug release or zero order sustained release from drug delivery systems at physiological pH in blood circulation.

To investigate the release behavior of the three drug-loaded *MaGICs*, in vitro release studies of anticancer drugs from the *MaGICs* were performed at pH 7.4 and 4.5 at 37 °C in the presence of 0.14 M NaCl to simulate blood pH and intracellular pH conditions respectively. In this method, free drugs or drug-loaded *MaGICs* were dispersed in either PBS (pH 7.4) or ABS (pH 4.5) and placed in a dialysis cassette. The cassettes were fully submerged in a beaker containing receptor medium to establish sink

conditions. Release of the drugs into the receptor medium was measured at respective time points.

As shown in Figure 6.8 (a) free doxorubicin fully diffused through the membrane into the receptor medium within 9 hours. In contrast, release of the doxorubicin from the *MaGICs* was sustained significantly longer and was dependent on the drug concentration in the particles. Higher drug concentrations released at faster rate. The drug release rate was also dependent on the pH. Approximately 44 % and 67 % of doxorubicin were released from *MaGICs-DOX 14.5* at pH 7.4 and 4.5 within 48 hours, respectively. At pH 4.5, the net negative charge on the ammonium bisphosphonate units was lower than at pH 7.4. This could lead to weakening of the electrostatic interaction between the bisphosphonate and doxorubicin, thereby leading to faster release of drug molecules. These results suggest that the *MaGICs* should sufficiently release the drug in the acidic environment found in cellular compartments.

Unlike doxorubicin, the release behavior of cisplatin from *MaGICs* is much slower even at pH 4.5 indicating strong interactions between *MaGICs* and cisplatin. This could be attributed to a combination of electrostatic interaction and chelation of platinum metal with the bisphosphonate moieties. As shown in Figure 6.9, at the 48-hour time points, only about 13 % and 17 % of Pt were released from *MaGICs-CPt 16.0* at pH 7.4 and 4.5, respectively. It has been reported that release of Pt from polymeric carboxylate complexes was initiated by dissociation of particles accompanied by an inverse ligand exchange reaction of Pt(II) with chloride ions in physiological saline.[8] The very slow release from the bisphosphonate complexes may likely be due to much slower inverse ligand exchange with ions in the media.

The release rate of carboplatin from *MaGICs* was faster than that of cisplatin but slower than doxorubicin. The *MaGICs-CBPt 13.0* released about 34 % and 52 % of Pt at pH 7.4 and 4.5 respectively. Since the coordination bonds between the cyclobutanedicarboxylate ligand and Pt in carboplatin were stronger than that of chloride ions and Pt in cisplatin, the reaction between carboplatin and *MaGICs* might result in the formation of only one coordination bond between the bisphosphonate groups of *MaGICs* and Pt of carboplatin. This may explain the faster release rate of Pt from *MaGICs-CBPt* compared to *MaGICs-CPt*. In addition, the higher water solubility of carboplatin compared to cisplatin could lead to a better diffusion rate of the carboplatin from *MaGICs* to the surrounding medium. (Figure 6.10)

Overall, we envision that *MaGICs* could be utilized to carry and sufficiently release the payloads in both physiological media, particularly in the intracellular acidic environment.

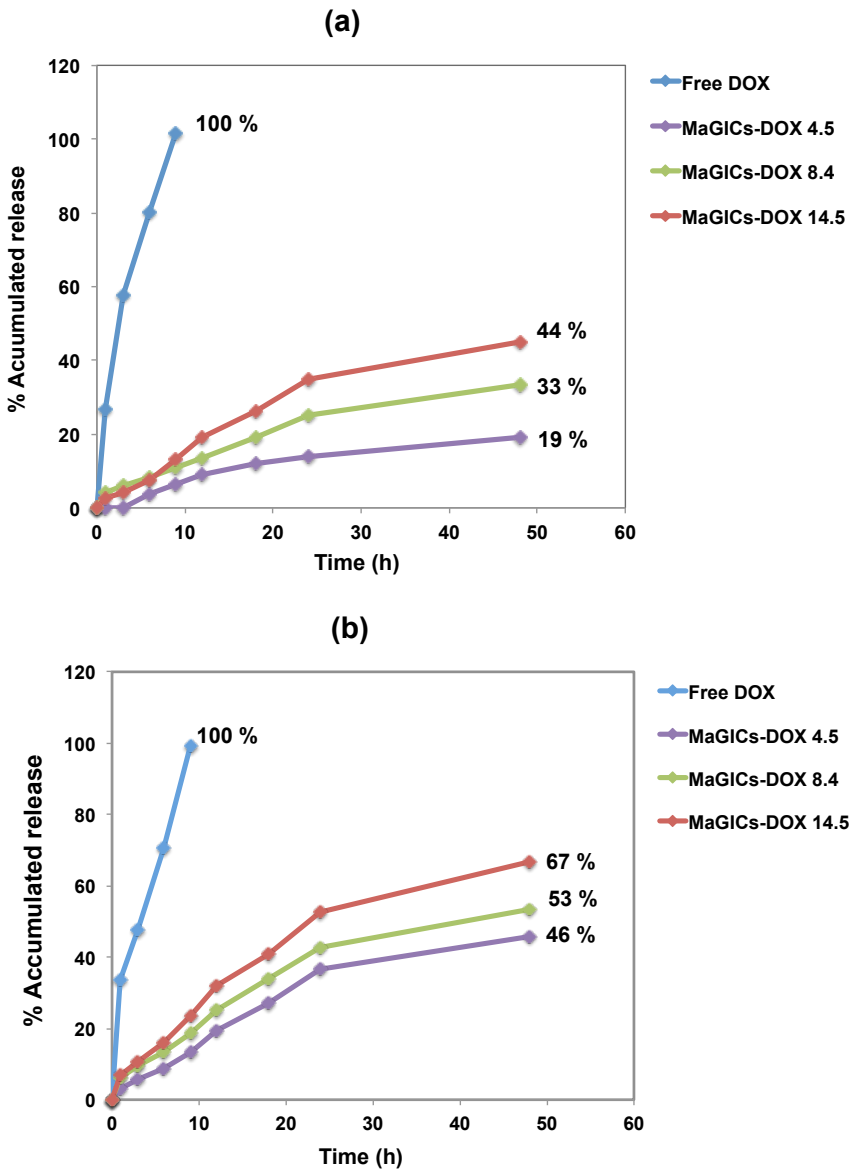

Figure 6.8 Release behavior of doxorubicin from *MaGICs* at a) pH 7.4 b) pH 4.5

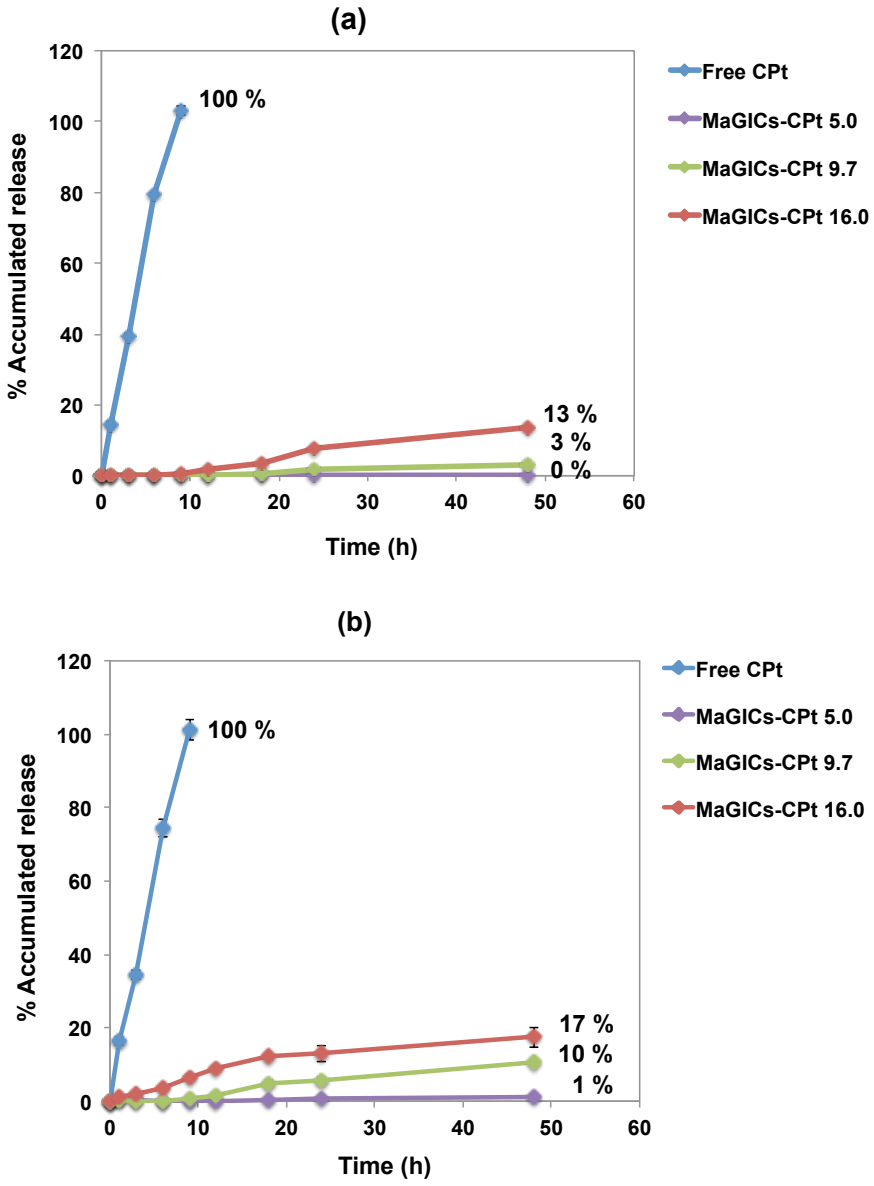

Figure 6.9 Release behavior of cisplatin from *MaGICs* at (a) pH 7.4 (b) 4.5

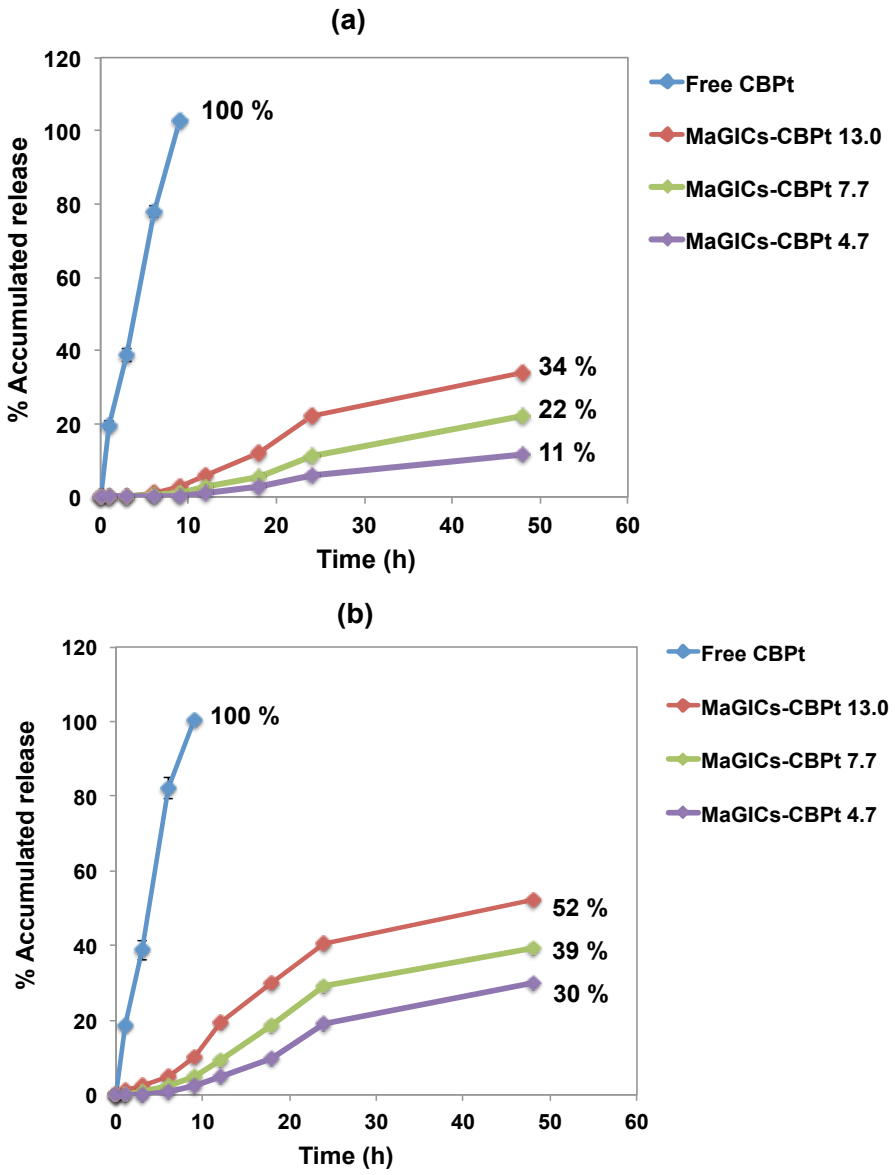

Figure 6.10 Release behavior of carboplatin from *MaGICs* at (a) pH 7.4 (b) pH 4.5

6.3.4 In vitro cytotoxicity of anticancer drug loaded *MaGICs*

Breast cancer MCF-7 cells were exposed to various doses of drug-loaded *MaGICs* for 48 hours to examine the in vitro anticancer efficacy. The cytotoxic effects were evaluated using a standard MTT assay and the results are presented in Figures 6.11-6.13. These investigations clearly demonstrated that the cytotoxicities of doxorubicin-loaded

MaGICs against breast cancer cells were similar to the free drug even though the complexes likely only partially releases the drugs. Previously reported anticancer activities of various doxorubicin-loaded nanocarriers against non-resistant cells have been mixed.[5, 6, 34-37] Some formulations led to comparable or superior activities, whereas some nanocariers resulted in reduced activities. For example, Alakhov et al. demonstrated that doxorubicin-loaded Pluronic L61 copolymer micelles had similar cytotoxic activity against MCF-7 cells relative to free doxorubicin.[34] Gokhale et al. also reported that liposomes encapsulating doxorubicin showed the same range of cytotoxicity on HL60 cells relative to free doxorubicin.[35] Increased cytotoxicities compared to free drugs have also been observed with polymeric nanoparticles and liposomes carrying doxorubicin. Couvreur et al. have shown that doxorubicin-loaded polyalkylcyanoacrylate nanoparticles were more cytotoxic than free doxorubicin against P388 leukemia cells.[36] Solid lipid nanospheres comprised of stearic acid and sodium taurocholate enhanced the cytotoxicity of doxorubicin about 10-fold with MCF-7 cells.[37] On the contrary, Kamimura et al. have reported that doxorubicin-loaded PEG-*b*-poly(4-vinylbenzylphosphonate) micelles reduced cytotoxic activity of the drug against MCF-7 cells by ~2 fold due to sustained release of the drug.[6] Bronich et al. have shown that doxorubicin-loaded non-degradable crosslinked micelles based on poly(ethylene oxide)-*b*-poly(methacylic acid) displayed 16 times lower cytotoxic activity against A2780 ovarian carcinoma cells than free drug, while degradable complexes were 2.5 times less potent than the free drug.[5] Indeed, there is an interplay between release properties and intracellular uptake on antitumor efficacy of drug-loaded nanocarriers. Enhanced uptake of nanocomplexes into cancer cells increases overall intracellular drug concentration. However, if drug molecules are

released in a controlled or slow fashion in the cells, this may affect efficacy in comparison to free drug.

In contrast to doxorubicin-*MaGICs*, the cisplatin-loaded nanocarriers showed a decrease of anti-proliferative effect relative to cisplatin by 3-fold. This is likely caused by very slow release of platinum species from cisplatin-loaded *MaGICs* even at low pH (figure 6.9 a and b). This is consistent with the results reported previously by others. For example, poly(ethylene oxide)-*b*-poly(methacylic acid) micelles displayed ~10-fold lower cytotoxic activity than free cisplatin against A2780 ovarian carcinoma cells.[4] Kataoka and Kakizoe et al. also reported that cisplatin incorporated into poly(ethylene glycol)-*b*-poly(glutamic acid) micelles was ~10 times less potent against LLC, C 26, and MCF-7 cell lines than free cisplatin due to the slow release of Pt.[8, 38]

Carboplatin-loaded *MaGICs*, quite remarkably, enhance the anti-proliferative effect relative to free carboplatin by almost 30-fold. This is highly advantageous since carboplatin, though with less side effects, has much lower anticancer activity relatively to cisplatin. Not only do carboplatin-loaded *MaGICs* exhibit activity far exceeding carboplatin, these complexes also show superior killing efficacy against MCF-7 cells relative to cisplatin by about 2-fold. Our finding is contrary to what others have previously reported regarding polymeric-platinum drug complexes and their anticancer activities. For example, Huynh and Stenzel et al. have reported that block copolymer micelles with 1,3-dicarboxylate pendants efficiently formed chelating complexes with cisplatin. Indeed, those micelles exhibited activities against cancer cell lines comparable to carboplatin, but none of the complexes showed antiproliferative activity exceeding that of cisplatin.[39, 40]

The reasons why the polyammonium bisphosphonate-carboplatin complexes show such remarkable enhancement of activity are not clear. There are large bodies of work that have addressed structure-activity relationships of anticancer platinum compounds.[19, 41] Changes in platinum ligands have led to development of more potent compounds. Thus, it is reasonable that if one or both of the carboxylate ligands on carboplatin are exchanged with ammonium bisphosphonate moieties on the *MaGICs* complexes, the activity of such new complexes would be changed. The large enhancement of activity observed with the *MaGICs*-carboplatin against MCF-7 cells however is promising and warrants considerable further studies. This could pave the way toward development of new macromolecular carriers that promote therapeutic efficacy against cancer cells and where biodistribution can be non-invasively tracked.

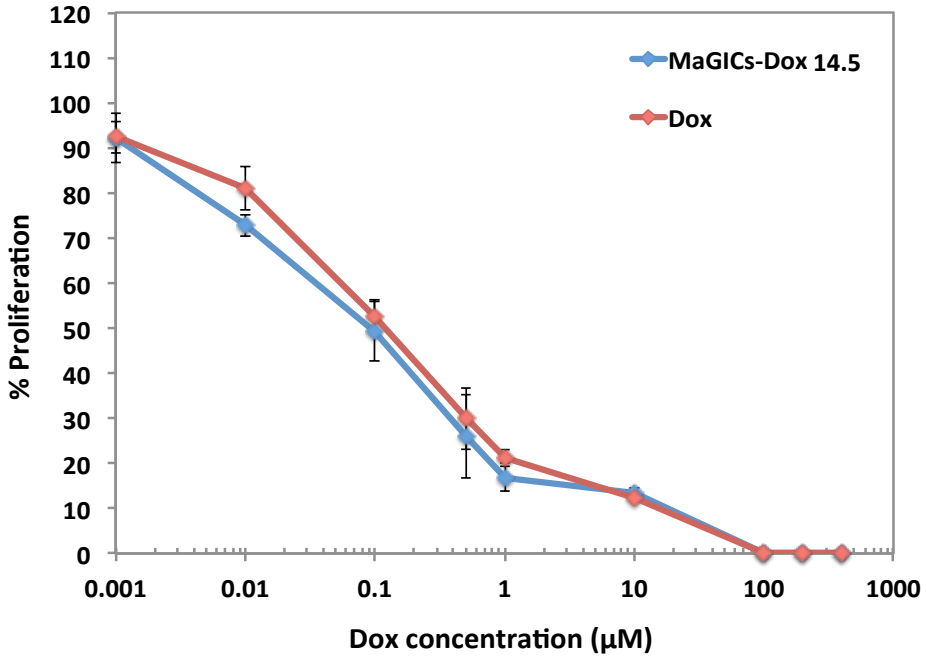

Figure 6.11 Cytotoxic effect of *MaGICs-DOX 14.5* and free DOX

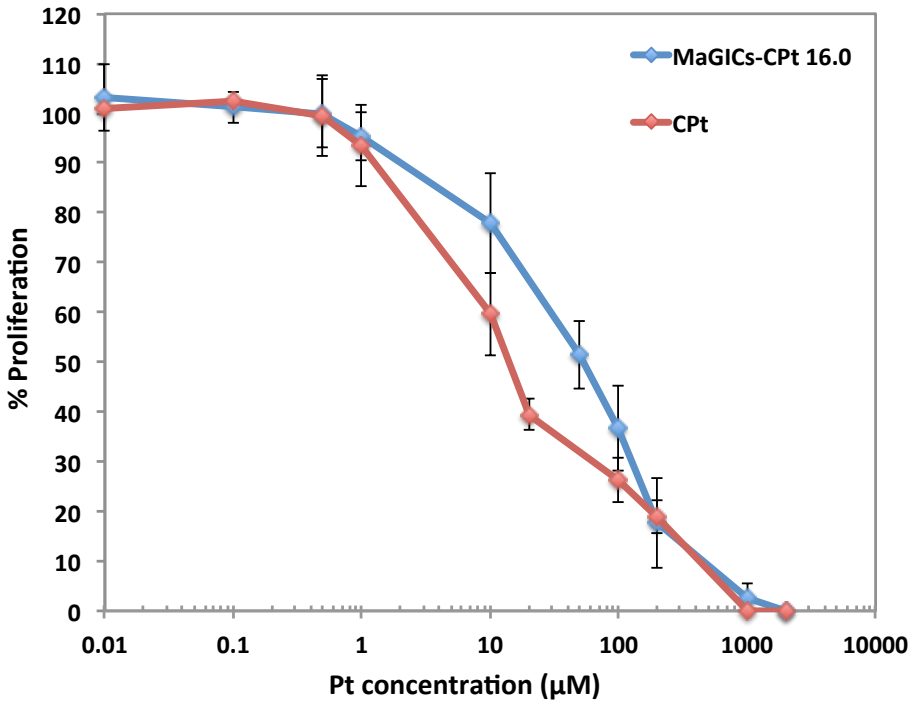

Figure 6.12 Cytotoxic effect of *MaGICs-CPt 16.0* and free CPt

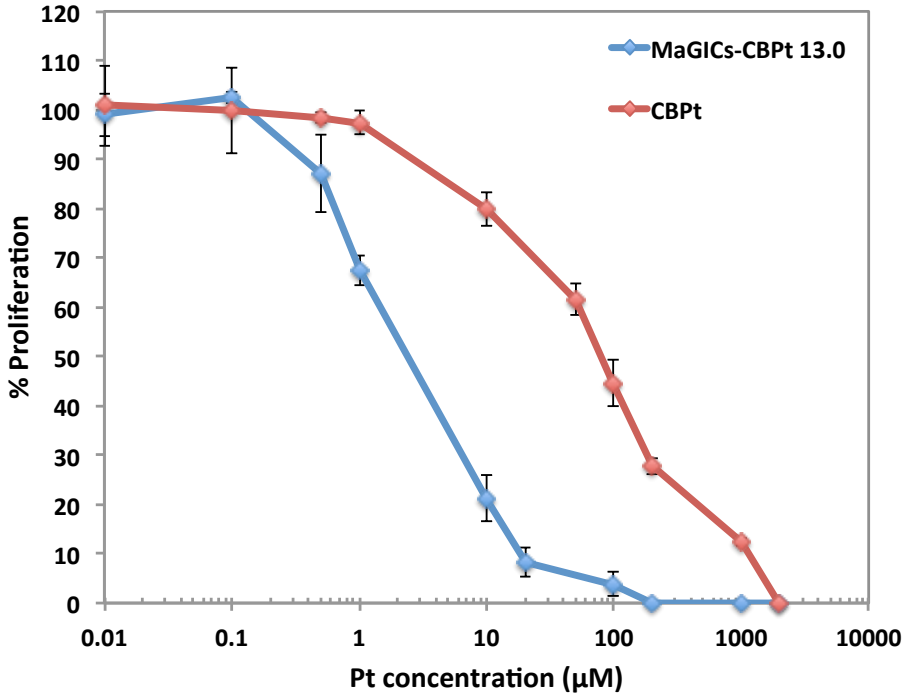

Figure 6.13 Cytotoxic effect of *MaGICs-CBPt 13.0* and free CBPt

6.4 Conclusion

In conclusion, we have successfully developed MRI active manganese based nanocarriers that can be used to encapsulate chemotherapeutic drugs, with emphasis on doxorubicin, cisplatin and carboplatin. Drug release behavior was sustained and depended on pH, drug structures and payload. In vitro anti-proliferative efficacies of drug-loaded *MaGICs* revealed that the complexes are potent. These pH-responsive manganese nanocarriers have excellent relaxometric properties and also anticancer activity against MCF-7 breast cancer cells. The binding of carboplatin molecules into the polymeric carriers increased the cytotoxic activity remarkably. Therefore, these multifunctional nanocarriers may have potential as theranostic agents for cancer chemotherapy.

6.5 References

1. S. Prakash, M. Malhotra, W. Shao, C. Tomaro-Duchesneau, S. Abbasi, *Advanced Drug Delivery Reviews*, 2011, **63**, 1340.
2. K. K. Upadhyay, H. G. Agrawal, C. Upadhyay, C. Schatz, J. F. Le Meins, A. Misra, S. Lecommandoux, 2009, **26**, 157.
3. D. Peer, J. M. Karp, S. Hong, O. C. Farokhzad, R. Margalit, R. Langer, *Nature Nanotechnology*, 2007.
4. S. Bontha, A. V. Kabanov, T. K. Bronich, *Journal of Controlled Release*, 2006, **114**, 163.
5. J. O. Kim, G. Sahay, A. V. Kabanov, T. K. Bronich, *Biomacromolecules*, 2010, **11**, 919.

6. M. Kamimura, J. O. Kim, A. V. Kabanov, T. K. Bronich, Y. Nagasaki, *Journal of Controlled Release*, 2012, **160**, 486.

7. K. Kataoka, A. Harada, Y. Nagasaki, *Advanced Drug Delivery Reviews*, 2001, **47**, 113.

8. N. Nishiyama, S. Okazaki, H. Cabral, M. Miyamoto, Y. Kato, Y. Sugiyama, K. Nishio, Y. Matsumura, K. Kataoka, *Cancer Research*, 2003, **63**, 8977.

9. G. Kwon, S. Suwa, M. Yokoyama, T. Okano, Y. Sakurai, K. Kataoka, *Journal of Controlled Release*, 1994, **29**, 17.

10. M. Yokoyama, T. Okano, Y. Sakurai, H. Ekimoto, C. Shibazaki, K. Kataoka, *Cancer Research*, 1991, **51**, 3229.

11. G. S. Kwon, M. Yokoyama, T. Okano, Y. Sakurai, K. Kataoka, *Journal of Controlled Release*, 1994, **28**, 334.

12. K. Chatterjee, J. Zhang, N. Honbo, J. S. Karliner, *Cardiology*, 2010, **115**, 155.

13. S. A. Abraham, D. N. Waterhouse, L. D. Mayer, P. R. Cullis, T. D. Madden, M. B. Bally, in *Methods in Enzymology*, ed. D. Nejat, Academic Press, 2005, pp. 71.

14. A. J. DeFail, H. D. Edington, S. Matthews, W.-C. C. Lee, K. G. Marra, *Journal of Biomedical Materials Research Part A*, 2006, **79A**, 954.

15. *Doxorubicin loaded pH-sensitive micelle targeting acidic extracellular pH of human ovarian A2780 tumor in mice*, 2005, **13**, 391.

16. G. D. Kang, S. H. Cheon, S.-C. Song, *International Journal of Pharmaceutics*, 2006, **319**, 29.

17. K. Kataoka, T. Matsumoto, M. Yokoyama, T. Okano, Y. Sakurai, S. Fukushima, K. Okamoto, G. S. Kwon, *Journal of Controlled Release*, 2000, **64**, 143.

18. E. S. Lee, K. Na, Y. H. Bae, *Journal of Controlled Release*, 2005, **103**, 405.

19. I. Kostova, *Recent Pat Anticancer Drug Discov*, 2006, **1**, 1.

20. C. A. Rabik, M. E. Dolan, *Cancer Treat Rev*, 2007, **33**, 9.

21. B. Schlechter, A. Neumann, M. Wilchek, R. Arnon, *Journal of Controlled Release*, 1989, **10**, 75.

22. B. Schechter, M. Wilchek, R. Arnon, *International Journal of Cancer*, 1987, **39**, 409.

23. M. Yokoyama, T. Okano, Y. Sakurai, S. Suwa, K. Kataoka, *Journal of Controlled Release*, 1996, **39**, 351.

24. N. Nishiyama, M. Yokoyama, T. Aoyagi, T. Okano, Y. Sakurai, K. Kataoka, *Langmuir*, 1998, **15**, 377.

25. A. B. Richard Barakat, Maurie Markman, Marcus E. Randall 2013.

26. J. Xie, S. Lee, X. Chen, *Advanced Drug Delivery Reviews*, 2010, **62**, 1064.

27. N. Ahmed, H. Fessi, A. Elaissari, *Drug Discovery Today*, 2012, **17**, 928.

28. S. M. Janib, A. S. Moses, J. A. MacKay, *Advanced Drug Delivery Reviews*, 2010, **62**, 1052.

29. T. K. Jain, J. Richey, M. Strand, D. L. Leslie-Pelecky, C. A. Flask, V. Labhasetwar, *Biomaterials*, 2008, **29**, 4012.

30. N. Pothayee, N. Pothayee, N. Jain, N. Hu, S. Balasubramaniam, L. M. Johnson, R. M. Davis, N. Sriranganathan, J. S. Riffle, *Chemistry of Materials*, 2012, **24**, 2056.

31. A. S. Hasan, M. Socha, A. Lamprecht, F. E. Ghazouani, A. Sapin, M. Hoffman, P. Maincent, N. Ubrich, *International Journal of Pharmaceutics*, 2007, **344**, 53.

32. K. Fu, R. Harrell, K. Zinski, C. Um, A. Jaklenec, J. Frazier, N. Lotan, P. Burke, A. M. Klibanov, R. Langer, *Journal of Pharmaceutical Sciences*, 2003, **92**, 1582.

33. X. Huang, C. S. Brazel, *Journal of Controlled Release*, 2001, **73**, 121.

34. A. Venne, S. Li, R. Mandeville, A. Kabanov, V. Alakhov, *Cancer Research*, 1996, **56**, 3626.

35. P. C. Gokhale, B. Radhakrishnan, S. R. Husain, D. R. Abernethy, R. Sacher, A. Dritschilo, A. Rahman, *Br J Cancer*, 1996, **74**, 43.

36. P. Couvreur, C. Vauthier, *Journal of Controlled Release*, 1991, **17**, 187.

37. A. Miglietta, R. Cavalli, C. Bocca, L. Gabriel, M. Rosa Gasco, *International Journal of Pharmaceutics*, 2000, **210**, 61.

38. H. Uchino, Y. Matsumura, T. Negishi, F. Koizumi, T. Hayashi, T. Honda, N. Nishiyama, K. Kataoka, S. Naito, T. Kakizoe, *Br J Cancer*, 2005, **93**, 678.

39. V. T. Huynh, P. de Souza, M. H. Stenzel, *Macromolecules*, 2011, **44**, 7888.

40. V. T. Huynh, J. Y. Quek, P. L. de Souza, M. H. Stenzel, *Biomacromolecules*, 2012, **13**, 1010.

41. R. A. Alderden, M. D. Hall, T. W. Hambley, *Journal of Chemical Education*, 2006, **83**, 728.

Chapter 7
Conclusions and Recommendations

In conclusion, we have successfully developed multifunctional nanocarriers that combine unique features of ion-containing block and graft copolymers, robust MRI contrast agents and drugs that can be used as novel platforms for simultaneous real-time imaging of disease and biodistribution and drug delivery.

Firstly, this research demonstrated that magnetite nanoparticles can be efficiently complexed with PEO-*b*-PAA block copolymers through binding of a portion of the anionic segment of the copolymer with the metal oxide surfaces. The remainder of the carboxylates can then be utilized to bind high concentrations of cationic antibiotics. The resultant polymer-magnetite-drug nanoparticles have excellent colloidal stability in media simulating physiological conditions. Mouse macrophages take up these complexes over a range of incubation concentrations and complex sizes. These complexes appeared to enhance intracellular antimicrobial activities of gentamicin.

Furthermore, a series of magnetic block ionomer clusters *(MBIClusters)* with some of the highest T2 relaxivities ever reported were prepared. Small aggregates of magnetite-polymer nanoparticles (*MBICs*) were first assembled by adsorbing the polyacrylate block of an aminofunctional poly(ethylene oxide-*b*-acrylate) (H_2N-PEO-*b*-PAA) copolymer onto magnetite nanoparticles. Amine groups at the tips of the H_2N-PEO corona were then crosslinked through reaction with a poly(ethylene oxide) diacrylate oligomer to yield *MBIClusters.* The extremely high relaxivities of the *MBIClusters* were attributed to the hydrophilic intracluster spacing between the magnetite particles and the cluster sizes. The transverse relaxivities increased as their average size was increased.

MRI scans focused on the livers of mice demonstrated that these *MBIClusters* are significantly sensitive contrast agents. The *MBIClusters* were also efficiently loaded with high concentrations of the multi-cationic drug gentamicin. Therefore, these multifunctional nanocarriers have potential as theranostic agents for dual imaging and drug delivery.

Novel manganese graft ionomer complexes *(MaGICs)* that contain Mn ions complexed with a novel polyaminobisphosphonate-*g*-PEO for T1 weighted MRI positive contrast agents were developed. These materials contained a family of new polymeric bisphosphonates that had unprecedented binding capacities for metal ions. The complexes exhibited excellent colloidal stability without any release of free manganese in simulated physiological media. Moreover, the manganese did not ion exchange with calcium ions, even at high concentrations. This is important because free manganese salts can lead to toxicity. It was discovered that neither the polymers nor the *MaGICs* cause any in vitro toxicity against mouse hepatocytes. The T1 relaxivities of the *MaGICs* were superior to those of free manganese ions and commercial positive contrast agents, suggesting their applicability as effective T1 weighted MRI contrast agents.

Finally, imageable nanocarriers for chemotherapy drugs were created from the *MaGICs*. The manganese based nanocarriers were loaded with anticancer drugs including doxorubicin, cisplatin and carboplatin. Drug release behavior was sustained and depended on environmental pH (faster in acidic environments), drug structures and drug concentration in the *MaGICs*. These manganese nanocarriers also have excellent relaxometric properties together with anticancer activity against cancer cells. In particular, the binding and release properties of the carboplatin-loaded *MaGICs* were

remarkable. The complexes enhanced the anti-proliferative effect of MCF-7 breast cancer cells relative to free carboplatin by almost 30-fold. Thus, these drug-loaded *MaGICs* have excellent potential as simultaneous diagnostic and chemotherapeutic agents.

It is recommended that the *MBICs* and *MBIClusters* be prepared with larger magnetite cores to achieve high specific absorption rates (SAR) when exposed to AC magnetic fields. An external alternating magnetic field (AMF) could then be applied to generate energy, and the resulting energy dissipation may be useful for triggering release of chemotherapeutic drugs. Moreover, if the energy dissipated results in a local temperature rise, this might provide simultaneous hyperthermia-based treatment of cancer. It is also recommended that the *MaGICs* should be made with polyaminobisphosphonate-*g*-PEO-amine. This would allow for conjugation of targeting moieties e.g., antibodies, peptides, or aptamers to create multifunctional *MaGICs* with enhanced uptake and retention in cancer cells, and with increased specificity in combination with anticancer efficacy.